

**AN INVESTIGATION OF POLY(CAPROLACTONE-CO-GLYCOLIDE)
INTERACTION WITH BIOACTIVE PROTEINS AND CELLULAR RESPONSES**

By

HAN CUI

A Dissertation submitted to the
Graduate School-New Brunswick
Rutgers, The State University of New Jersey
in partial fulfillment of the requirements
for the degree of
Doctor of Philosophy
Graduate Program in Pharmaceutical Science

written under the direction of

Patrick J. Sinko, Ph.D.

and approved by

New Brunswick, New Jersey

May, 2010

ABSTRACT OF THE DISSERTATION
AN INVESTIGATION OF POLY(CAPROLACTONE-CO-GLYCOLIDE)
INTERACTION WITH BIOACTIVE PROTEINS AND CELLULAR
RESPONSES

by Helen Han Cui

Dissertation director: Patrick J. Sinko, Ph.D.

The objective of the present investigation is to systematically evaluate the role of polymer crystallinity on osteoblast adhesion, proliferation, osteogenic gene expression and bioactive protein adsorption using a series of poly(caprolactone-*co*-glycolide) (PCL-PGA) polymers.

Five compositions of pure PCL and PGA, and PCL-PGA intermediate copolymeric compositions in ratios of 25:75, 35:65 and 45:55, were selected. These polymers were fabricated into thin films by compression molding. The samples were characterized using scanning electro microscopy (SEM) for surface morphology, differential scanning calorimetry (DSC) for crystallinity, contact angle measurement for hydrophobicity (CA), and atomic force microscopy (AFM) for nanotopography. The PCL-PGA films

demonstrated similar morphology, hydrophobicity and nanotopography whereas they differed significantly in crystallinity.

Cell adhesion and proliferation, as well as osteogenic gene expression were evaluated with osteoblasts (HEPM 1486) on PCL-PGA surfaces. Recombinant human growth and differentiation factor 5 (rhGDF-5) and Fibronectin (Fn) were adsorbed from single protein solutions using depletion method and quantified using bicinchoninic acid (BCA) protein and radiolabelling assay. The protein-adsorbed surface nanotopography was analyzed using AFM.

In the cellular responses experiments, amorphous/flexible PCL-PGA 35:65 supports osteoblast growth and promotes osteogenic gene expression significantly better than the crystalline PCL and PGA. These studies demonstrated that crystallinity and rigidity played major roles in determining cell responses with PCL-PGA polymers.

Protein adsorption study results indicate that rhGDF-5 adsorbed to a higher extent on PCL surfaces and least on PGA surfaces. Reduced rhGDF-5 (a more hydrophilic and flexible protein form) adsorbed significantly in greater amounts on all PCL-PGA substrates, demonstrating that the conformation and hydrophobicity of rhGDF-5 played a major role in its adsorption to PCL-PGA surfaces.

Fn, a 450 kDa protein, contains multiple binding motifs with varied hydrophobicity.

Binding motifs of Fn fragments strongly impacted their adsorption to PCL-PGA surfaces.

The adsorption of Fn 70 kDa fragment on PCL-PGA polymers was found to favor

binding to PCL material with the greatest adsorption on pure PCL surfaces, similar to the full length of Fn molecule. Collectively, these studies demonstrate that Fn (70 kda) played a major role in full-length Fn adsorption to PCL-PGA substrates.

LIST OF PAPERS

This thesis is based on the following papers:

Helen Cui and Patrick Sinko. The Role of Crystallinity on Differential Attachment and Proliferation of Osteoblasts and Fibroblasts on Poly(caprolactone-*co*-glycolide) Polymeric Surfaces. To be submitted to J. of Biomed. Mater: Mater in Tissue E. and Reg. Med.

Helen Cui, Jeffrey Geesin and Patrick Sinko. Fn Adsorbed to Poly(caprolactone-*co*-glycolide) Surfaces via Its Heparin/Collagen Binding Motif Module under influence of varied crystallinity of the matrix. To be submitted to Biomat.

Helen Cui, Jeffrey Geesin and Patrick Sinko. Does crystallinity play a major role in rhGDF-5 adsorption to Model Polyester Surfaces. In preparation

Helen Cui, Patrick Sinko. The role of crystallinity on differential osteogenic gene expression on poly(lactide-*co*-glycolide) Polymers. In preparation

ACKNOWLEDGEMENT

Many People have helped and supported me and I would like to express my sincere gratitude to all of you: family, friends, colleagues, and teachers. Where would I have been without you.

The following people deserve special thanks:

Professor Patrick Sinko, my supervisor

I am extremely grateful that you allowed me the opportunity to be part of your achieving and high quality group. You and I, together, created the independent critical researcher I am today.

Dr. Jeffrey Geesin, my supervisor at work

Jeff, thank you, for always kindly sharing your vast and diverse knowledge in science.

Dr. Kathryn Uhrich and Dr. Stanley Stein, the experts

Thank you for your time and expertise! You are all professional in summarizing a vast deal of knowledge into effective key instructions guiding me through my research.

Dr. Fuzhai Cui, My father and expert in biomaterials research

I know how lucky I am to have you guiding me through my whole life,
including my career.

Eric Hu, Wanlan Huang, AnnaBelle, Arnold, my family,

One word-LOVE

Somerville, NJ, USA, January 30, 2010

Helen H. Cui

LIST OF TABLES

Table 2- 1. Properties of common biodegradable polymers.	32
Table 4- 1 Physicochemical properties of Poly (caprolactone- <i>co</i> -glycolide) (PCL-PGA) polymers.....	76
Table 4- 2. Processing Temperatures for Compression Molding of PCL-PGA Films	77
Table 4- 3. Thickness of Crystallinity-Induced PCL-PGA Polymeric Films	77
Table 4- 4. Basic Physicochemical Properties: Thermal Properties of PCL-PGA films and hydrophobicity.	78
Table 4-5. RMS Roughness for Wet and Dry PCL-PGA Films.....	78
Table 6- 1 AFM Nanotopography Images of Fn, Fn 30 KDa, Fn 70 KDa and Fn 120 KDa Adsorbed PLGA Surfaces.	148

LIST OF FIGURES

Fig. 2- 1 Growth and Differentiation Factor 5, chemical name rhGDF-5: sequence and molecular.....	27
Fig. 2- 2 Schematic structure plot of Fn	30
Fig. 4- 1 Schematic Model of Fn and Its Major Domains [156].....	80
Fig. 4- 2 Thickness of PCL-PGA Films.....	80
Fig. 4- 3 Differential Scanning Calorimetry thermograms of PCL-PGA Films.	81
Fig. 4- 4 DSC Thermograms on Dry and Wet PCL-PGA 35:65 and PGA polymeric Films..	82
Fig. 4- 5 SEM Images of PCL-PGA Films..	83
Fig. 4- 6 Contact Angle Measurement of PCL-PGA Films.....	84
Fig. 4- 7 Representative AFM surface topographic features (Tapping mode) for PCL-PGA Films..	85
Fig. 4- 8 Roughness of PCL-PGA Films Comparison: Pre- and Post-Hydration.....	86
Fig. 4- 9. Roughness Pre-osteoblasts Attachment and Proliferation on PCL-PGA Polymeric Films at 24, 72 and 168 hours..	87
Fig. 4- 10. Osteoblasts morphology (optical microscopy) post seeding on PCL-PGA Films.	90
Fig. 4- 11. FAK Gene Expression on PCL and PCL-PGA 35:65 Films at 24 and 72 hours.....	91
Fig. 4- 12. cbfa-1 Expression on PCL and PCL-PGA 35:65 Films at 24 and 72 hours.. ..	91
Fig. 4- 13. Osteocalcin Expression on PCL and PCL-PGA Films at 24 and 72 hours.....	92

Fig. 4- 14. Collagen Type I gene expression on PCL and PCL-PGA 35:65 films at 24 and 72 hours.....	92
Fig. 4- 15. Osteocalcin Expression on PCL-PGA Films at 72 hours and 1 week..	93
Fig. 4- 16. The Thickness of PLGA 85:15 Films..	93
Fig. 4- 17. Effect of the Induced Crystallinity on the Tensile Strength and Percentage Elongation of PLGA 85:15 Films.	94
Fig. 4- 18. X-ray Scattered Plot of PLGA 85:15 Films with Induced Crystallinity.	95
Fig. 4- 19. X-ray Diffraction for PLGA 85:15 Films with Induced Crystallinity.....	96
Fig. 4- 20. Contact Angle Measurement of PLGA 85:15 Films with Induced Crystallinity.....	97
Fig. 4- 21. Kinetic DSC on Dry and Wet PLGA 85:15 Films	98
Fig. 4- 22. RMS Roughness for Dry and Wet PLGA 85:15 Films.....	99
Fig. 4- 23. AFM Nanotopography Images of Dry and Wet PLGA 85:15 Films.	100
Fig. 4- 24. Pre-osteoblast Cell Attachment and Proliferation on Crystallinity-Induced PLGA 85:15 Films.....	101
Fig. 4- 25. Osteogenic Gene Expression from Crystallinity-Induced PLGA 85:15 Films. .	102
Fig. 5- 1 rhGDF-5 Adsorption onto PCL-PGA Films..	120
Fig. 5- 2 rhGDF-5 Desorption from PCL-PGA Films over the course of 24 h..	121
Fig. 5- 3 Chromatographic Figure of rhGDF-5 which Underwent Kinetic Reduction of rhGDF-5.....	121
Fig. 5- 4 Amount of rhGDF-5 and Reduced rhGDF-5 Adsorption on PCL-PGA Surfaces..	122
Fig. 5- 5 Surface Roughness of rhGDF-5 Adsorbed PCL-PGA Surfaces..	123

Fig. 5- 6. Surface Roughness of RhGDF-5 and Reduced rhGDF-5 Adsorbed PCL-PGA Surfaces.....	124
Fig. 5- 7 Roughness of rhGDF-5 and Reduced rhGDF-5 Adsorbed PCL-PGA Surfaces..	125
Fig. 5- 8 AFM Nanotopography Images of rhGDF-5 and Reduced rhGDF-5 Adsorbed PCL-PGA Surfaces..	127
Fig. 5- 9 rhGDF-5 and Reduced rhGDF-5 Adsorption on PLGA 85:15 Surfaces..	127
Fig. 5- 10. rhGDF-5 Desorption from Stretched PLGA 85:15 Surfaces..	128
Fig. 5- 11. rhGDF-5 and Reduced rhGDF-5 Adsorbed Surface Roughness for PCL-PGA Surfaces.....	129
Fig. 5- 12 AFM Nanotopography Images of rhGDF-5 and Reduced rhGDF-5 Adsorbed PLGA 85:15 Surfaces..	130
Fig. 6- 1 Fn Adsorption onto PCL-PGA Surfaces..	149
Fig. 6- 2 Fn Desorption from PCL-PGA Surfaces.....	150
Fig. 6- 3. Fn 30 kDa Fragments and Fn Adsorption on PCL-PGA Surfaces.	151
Fig. 6- 4. Fn 70 kDa Fragments and Fn Adsorption on PCL-PGA Surfaces.....	152
Fig. 6- 5. Fn 120 KDa and Fn Adsorption on PCL-PGA Surfaces.....	153
Fig. 6- 6. RMS roughness for Fn Adsorbed PCL-PGA Surfaces..	153
Fig. 6- 7. Roughness for Fn 30 KDa Fragment Adsorbed PCL-PGA Surfaces.....	154
Fig. 6- 8. Roughness for 70K Fn Fragment and Fn..	155
Fig. 6- 9. Surface Roughness for 120K Fn Fragments..	156
Fig. 6-10. AFM nanotopography Images of Fn, Fn 30 KDa, Fn 70 KDa and Fn 120 KDa Fragment Adsorbed PCL-PGA Surfaces..	157

Fig. 6- 11. Fn Adsorption on PLGA 85:15 Surfaces..	158
Fig. 6- 12 Fn Desorption from PLGA 85:15 Films with Different Degree of Induced Crystallinity.....	158
Fig. 6- 13. Fn and Fn 30 kDa Fragment Adsorption on PLGA 85:15 Surfaces..	159
Fig. 6- 14. Fn and Fn 70 kDa Fragment Adsorption on PLGA 85:15 Surfaces..	160
Fig. 6- 15. Fn and Fn 120 kDa Fragment Adsorption on PLGA 85:15 Surfaces.	160
Fig. 6- 16. Roughness of PLGA 85:15 Films Adsorbed with Fn 30 KDa Fragments.	161
Fig. 6- 17. Roughness of PLGA 85:15 Films Adsorbed with Fn and Fn 70 KDa Fragments.....	161
Fig. 6- 18. Roughness of PLGA 85:15 Films Adsorbed with Fn 120 KDa Fragments. ...	162

TABLE OF CONTENTS

ABSTRACT OF THE DISSERTATION.....	ii
LIST OF PAPERS	v
ACKNOWLEDGEMENT.....	vi
LIST OF TABLES	viii
LIST OF FIGURES	ix
1 INTRODUCTION	1
2 BACKGROUND AND SIGNIFICANCE.....	3
2.1 Cell adhesion	3
2.2 Cell proliferation and differentiation.....	6
2.3 The interaction of proteins with solid surfaces: protein adsorption and interface composition.....	7
2.3.1 Principles of protein adsorption	12
2.3.1.1 Protein adsorption isotherm	17
2.3.2 Factors affecting protein-surface interaction:	18
2.3.3 Protein mediation of cell responses to surface characteristics	24

2.4 Proteins of interest	26
2.4.1 rhGDF-5	26
2.4.2 Fibronectin (Fn)	29
2.5 Surfaces of interest	30
3 SPECIFIC AIMS	34
4 POLY (CAPROLACTONE-CO-GLYCOLIDE) SURFACES AND OSTEOGENIC CELLULAR RESPONSES	36
4.1 Introduction	36
4.1.1 Polymeric material selection	38
4.1.2 Cells and osteogenic gene marker selections	41
4.2 Materials and methods	41
4.2.1 Materials	41
4.2.2 PCL-PGA polymer surface preparation	43
4.2.3 Polymeric surface characterization	43
4.2.3.1 Scanning electron microscopy (SEM)	43
4.2.3.2 Contact angle measurement (CA)	44
4.2.3.3 Differential scanning calorimetry (DSC) analysis	44

4.2.3.4 Atomic force microscopy (AFM).....	45
4.2.4 Pre-osteoblast attachment and proliferation on PCL-PGA surfaces	46
4.2.5 Osteogenic gene expression	48
4.3 Crystallinity induced poly(L-lactide-co-glycolide) PLGA 85:15 and cellular responses	49
4.3.1 Materials and methods	49
4.3.1.1 Surface preparation: poly(L-lactide-co-glycolide) 85:15 polymer film preparation and crystallinity induction:	50
4.3.1.2 Crystallinity-induced PLGA 85:15 surface characterization	50
4.3.1.2.1 Scanning electron microscopy (SEM)	50
4.3.1.2.2 X-ray diffraction (XRD)	51
4.3.1.2.3 Contact angle measurement (CA)	51
4.3.1.2.4 Mechanical tests	52
4.3.1.3.5 Atomic force microscopy (AFM).....	52
4.3.1.3 Pre-osteoblast attachment and proliferation.....	53
4.3.1.4 Osteogenic gene expression	53
4.4 Results and discussions	53
4.4.1 PCL-PGA films: Physicochemical properties and cell responses.....	53

4.4.1.1 Thickness of PCL-PGA films	54
4.4.1.2 Differential scanning calorimetry (DSC)	54
4.4.1.3 SEM	55
4.4.1.4 Contact angel measurement	55
4.4.1.5 Atomic force microscopy	56
4.4.1.6 Osteogenic gene expression	58
4.4.2 Crystallinity-induced PLGA 85:15 films physicochemical properties and cellular responses	68
4.4.2.1 Thickness of PLGA 85:15 films	68
4.4.2.2 Mechanical strength	68
4.4.2.3 X-ray diffraction	69
4.4.2.4 Contact angel measurement	70
4.4.2.5 DSC for dry and wet PLGA 85:15 films.....	71
4.4.2.6 AFM for hydrated films:	71
4.4.2.7 Osteogenic cellular responses	71
4.4.2.8 Osteogenic gene expression	72
4.5 Conclusions	74
4.6 Tables	76
4.7 Figures.....	80

5 rhGDF-5 ADSORPTION ON POLY (CAPROLACTONE-CO-GLYCOLIDE)	
SURFACES	103
5.1 Introduction.....	103
5.2 Materials and methods	107
5.2.1 Materials	107
5.2.2 rhGDF-5 adsorption to PCL-PGA surfaces	108
5.2.2.1 Radiolabelling rhGDF-5 using Iodine monochloride (ICL)	108
5.2.2.2 rhGDF-5 adsorption to PCL-PGA surfaces	109
5.2.2.3 rhGDF-5 displacement (desorption)	110
5.2.2.4 AFM for rhGDF-5 modified PCL-PGA surfaces.....	110
5.2.3 Reduced rhGDF-5 adsorption to PCL-PGA surfaces	110
5.2.3.1 Reduction of rhGDF-5 and characterization	110
5.2.3.2 Adsorption of reduced rhGDF-5 on PCL-PGA surfaces	110
5.2.3.3 AFM for reduced rhGDF-5 adsorbed surfaces.....	111
5.2.4 rhGDF-5 and reduced rhGDF-5 adsorption on PLGA 85:15 surfaces.....	111
5.2.4.1 rhGDF-5 and reduced rhGDF-5adsorption studies	111
5.2.4.2 AFM on PLGA 85:15 adsorbed with rhGDF-5 and reduced rhGDF-5 surfaces .	111
5.3 Results and discussions.....	111

5.3.1 rhGDF-5 adsorption and desorption from PCL-PGA surfaces	111
5.3.2 Reduced rhGDF-5 adsorption to PCL-PGA surfaces	112
5.3.3 AFM for rhGDF-5 and reduced rhGDF-5 adsorbed PCL-PGA surfaces.....	113
5.3.4 rhGDF-5 adsorption and desorption from PLGA 85:15 surfaces	114
5.3.5 AFM for rhGDF-5 and reduced rhGDF-5 adsorbed PLGA 85:15 surfaces.....	115
5.4 Conclusions.....	119
5.5 Figures.....	120
6. FIBRONECTIN AND ITS FRAGMENTS ADSORPTION ON PCL-PGA SURFACES	
.....	131
6.1 Introduction.....	131
6.2 Materials and methods	133
6.2.1 Materials	133
6.2.2 Fn adsorption and desorption from PCL-PGA surfaces and PLGA 85:15 surfaces	134
6.2.2.1 Fn and fragments adsorption:.....	134
6.2.2.1 Fn desorption:	134
6.2.2.3 AFM on Fn and Fn adsorbed polymer surfaces	135
6.3 Results and discussion	135

6.3.1 Fn adsorption on PCL-PGA surfaces.....	135
6.3.2 Fn fragments adsorption on PCL-PGA surfaces	136
6.3.3 AFM results of Fn and its fragments adsorbed on PCL-PGA surfaces	137
6.3.4 Adsorption of Fn and fragments on crystallinity-induced PLGA 85:15 surfaces	140
6.3.4.1 Fn sdsorption/desorption on PLGA 85:15 surfaces	140
6.3.4.2 Fibronectin fragments adsorption on PLGA 85:15 Surfaces	140
6.3.4.2 AFM results on Fn adsorbed PLGA 85:15 surfaces.	142
6.4 Discussion	143
6.5 Conclusions.....	147
6.6 Tables	148
6.7 Figures.....	149
7 SUMMARY AND CONCLUSIONS	163
ABBREVIATIONS.....	165
8 REFERENCES	166
9 CURRICULUM VITA.....	183

1 INTRODUCTION

The goal of tissue engineering research is to reconstitute living cells and other natural substances in the form of tissue substitutes that can be used to repair, maintain or enhance normal body structure and function. Such tissue regeneration is often achieved with the aid of biodegradable polymers, onto which cells may be seeded, and which are introduced into a patient where the material gradually resorbs, leaving behind a matrix of connective tissue and cells with the appropriate structural and mechanical properties[1-2].

The interaction of cells with materials is a highly complicated subject, but one that is important in cell biology and a broad range of medical applications. The responses of cells to structured surfaces suggests they are sensitive to surface physicochemical properties, such as substrate topography [3-5], surface charge [6], chemistry [7] and surface free energy/hydrophobicity [8-11].

Complications of implantable medical devices are largely based on both the effects of the implant on the host tissue and the effects of the host on the implant. When cells approach an implant material, they will not make direct contact with its surface. Rather, the rapid adsorption of proteins from blood (or serum) effectively translates the structure and composition of the foreign surface into a biological language [12]. It is to that language that the cells respond, contributing to the ultimate outcomes in implantations.

Cells rely on specific proteins for anchoring and extracellular guidance; the composition of an adsorbed protein layer plays an important role in influencing cellular responses. If the required proteins were correctly presented, a constructive cell response can be expected, favoring wound healing and tissue integration, whereas proteins in an unrecognizable state might direct implants to be removed or isolated. Osteogenesis requires a sufficient number of pre-osteoblastic cells with subsequent differentiation and bio-metabolic activities. Therefore, osteointegration requires that the proteins encountered by the cells must support or actively promote these activities, subsequent to attachment and proliferation. In the same manner, the protein adsorbed to a tissue-engineering scaffold must support cell adhesion, migration and proliferation to populate the scaffold.

2 BACKGROUND AND SIGNIFICANCE

The concepts that relate to the significance of cellular responses and protein adsorption to biomaterials are discussed in this chapter. The references cited throughout the chapter provide more detailed insight to each topic that is presented.

2.1 Cell adhesion

For most cell types, including connective tissue cells such as osteoblasts and fibroblasts, survival is hinged upon their initial adhesion to extracellular matrix [13-15]. In addition, a cell's growth and phenotypic behavior are regulated, at least partially, by its ability to adopt an appropriate morphology [13-14, 16-17]. Therefore, cell adhesion to any substratum is a critical factor of ultimate cellular responses.

Cells in their native environment are anchored by discrete attachments to proteins in the extracellular matrix. *In vitro*, cell attachment to culture surfaces is usually mediated by adhesion proteins contained in the cell culture medium. Osteoblastic cells *in vitro* have been shown to depend primarily on adsorbed fibronectin (Fn) or vitronectin for initial adhesion and spreading on such materials as tissue culture polystyrene, titanium, stainless steel and hydroxyapatite [18-20]. Thus the ability of materials to adsorb proteins from serum determines their ability to support cell adhesion and spreading [21-22] and, hence, is an important aspect of their biocompatibility.

Previous studies showed that enhancement of both Fn and vitronectin adsorption [23] on hydroxyapatite, compared with titanium and stainless steel, correlated with a significant increase in osteoblast precursor attachment. Adhesion proteins can effectively mask otherwise hostile surfaces. Osteoblasts in culture show substantially improved adhesion if the culture surface is precoated with Fn or vitronectin [23]. In a similar manner, the suppression of cell adhesion on a hydrophobic surface was alleviated by a synthetic protein: osteopontin which is one of the bone matrix adhesion proteins [24].

The primary interaction between cells and adhesion proteins takes place via integrins (heterodimeric receptors in the cell membrane), as demonstrated by the decrease in cell attachment observed when antibodies are introduced to prevent these interactions [25]. Researchers have concluded that differences in integrin expression observed on different materials may account for observed variations in cell attachment [26].

Even though the initial stage of interaction between cells and surfaces is critical, it should be noted that this system is of dynamic nature. Cells might be able to change the nature of their extracellular adhesion by secreting Fn [27-28] or by manipulating the composition of the extracellular matrix. In addition, cells have the ability to adapt to their environment. It has been shown that nonadherent fibroblasts produce less Fn [29]. On the contrary, collagen production is seen to increase on rough surfaces [30]. Cells also adapt by changing the collection and distribution of integrins expressed, and the differentiation

state of the cells based on ligand availability [31-32]. Because of this cell adaptability, caution should be taken in extrapolating *in vitro* findings into *in vivo* situations.

Obviously, there will be differences in the molecular and cellular composition between implant sites and cell culture medium. However, many of the adhesion proteins associated with osteoblasts *in vitro* have shown similar behavior *in vivo*. Both vitronectin and Fn are found in bone extracellular matrix, along with various other proteins containing the integrin-binding arginine-glycine-aspartic acid (RGD) amino acid sequence, although each protein is present in distinct regions of bone [25].

Prediction of the osteoblast-implant interface *in vivo* are further complicated by the progressive changes in composition as proteins are exchanged, as fibrin clot forms and is remodeled, and cells secrete extracellular matrix. Depending on the stage of tissue repair, a different suite of adhesion proteins will be available. The affinities of various osteoblasts or related cells for these proteins are equivalent, in adhesive potency, to that shown for many of the RGD-containing proteins found in bone [25]. Laminin-1 was found to preferentially bind the preosteoblastic cells from a primary bone-derived culture [33]. Studies have been shown that various adhesion proteins promote different osteoblast responses, with fibrinogen in particular exhibiting the least adhesion affinity [29, 34-35]. Fn, collagen-I and thrombospondin also function employing cell binding motifs other than the RGD-integrin binding mechanism [25].

Cell attachment is a process related to adhesion and usually involves similar extracellular proteins. Proteins such as Fn and vitronectin are required for the formation of focal contacts and essential intracellular structures [21]. Researchers estimate that a ligand spacing of 141 nm or less was needed for these structures to form, although response to ligand density could be altered by surface topography [36]. The distribution of ligands on the substratum and the availability of the appropriate binding sites are thus important in cell adhesion, spreading and subsequent functions.

Cell mobility and migration also depend on the nature of adhesion to the substratum. Adhesive protein ligands are required and may provide a haptotactic signal [37-38], while a peak in migration rates has been observed at intermediate ligand concentrations on the surface. The ligand density is reduced with increasing strength of cell binding [38]. However, cell migration rate and binding strength always show opposite trends [39]. It is apparent that maximal cell motility requires adhesion strength sufficient to maintain substratum contact, but not to the extent that release of contact is inhibited.

2.2 Cell proliferation and differentiation

It is well established that cell adhesion, spreading and morphology influence subsequent cellular responses such as proliferation and differentiation. Early on Folkman and Moscona [14] verified that composition of tissue culture plastic polystyrene can affect cell shape, and corresponding cell growth. These effects have been utilized to design engineered patterns to regulate cell shape [40-43].

With respect to osteoblasts and adsorbed proteins, Fn appears to be very important as the cell differentiates [44-45]. Because it is known that osteoblasts secrete their own Fn, Fn coated culture environment might be a benign environment for osteoblasts. Although adhesion might be clearly essential in osteoblast development, excessive adhesion strength may actually inhibit subsequent cell activities, such as cell motility. Qiu[46] et al showed increased marrow stromal cell attachment on positively charged surfaces, but these cells also showed reduced spreading and differentiation. This stressed the importance of these facts that adhesion alone is not an adequate indicator of biocompatibility when a specific function is required.

Implant surface in combination with present growth factors and other signaling molecules might synergistically influence proliferation and/or differentiation together. Adsorbed proteins might provide binding sites for other molecules, mimicking the structure of the extracellular matrix in vivo. For example, insulin-like growth factor II (IGF-II) is stored in bone as a complex with IGF-binding protein 5 (IGFBP-5), which in turn binds to bone matrix hydroxyapatite [47]. Such a co-localization strategy might provide further benefits where signal transduction results from cooperation between receptors [48-49].

2.3 The interaction of proteins with solid surfaces: protein adsorption and interface composition

The interaction of proteins with solid surfaces is not only a fundamental phenomenon but is also key to several important and novel applications. New biotechnological methods of

protein production depend on protein interfacial properties in downstream protein purification and separation. In addition, the adsorption of proteins at solid/liquid interfaces has enabled the development of diverse biomedical applications, such as biosensors, immunological tests and drug delivery applications [50].

In the biomaterials field, protein adsorption is the first step in the integration of an implanted device or material with tissue. After administration, proteins become absorbed immediately onto the surface of the biomaterial, thus determining its fate, e.g., complement activation, platelet activation, coagulation activities, adherence of cells and bacteria. For example, the adsorption of serum proteins, such as fibrinogen, Fn or vitronectin, can influence the adhesion of leukocytes, macrophages or platelets, and ultimately lead to fibrous encapsulation [12].

In the field of protein formulation for protein therapeutics, or as development of novel controlled release systems, the fine balance between the folded and unfolded states of proteins can be greatly affected by the surrounding physical conditions, such as temperature, solvent composition, or level of hydration; consequently, many recent studies have focused their attention on means of increasing the stability of the protein structure [51]. One of the most common stabilization procedures consists of preparing protein formulations in the solid state by freeze or spray drying. However, these methods, although rendering reasonably stable products, can have deleterious effects on the protein structure and subsequently on the long-term stability and recovery of protein activity

upon rehydration. One route of enhancing the stability of dried protein formulations is the addition of excipients to protein solutions prior to drying [52]. This has been shown to inhibit drying-induced damage, improve the activity of proteins upon rehydration and enhance the stability of biological systems during storage. Various hypotheses have emerged to explain the modes of action of these excipients on protein stability.

A detailed mechanistic understanding of the protein-surface would be of value to these fields, and the ability to tailor specific protein-surface interactions would benefit protein-surface technologies. Fundamentally, the interaction of proteins and surfaces involves both protein binding and unfolding; therefore investigations of this kind may increase our knowledge of protein biophysics.

Because of the great relevance of the protein-surface interaction phenomenon, much effort has gone into the development of protein adsorption experiments and models. The ultimate goal of such studies would be to measure, predict and understand the protein conformation, surface coverage, superstructure and kinetic details of the protein-surface interaction. In addition, bio-protection rendered by excipients (sugars) also elicits various theoretical explanations. One being that the formation of glassy matrices restricts molecular motion thus reducing degradation. Others explained the stabilization of excipients on proteins by providing hydrogen bonds between proteins and disaccharides, replacing essential protein-bound water molecules to maintain the secondary protein structure.

Proteins are often thought to denature at both solid-liquid and vapor-liquid interfaces, although they retain more structure on electro statically neutral hydrophilic surfaces than on hydrophobic or charged surfaces. Kinetic measurements of absorbed protein as a function of time and equilibrium adsorption isotherms have been measured using a variety of informative techniques, such as optical waveguide light mode spectroscopy (OWLS) [53], ellipsometry and total internal reflectance fluorescence (TIRF) [54]. Studies have identified systematic effects of salt concentration, protein charge or dipole moment, and surface charge or hydrophobicity. Kinetic effects are often complex, in that long-term behavior can differ from short-term behavior, and the final surface coverage can vary based on the rate at which protein was introduced into the system. Behavior is highly dependent on the individual nature of the protein and the surface involved. These complexities are often interpreted as arising from underlying structural phenomena.

Current technology doesn't allow direct observation of atomic-scale morphology yet, but progress has been made toward determining protein structure on a surface and useful structural information can be inferred. Because most protein-interaction samples are heterogeneously presented in a monolayer on a surface, the traditional biophysical methods for determining protein structure in solution, such as CD, IR spectroscopy, NMR and crystallography, are somewhat limited. However, attenuated total reflection Fourier transform IR (ATR-FTIR) spectroscopy has been used to track the loss of secondary structure during insulin unfolding on a model lipid-water interface [55].

Giamelli and Norde have used CD together with probes of thermal stability to measure changes in the secondary structure of BSA before and after thermal denaturation [56]. Long et al. used solid-state NMR techniques to determine the structure of the terminal helix of statherin on hydroxyapatite [57]. This first high-resolution structural and dynamic characterization of a hydrated biomineralization protein adsorbed to its substrate is based on accurate measurements of distances between backbone carbonyl carbons and backbone nitrogen.

Biochemical techniques have enabled investigators to infer much knowledge about the morphology of proteins on surfaces. Mutagenesis experiments, radioisotope labeling, antibody or epitope binding surfactant elutability and catalytic activity have all been used to infer knowledge about the changing state of the protein on the surface [58]. Nanoscale imaging techniques have also been utilized. Atomic force microscopy (AFM) has been employed to study lysozyme [59] and insulin[60] at surfaces, including the observation of surface denaturation. Scanning force techniques have been explored to study lysozyme and albumin topology and adhesion force [59], and scanning tunneling microscopy (STM) has also been used with lysozyme [61].

To provide information about particular regions of the protein, several methods have been employed. Hydrogen-exchange mass spectroscopy has been used to identify regions of lysozyme and α -lactalbumin that are accessible to solvent during chromatography under a range of solution conditions [62]. Time-of Flight secondary ion mass spectroscopy (ToF-

SIMS) has been used to investigate the orientation of the protein or its state of unfolding on the surfaces. In this technique, an adsorbed protein layer is bombarded with ions, breaking off short segments (as much as several peptides) from the upper nanometer of the adsorbed layer; these bombarded segments are then analyzed by mass spectroscopy. Simultaneous contributions from multiple types of proteins at the surface can be distinguished. In theory, this technique can be applied in general to most typical proteins at different interfaces to provide structural information.

In summary protein-surface interactions are highly dependent on the individual properties of the system. Many methods have being developed to observe structure and significant information is already available to begin to decode the complex phenomenon.

2.3.1 Principles of protein adsorption

Protein easily accumulates at interfaces [63]. Protein is an amphoteric polyelectrolyte [64]. For some proteins, the tendency to adsorb is due to the nature of side chains present on the surface of the protein. Its amino acids have different characteristics: some are apolar and like to be buried inside the protein globule, whereas others are polar and charged and are often found on the outside protein surface. Upon biomaterial implantation, absorbed proteins affect blood coagulation, complement activation, bacterial and cell adhesion as well as biomaterial surface properties and degradation. Many theories have been proposed on blood-compatible polymers that showed

interactions of blood with surfaces leading to thrombus formation were governed by many chemical, physical and biological parameters.

Soon after elucidating the unique secondary, tertiary and quaternary structures of proteins, the potential to determine conformational changes in protein structure at liquid/solid interface was realized. The surface of protein is often complex in nature, with different characteristics such as hydrophilicity and charge. Protein adsorption is complex and includes the diffusion of the protein particles through the aqueous solution and the collision and interaction of the protein at the interface. Regardless of the biomaterial and biological environment, the adsorption principles are similar. Proteins can interact with the solid surface in a variety of different ways, depending on the particular orientation by which it approaches and the overall binding energy [65]. Thermodynamically, the adsorption process can only occur if the Gibbs free energy of the system decreases:

$$\Delta_{ads}G = \Delta_{ads}H - T \Delta_{ads}S < 0$$

Where H, S and T refer to enthalpy, entropy and absolute temperature respectively and Δ_{ads} indicates thermodynamic changes of functions of state resulting from the adsorption process. Enthalpy (heat of reaction) refers to the making and breaking of chemical bonds; making bonds is energetically favorable ($\Delta_{ads}H < 0$), and entropy refers to the free energy gain ($\Delta_{ads}S > 0$) when going from order to disorder. Norde and Lyklema [66] considered various types of contributions to the total Gibbs energy of the adsorption process, Δ_{ads}

and concluded that the affinity between a protein and a sorbent surface increases by increasing hydrophobicity of the sorbent surface and the protein exterior. They demonstrated that opposite values of electrokinetic potentials of the sorbent and protein leads to higher adsorption. Several authors discussed and modeled the protein adsorption kinetics at solid-liquid interfaces [67-68]. Most of these models assume that proteins undergo time-dependent conformational changes due to adsorption onto a surface. However, Andrade and Haldy[69-70] defined a more general kinetic model. They suggested that any protein desorbed in a denatured state rapidly denatures in solution. Studies on kinetic and thermodynamic controls of protein adsorption have shown that some polymers and natural lipids can be used as surface modifiers to reduce protein adsorption. Although many attempts have been made to prevent protein adsorption, the amount of adsorbed proteins remains significant.

Interactions between entrapped proteins and polyester materials are often responsible for protein aggregation and subsequently slower and incomplete release in vitro. These interactions are often hydrophobic in nature, but ionic interactions might also contribute to protein adsorption onto the polymer [71-73].

Clocked (capped) or free carboxyl end groups have influence on protein release. Proteins formulated at neutral pH (lower than their pI) are often positively charged and thus might interact with negatively charged PLGA containing free carboxyl end groups [74-75]. The

interaction depends on the content of free carboxyl end groups: the more numerous, the stronger the interaction.

Electrostatic interactions generally increase encapsulation efficiency [76] and for some proteins, non-specific adsorption onto the polymer surface might represent a useful delivery system instead of loading inside the particle core [73]. This was ascribed to the probable higher rate of solidification of the microspheres resulting from higher PLGA concentrations [77].

There is reversible and irreversible interactions of protein with biodegradable matrix. The interface between water and a solvent is a well-known destabilizing factor [78]. Typically, proteins become prone to aggregation from the moment they migrate and adsorb at the interface. They undergo unfolding by exposing their hydrophobic regions, which are usually buried in the molecular structure, to the organic solvents. It has been shown that protein in pure organic solvent displays less conformational flexibility than in aqueous/organic mixtures leading to a more preserved secondary structure and impaired denaturation.

Crystalline proteins are usually less prone to chemical degradation than the amorphous form and X-ray can aid in the investigation of crystal structure of PLGA microparticles[79].

Protein concentration is of importance since unmodified proteins exhibit a “self-protecting” behavior, when used at high concentrations in emulsion-based techniques of encapsulation. This interesting effect is probably due to the proportional distribution of the protein between the water phase and the water/organic interface, regardless of the initial amount of protein added in the water phase. Once a fraction of protein has adsorbed onto the interface, it aggregates and shields the nonadsorbed protein fraction that is thereby prevented from aggregation [80-81].

Preferential hydration: A protein in an aqueous environment is in equilibrium between the native and the denatured states. The protein is preferentially hydrated and folds back to its native state. Strategies to counteract protein degradation related to interfacial phenomena include protocols to avoid partial or total use of water. One way is to have the protein suspended in organic solvents. Protein can be solubilized in organic solvents by first precipitating the protein at its isoelectric point (PI) [74]. Then, lyophilize the protein at a pH away from its pI before formulating it. This could increase protein solubility and stability in various polar and water-miscible organic solvents like DMSO [73, 75-76]. Ion-pairing can be anchored by adding an oppositely charged surfactant that binds to the protein, so as to obtain a neutral hydrophobic entity and to reduce direct contact between the protein and the organic solvent [77, 82]. An aggregated protein can then be encapsulated in a reversibly dissociable form, in order to avoid the formation of

irreversible aggregates during processing and to promote the sustained release of the native monomeric form [83].

2.3.1.1 Protein adsorption isotherm

The adsorption isotherm is a function that relates the measured adsorbed amount of a protein (per unit area), Γ_p , to the solution concentration of protein, c_p . Typically, Γ_p increases sharply at low solution concentrations of protein and levels off at higher protein concentrations approaching a limiting Γ_p value. The existence of a Γ_p adsorption “plateau” has been interpreted as a sign that the adsorbing surface is “saturated” with protein molecules; any further increase in the solution protein concentration typically does not affect Γ_p . The amount of adsorbed protein at the “plateau” of the adsorption isotherm is often close to the amount that can fit into a closed-packed monolayer; hence, the notion of a saturating monolayer coverage is often applied to protein adsorption.

Under ideal conditions, the shape of the adsorption isotherm can provide information about the affinity between protein and surface. The evaluation of the affinity, however, does require a model for the protein–surface interactions; a model from which the adsorption isotherm function, $\Gamma_p(c_p)$, can be derived and compared with the experimental results. Most experimentally measured protein adsorption isotherms may not be the true equilibrium isotherms [84], [69] It may take a relatively long time for a protein adsorbing to a surface to reach true equilibrium. Other processes, such as protein conformational

change, may run concurrently with the adsorption process and affect the adsorbed amount. Hence, the information contained in the adsorption isotherm may not refer to identical molecules. The existence of several protein conformers in solution, each with slightly different adsorptivity, may result in an isotherm that will reflect the competition between conformers for a limited adsorption surface area.

2.3.2 Factors affecting protein-surface interaction:

Material surface properties influence how proteins approach and arrange on the interface. Reviews by Norde [66, 85] have provided a comprehensive description of such interactions.

There are two main contributors to influencing protein-surface interactions. Firstly protein properties impact protein-surface interaction as described below.

Size: proteins that are larger in size contain more contact sites with surfaces. For example, albumin with 67 KDa in molecular weight has 77 contacts with silica; whereas fibrinogen with 340kDa has 703 contacts per molecule. Thus fibrinogen has higher affinity for silica surfaces.

Charge: Protein is more reactive when it is at its isoelectric point. Charged amino acids tend to be on the outside of the molecule. Consequently more features than just many adsorption sites on the surface and reduced isoelectric repulsions allow more absorption-also charged amino acids may change protein structure/conformation.

Structure and folding: unfolding of protein will increase the number of contact points. Thus proteins with low intramolecular bonding are likely to unfold more and faster than crosslinked proteins. In addition, unfolding will enable exposure of new portions (hydrophobic) of protein to surfaces.

Several other aspects of biomaterials properties indicated below might participate in contributing to protein-surface interactions.

Surface roughness: One of the predominant research topics in tissue engineering is that of scaffold architecture, particularly with respect to optimizing cell colonization. In orthopedic applications, surface roughness seems to increase osteointegration [86]. Various studies revealed few consistent trends in the effects of surface topography on initial cell adhesion. Interpretation and comparison of results is frequently complicated by differences and inadequacies in characterizing the morphology, as well as magnitude of surface topography [87]. Furthermore, methods used to produce surface textures, for example, sand blasting, grinding, and plasma-spraying may variously alter surface chemistry or physicochemical properties. The type of cells used also influences these studies. Surface topography is frequently seen to have a significant effect on both proliferation and differentiation of osteoblastic cells. The most commonly observed trends are that as the roughness gets greater, there was less cell proliferation [88]. Although responses to differences in surface chemistry and wettability may be attributed substantially to the composition and bioactivity of the adsorbed protein layer, its

involvement in directing reactions to surface topography is less clear. There is some evidence, although relatively scarce, that proteins adsorb differentially with variations in surface roughness. Although it is difficult to evaluate from the selection of images presented, perhaps the most compelling evidence comes from Schneider et al [86] that serum Fn deposition was induced on grooved surfaces. Some researchers have found that greater texture increases absolute surface areas, thus increasing chances for protein-surface interactions [89]. The increase in Fn adsorption on Ti-6Al-4V was accompanied by increases in bone marrow cell attachment and over a prolonged time frame, proliferation [90]. Apart from increasing the surface area, topographic features also create confined spaces. It has been speculated that these may interfere with wetting of the surfaces [91], leading to a localized dilution of the coating solution. Studies showed variations in protein species adsorbed from serum depending on gap width and serum dilution. The differences were explained by limited displacement of abundant proteins by those with high affinities. Given that protein exchange limitations were apparent with lens-surface clearances of up to tens of microns, it is not unreasonable to expect that similar effects might be significant in protein adsorption to surface micro topography [92].

Chemistry: One of the most studied elements of protein adsorption is its variation with surface wettability (hydrophilia or hydrophobia). Because water is a polar solvent, it does not readily interact with nonpolar solutes and surfaces. Hence, contact between water and

these hydrophobic surfaces increases self-association by hydrogen bonding within the neighboring water molecules [92]. This increase in order creates an entropic penalty. The various interaction of basic, polar, acidic and nonpolar amino acid side chains with water and each other create the folded structure of a protein with hydrophobic residues preferentially located towards water excluding core of the protein. For a protein to adsorb, both adsorbate and surface must at least partially dehydrate. This is thermodynamically favorable for similarly hydrophobic sorbents and adsorbates, as it increases the water entropy [85]. Conversely, displacement of water molecules from hydrophilic surfaces presents a substantial energy barrier to protein adsorption [70]. Experiments have shown significantly less protein adsorption on surfaces with tightly bound water [93]. However, evidence does show that adsorption occurs on hydrophilic materials, where charge interaction and protein conformation provide the necessary driving force.

In addition, functional species will alter interactions between protein and surfaces. For example, Oxides, Metals, Carboxyl, Aromatic, Carbonyl groups have different affinity for different biomolecules. Spatial variation of material surfaces will contribute differently to the interactions, such as alloy phases, grain boundaries, polymer crystallinity and segregations.

Electrical potential: The charge on a surface is minimized at its isoelectric point: a pH below this creates a positive charge and vice versa. The presence of ions such as Na^+ , K^+ ,

Ca^{2+} and Cl^- results in the formation of an electrical double layer at charged surfaces, the composition of which is determined by the opposing influences of charge negation and osmolar pressure [69]. Although microscopic and molecular change might occur in protein/surfaces system, the dominant driving force in protein adsorption interactions appear to be electrostatic forces [94]. When the process is opposed by like[95] charges at physiological pH, maximum adsorption generally occurs at the isoelectric point of the protein-surface system. Coadsorption of counter ions may contribute to this process and the presence of such ions is implied by adsorption of proteins to like-charged surfaces [85].

Protein conformation change: While dehydration effects are significant, structural changes within the adsorbed protein molecule can also increase the entropy of the system. A loss of the secondary structure increases the bond mobility and thus entropy, within the molecule. Structural rearrangement also permits increasing contact between the protein and surface. Such changes result in strengthening of protein attachment with residence time [96]. In addition, the flexibility and stability of a protein's conformation contribute to its adsorption kinetics. Highly hydrated, flexible molecules are able to rapidly form many noncovalent bonds with a surface, whereas adsorption of more compact/stable proteins depends on surface-surface interactions-either hydrophobic or electrostatic. Conformational change is the main driving force for adsorption of proteins to otherwise prohibitive surfaces: hydrophilic and or carrying a like charge. Studies using various

proteins and surfaces suggest some structural changes occur in most protein adsorption [56]. These studies show that adsorbed proteins are not fully denatured (unfolded) on adsorption: adsorbed proteins contain considerable ordered secondary structure and are internally more stable compared to their dissolved form. The ability of a protein to regain its native structure on desorption depends on the surface hydrophobicity and the protein's internal stabilizing forces. For example, bovine serum albumin, which is a flexible protein, adopted a different conformation while adsorbed to hydrophilic silica, but returned to its native structure once desorbed; the hen's egg lysozyme (a hard protein) regained its native structure even when desorbed from hydrophobic polytetrafluoroethylene [56].

The re-arrangement of protein structure progresses at variable rates, resulting in a heterogeneous distribution of conformations among the adsorbed proteins. These distinct populations of proteins thus have different ability to desorb and/or rate of exchange with similar molecules in solution. The composition of the proteinaceous layer on the surface thus will depend on competing protein adsorption, spreading along with desorption.

Protein-surface interaction presents opportunities and challenges for implantation success and much research has been directed at understanding and controlling protein/surface interactions. Despite extensive study and superb descriptions on the colloidal scale, basic questions concerning the structural details of a protein in its adsorbed state are still difficult to answer. Some of these questions include: does the protein denature; is the

protein still active; if the protein has not unfolded, what is its orientation; what conformation does the protein assume; what is the effect of crowding on the surface by other proteins; what are good strategies for controlling protein adsorption to create a biocompatible surface? The more understanding we obtain about protein-surface interaction, the more new ideas and strategies we have for controlling and directing new structures and material, and developing applications in biomaterials, biotechnology and protein therapeutic formulations.

2.3.3 Protein mediation of cell responses to surface characteristics

The fields of tissue engineering and biopharmaceutics provide a number of complex opportunities for the design of new implantable scaffolds for protein delivery [97]. For example, bone regeneration under clinical circumstance requires a morphogenetic signal, a respondent cell population capable of assuming an osteogenic phenotype and a matrix to deliver the signal and act as a scaffold for cell recruitment, attachment, proliferation and differentiation [98]. Various growth and differentiation factor (GDF) delivery strategies are undergoing evaluation for clinical use. GDFs act locally and therefore must be delivered directly to the site of regeneration via a carrier matrix. For applications that require the creation of large volumes of bone, an optimal carrier would be both a controlled release system and a scaffold. In the former role, the carrier must prevent rapid factor clearance and ideally meter out the factor in a predictable manner allowing therapeutic doses of the protein to stimulate target cells for the appropriate duration. In

the latter role, the material should act as a permissive environment into which bone cells would be enticed to migrate and begin the process of depositing bone matrix in the carrier template. In addition to osteoprogenitor cells, endothelial cells must be able to migrate into or near the matrix and form vascular beds to nourish the newly formed tissue.

Local delivery of GDF through a scaffold offers several advantages, because 1) it provides GDFs at desirable concentration within their therapeutic window at the site where they are needed without eliciting potential toxicity associated with systemic delivery; 2) Carrier matrices also delay the otherwise rapid dispersion of the water-soluble, readily diffusible GDFs from the implant site without which, they, like other protein therapeutics, would likely have a short serum half life because of liver uptake and catabolism; and 3) the scaffold is a 3-D matrix suitable for permitting tissue ingrowth and regeneration.

Various materials, including inorganic materials [99-100], synthetic polymers [101-103], natural materials [104-105], and its combination [106] have been tested as promising GDF carriers. However, reproducible sourcing and processing, the possibility of contamination with adventitious agents, and the potential for immunogenicity associated with natural materials has moved the field in the direction of synthetic materials. Commonly used synthetic materials include calcium phosphates (such as hydroxyapatite, tricalcium phosphate and cements), and synthetic polymers such as the poly α -hydroxyl acids (e.g. polylactide, polyglycolide and their copolymers). Many of these materials lack

optimal biological properties, thus composite of them are also used. Many of the delivery systems designed for GDFs and other bone inducing factors were used as carriers for GDF as well as scaffolds for bone formation. The appropriate choice of the delivery system for a particular growth factor is essential to induce a specific biological effect, as demonstrated by several examples in the literature, where failure of bone repair was associated with the type of delivery device. For example, locally administered solutions of bFGF did not promote bone regeneration in rabbit skull defects in contrast to bFGF incorporated in gelatin hydrogels [107]. Failure of BMP in an insoluble bone matrix to induce bone growth around titanium implants was attributed to unsuitable carrier properties [108]. Finally, locally applied IGF-1 failed to induce bone repair when delivered by an osmotic pump directly into the osteotomy [109-110], but was successful when embedded in biodegradable microspheres to heal segmental long bone defects [111]. But there are few reports concerning the effect of the controlled release of GDFs from a carrier on bone formation in surrounding tissue, nor are there reports concerning the 3D structural conformation of the GDF, which usually translates into protein stability and bioactivity, after being incorporated into the scaffold.

2.4 Proteins of interest

2.4.1 rhGDF-5

rhGDF-5 is a human analogue of growth and differentiation factor-5 (GDF-5) which is a homodimer of two 119-amino acid residue monomers [112]. rhGDF-5 is a disulphide

cross linked homo-dimer with each monomer having seven (7) cysteine residues, which is common for other growth factors from the transforming growth factor beta (TGF- β) super family. These seven cysteine residue in each monomer form three intra molecular (monomer) disulfide bonds and one intermolecular disulfide bond (Figure 2-1). The multiple cysteines residues, especially those that are located on the surface of the molecules, created multiple opportunities for the occurrence of disulphide exchange.

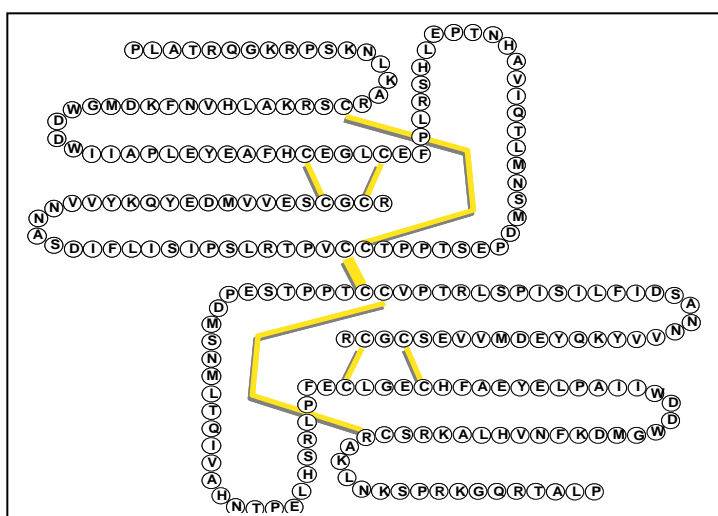


Fig. 2- 1 Growth and Differentiation Factor 5, chemical name rhGDF-5: sequence and molecular

The molecular weight of the protein is around 27 kDalton. Aqueous solubility is pH dependent. The protein forms precipitates above pH 4.5 and below 10 at concentration above 1-2 $\mu\text{g/mL}$. The isoelectric point is approximately 7.65.

The most noticeable attribute of this protein is its low aqueous solubility at physiologically relevant pH. The propensity for aggregation proves to be the major challenge for stabilizing the protein for controlled release purposes. In solvents with lower ionic concentration (strength), e.g., 10 –20 mM, protein solubility is 100 – 200 µg/mL when the pH value is below 5.2 and above 9.5. These attributes make rhGDF-5 prone to forming aggregates under stress on reconstitution. These stressful processes include lyophilization (cooling and drying stress) and the rehydration stress itself.

The protein-incorporated scaffold used to deliver GDF can serve a number of functions. In general, the scaffold physically delivers GDF locally and helps retain therapeutic concentration of the factor for sufficient length of time to stimulate an optimal healing response. rhGDF-5 has been incorporated in a collagen calcium phosphate matrix and evaluated in an animal model of spine fusion [82-83, 113]. Due to known reproducible sourcing and processing, the possibility of contamination with adventitious agents and potential for immunogenicity associated with natural polymers such as collagen, development of improved delivery matrices focused on the use of synthetic materials that provide the critical biological characteristics of natural extracellular environment that allows cells to migrate, divide and differentiate; such a device could expand the clinical applicability of GDFs.

2.4.2 Fibronectin (Fn)

Fn is a high-molecular-weight glycoprotein containing about 5% carbohydrate that binds to receptor proteins that span the cell's membrane, called integrins [114]. In addition to integrins, they also bind extracellular matrix components such as collagen, fibrin and heparin. Fn sometimes serves as a general cell adhesion molecule by anchoring cells to collagen or proteoglycan substrates. Fn also can serve to organize cellular interaction with the ECM by binding to different components of the extracellular matrix and to membrane-bound FN receptors on cell surfaces. The importance of Fn in cell migration events during embryogenesis has been documented in several contexts, e.g.: 1) mesodermal cell migration during gastrulation can be blocked by injection of Arg-Gly-Asp (RGD) tripeptides that block cellular Fn receptors (integrins); 2) injection of anti-Fn antibodies into chick embryos blocks migration of precardiac cells to the embryonic midline, and; 3) the patterns of Fn deposition in developing vertebrate limbs determines the patterns of precartilaginous cell adhesion to the ECM, thereby specifying limb-specific patterns of chondrogenesis.

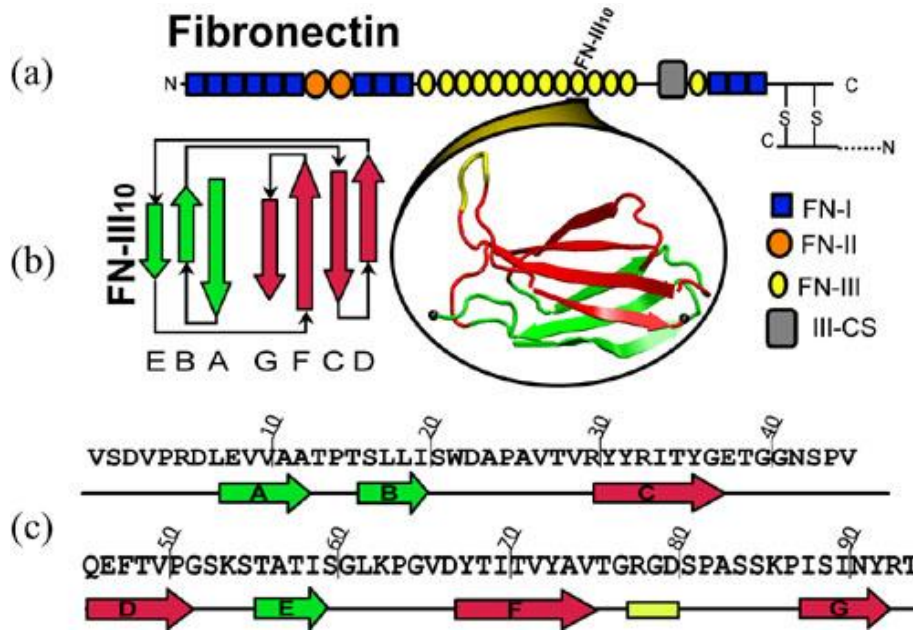


Fig. 2- 2 Schematic structure plot of Fn

Structurally, Fn is a 450 kDa dimer composed of homologous, repeating structural motifs (classified as Fn repeats Fn-I, Fn-II, and Fn-III) that are grouped together into functional domains[115]. Figure 1 shows the diagram of a Fn monomer, and the structure and sequence of the 10th type III Fn module, Fn-III-10. The Fn-III modules possess a beta-sandwich structure consisting of seven beta-strands (A-G) that are arranged in two anti-parallel sheets ABE and FGCD 1. (Figure 2-2.)

2.5 Surfaces of interests

Biodegradable polyester polymers found their applications for a variety of medical devices due to the fact that they can be used as an implant and will not require a second

surgical intervention for removal. For example, a fractured bone that has been fixated with a rigid, nonbiodegradable stainless implant has a tendency for re-fracture upon removal of the implant. Because the stress is borne by the rigid stainless steel, the bone has not been able to carry sufficient load during the healing process. However, an implant prepared from biodegradable polymer can be engineered to degrade at a rate that will slowly transfer load to the healing bone. Another exciting use for which biodegradable polymers offer tremendous potential is as the basis for drug delivery, either as a drug delivery system alone or in conjunction to functioning as a medical device [116].

Polymer	Melting Point (°C)	Glass-Transition Temp (°C)	Modulus (Gpa) _a	Degradation Time (months) _b
PGA	225—230	35—40	7.0	6 to 12
LPLA	173—178	60—65	2.7	>24
DLPLA	Amorphous	55—60	1.9	12 to 16
PCL	58—63	(—65)—(—60)	0.4	>24
PDO	N/A	(—10)—0	1.5	6 to 12
PGA-TMC	N/A	N/A	2.4	6 to 12
85:15 DLPLG	Amorphous	50—55	2.0	5 to 6

75/25 DLPLG	Amorphous	50—55	2.0	4 to 5
65/35 DLPLG	Amorphous	45—50	2.0	3 to 4
50/50 DLPLG	Amorphous	45—50	2.0	1 to 2
^a Tensile or flexural modulus.				
^b Time to complete mass loss. Rate also depends on part geometry.				

Table 2- 1. Properties of common biodegradable polymers.

(Obtained with permission from www.devicelink.com)

The general criteria for selecting a polymer for use as a biomaterial is to match the mechanical properties and the time of degradation to the needs of the application (see Table I). The ideal polymer for a particular application would be configured so that it:

- Has mechanical properties that match the application, remaining sufficiently strong until the surrounding tissue has healed.
- Does not invoke an inflammatory or toxic response.
- Is metabolized in the body after fulfilling its purpose, leaving no trace.
- Is easily processable into the final product form.

- Demonstrates acceptable shelf life.
- Is easily sterilized.
- Promotes or permits normal tissue repair or regeneration.

This study will explore the relationship of how the physicochemical properties of synthetic biodegradable polymers, i.e. PCL-PGA, affect adsorption of proteins, such as rhGDF-5 and Fn. Further, this study will examine the effect of polymer properties on the subsequent cellular responses as well as osteogenic gene expression. Surfaces were prepared by compression molding and they were thoroughly characterized: morphology by scanning electron microscopy (SEM), hydrophobicity by contact angles measurement, nanotopography by atomic force microscopy (AFM) and crystallinity by differential scanning calorimetry (DSC). Cellular responses were analyzed by osteoblast attachment and proliferation assays, followed by examination of osteogenic gene expression on these substrates. rhGDF-5 and Fn are used as model proteins to be absorbed onto PCL-PGA film substrates from single protein solutions. Bioactive protein adsorption on these substrates is investigated in terms of the absolute amount of protein adsorbed and the nanotopography of protein adsorbed material surfaces.

3 SPECIFIC AIMS

Poly(caprolactone-*co*-glycolide) (PCL-PGA) is a class of biodegradable polymers used for various tissue engineering applications. Previous research suggests that polymer crystallinity impacts biocompatibility. However, there have been no systematic studies to evaluate the role of crystallinity of PCL-PGA polymers in cellular responses and protein adsorption. The present investigation utilizes PCL-PGA polymers as substrate materials to study 1) cellular responses and 2) protein adsorption on these surfaces. The overall objectives of the proposed research are to evaluate the effect of PCL-PGA crystallinity on osteoblast cell attachment and osteogenic gene expression; and to determine how the physical properties of a bioactive protein are impacted upon adsorption to PCL-PGA polymeric surfaces. The specific aims of this dissertation are:

To assess the impact of the physicochemical properties of PCL-PGA polymeric films on osteoblast attachment, proliferation and osteogenic gene expression.

Hypothesis: PCL-PGA film *crystallinity* influences osteoblast attachment, proliferation and osteogenic gene expressions.

To evaluate the effect of surface differences in PCL-PGA films on protein adsorption, thus identifying critical relationships between PCL-PGA polymeric materials properties, protein properties and protein adsorption.

Hypothesis 1: PCL-PGA film *crystallinity* influences the surface adsorption of rhGDF-5.

Hypothesis 2: PCL-PGA surfaces determine adsorption of different Fn fragments with different *Biological Binding Motifs*.

4 POLY (CAPROLACTONE-CO-GLYCOLIDE) SURFACES AND OSTEOGENIC CELLULAR RESPONSES

4.1 Introduction

Recent advances in biology, medicine, and engineering have led to the discovery of new therapeutic agents and novel materials for the repair of large bone defects caused by trauma, congenital defects, or bone tumors. Osteointegration requires a sufficient number of osteoblastic cells as well as their subsequent differentiation and biosynthetic activities. It requires that proteins encountered by the cells support or promote attachment, proliferation and differentiation. For tissue engineering scaffolds, the scaffold surface must support these cellular responses to populate the scaffold.

For these applications, scaffolds hold two functional purposes: 1) serve as scaffold for cellular penetration and proliferation and 2) serve as controlled release platform for both therapeutic and plasma protein desorb from scaffold. These repair strategies often utilize degradable polymeric scaffolds for the controlled localized desorption/delivery of bioactive molecules to stimulate bone ingrowth as the scaffold degrades. Polymer composition, hydrophobicity, crystallinity, and degradability will affect the rate of either plasma or therapeutic protein desorbed from these scaffolds, as well as the rate of tissue ingrowth.

In the development of new materials for tissue engineering, the initial interaction of cells with material substrates is of fundamental importance and contributes to the ultimate

clinical success of implants [117]. The chemical and physical properties of the polymer surface such as chemical composition, topography, surface energy and wettability are important parameters to be considered in the interaction between the material and the biological environment [118-120]. Although previous reports suggest that the crystallinity of polymeric materials influences biocompatibility[43, 121-126], it has been difficult to delineate the effects of crystallinity from other physicochemical properties such as hydrophobicity and nanotopography [125]. Investigating cell-material interactions are further complicated by variation in cell populations and culture conditions [127]. Hence, more defined conclusions about the impact of crystallinity of polymers on cell responses have yet to be achieved.

In order to promote tissue formation, polymeric materials can be processed into a form that can provide the appropriate spatial and temporal cues and signals to enable successful tissue regeneration [2]. Such “scaffolds” must be mechanically stable and their strength and stiffness should ideally approach that of the target tissue that it intends to repair. Scaffolds can be in the form of films or foams that possess micro-porosity, the space into which cells will grow to regenerate tissue. Material properties should be properly characterized and optimized prior to the selection of materials as tissue engineering scaffolds. In biomaterials research, thin films are utilized to study cell growth and differentiation as a function of surface characteristics, such as hydrophobicity, morphology, and topography. Clapper et al studied the melt processed PCL thin films for

tissue engineering purposes [128]. Cheng et al have been successful in using acrylic acid and collagen to modify PCL films to improve attachment of fibroblasts and myoblasts [129].

4.1.1 Polymeric material selection

Synthetic polymers offer greater advantages than natural materials in that they can be tailored to give a wider range of properties and more predictable lot-to-lot uniformity than can materials from natural sources. Synthetic polymers also represent a more reliable source of raw materials, one free from concerns of immunogenicity. One of the exciting current areas for applications of biodegradable polymers is in tissue engineering. Several companies are investigating using these materials as a matrix for living cells. Important properties in this regard include porosity for cell in-growth, a surface that balances hydrophilicity and hydrophobicity for cellular attachment, and mechanical properties that are compatible with those of the tissue, and degradation rate and by-products. The polymer matrix may represent the device itself, or can be a scaffold for cell growth in vitro that is degraded by the growing cells prior to implantation. The device can also be formulated to contain additives or active agents for more rapid tissue growth or compatibility. For example, a bone implant may contain a form of calcium phosphate or a growth factor such as one of the bone morphogenetic proteins.

The factors affecting the mechanical performance of biodegradable polymers are those that are well known to the polymer scientist, and include monomer selection, initiator

selection, process conditions, and the presence of additives [130]. These factors in turn influence the polymer's hydrophilicity, crystallinity, melt and glass-transition temperatures, molecular weight, molecular-weight distribution, end groups, sequence distribution (random versus blocky), and presence of residual monomer or additives.

Poly(ϵ -caprolactone) (PCL). The ring-opening polymerization of ϵ -caprolactone yields a semicrystalline polymer with a melting point of 59 to 64°C and a glass-transition temperature of - 60°C . The polymer has been regarded as tissue compatible. Because the homopolymer has a degradation time on the order of 3 years, copolymers have been synthesized to accelerate the rate of bioabsorption. For example, a block copolymer of ϵ -caprolactone with glycolide, offering reduced stiffness compared with pure PGA, is being sold as a monofilament suture by Ethicon, Inc. (Somerville, NJ), under the trade name Monocryl. The FDA approved PCL has found applications in many medical devices concerned with drug delivery and is actively being considered for applications where slower rates of degradation are desirable, for example, as coating for urethral stents [131].

Copolymeric materials of poly(caprolactone-*co*-glycolide) (PCL/PGA) have been used as tissue engineering scaffold materials. Their applicability as candidate materials for tendon tissue engineering and small diameter vascular tissue grafts has been reported [118, 129, 132-136]. Of the many possible PCL/PGA compositions, PCL/PGA (25:75) has been employed in a commercialized, resorbable suture (Monocryl ®, Ethicon, Inc.) [136]. PCL/PGA materials with copolymeric ratios ranging from 25:75 to 50:50 possess

elasticity, which is favorable for applications such as smooth muscle tissue engineering [132, 135]. Surface modification of PCL/PGA scaffolds using collagen was also explored and tested for fibroblast growth for soft tissue regeneration [129]. PCL-derived polymers have been found in many applications ranging from both hard to soft tissue repair. [134] [132, 135] To date, systematic studies to discern osteoblast and fibroblast behavior as a function of copolymeric material composition have not been undertaken. In particular, the comparison of crystalline polymers such as PCL and PGA as well as their copolymer intermediate compositions, which are more amorphous and elastomeric, has not been reported.

In the present study, a series of polymeric films of PCL/PGA were fabricated using a compression molding approach. Films were produced using PCL, PGA and three intermediate copolymeric compositions (PCL/PGA, 25:75, 35:65 and 45:55). The surface properties of the films were thoroughly characterized with respect to surface hydrophobicity (Contact Angle Measurement), nanotopography (Atomic Force Microscopy), and crystallinity (Differential Scanning Calorimetry (DSC)). In addition, the ability of pre-osteoblasts to adhere and proliferate, as well as to express osteogenic genes on these surfaces was investigated.

This study further investigates how the more-rapidly degrading components, in forming copolymer with ϵ -caprolactone, influence the protein adsorption, and subsequent cellular

responses. Table 2-1 illustrates the basic physicochemical properties of poly(caprolactone-*co*-glycolide (PCL-PGA) polymers.

4.1.2 Cells and osteogenic gene marker selections

Pre-osteoblastic cells (HPEM 1486 from ATCC, Cambridge, MA, USA), were selected in the cell attachment and proliferation studies, as well as the osteogenic gene expression studies due to its wide use in tissue engineering [21, 137-138].

Runx2 is a master regulator that plays an essential role in osteoblast differentiation [139-140]. The expression of genes and proteins required for ECM production, such as collagen type I (col 1), osteocalcin and FAK [141], were selected in the osteogenic gene expression studies to explore the osteogenic potential among PCL-PGA substrates.

4.2 Materials and methods

4.2.1 Materials

Polycaprolactone (PCL) and polyglycolide (PGA) were obtained from Purac Biochem in Gorinchem, Holland. PCL-PGA polymer series (25:75, 35:65, 45:55) films were synthesized by Advanced Technologies and Regenerative Medicine, LLC, *Johnson & Johnson*. Human embryonic palatal mesenchymal pre-osteoblast cells were obtained from ATCC (HEPM 1486 preosteoblast, ATCC, Manassas, VA, USA). 70% Isopropyl alcohol, phosphate buffer saline (PBS) and cell culture grade water were obtained from Sigma (St. Louis, MO, USA). 96 well cell culture plates (96 well Corning Costar 3599)

were from Corning (Corning, NY, USA). The cell culture medium and supplies were obtained from Lonza (Allendale, NJ, USA), such as Eagle's minimum essential medium (EMEM) supplemented with Eagles' salts, L-glutamine (2mM), non-essential amine acids (0.1mM), sodium pyruvate (1mM), 10% fetal bovine serum (FBS), and 25µg/mL penicillin/streptomycin. Cells were counted using Guava flow cytometry counter EasyCyte Plus (Guava Technologies, USA). For gene expression studies, a TaqMan gold RT-PCR Kit (Perkin Elmer, Foster City, CA, USA), Gene markers, such as Osteocalcin, human Collagen I, Runx II and cfba-1, and Glyceraldehyde-3-phosphate dehydrogenase (GAPDH) were obtained by TaqMan Assay-By-Design service (Applied Biosystems, Foster City, CA). Master mix and target probes, high capacity cDNA reverse transcription kit with RNase inhibitor were obtained from Brinkmann Instruments (Westbury, NY). RNA storage solutions were obtained from Applied Biosystems (Scottsdale, AZ, USA). The cell morphology was observed using optical microscopy (Leica DM-LB, magnification 10x; Leica Microsystems Wetzlar GmbH, Wetzlar, Germany). Images were captured and acquired using ProgRes camera and ProgRes Capture Pro software 2.6 respectively (Jenoptik Laser, Optik System GmbH, Jena, Germany). The real-time PCR reactions were performed in 96-well Optical Reaction Plates (PerkinElmer) in an ABI Prism 7700 sequence Detection System (PerkinElmer). The morphological structures of the films were studied by a JSM-5900 LV scanning electron microscope of JEOL, Tokyo, Japan. The static contact angles for PCL-PGA polymeric films were determined using a sessile drop method using a static Knuss drop

shape analysis system (Knuss M 1020, Berlin, Germany). Thermo properties of the films were examined by a DSC analyzer (TA instruments Q200, New Castle, DE, USA). Atomic force microscopy was recorded at ambient temperature by using a multimode nanoscope IV (Digital Instruments, Santa Barbara, CA, USA). The XRD analyses were performed on a Fillips instrument (X'Pert APD, Netherland). The mechanical testing was done by an instron testing machine (Instron corporation, Lincoln, NE, USA)

4.2.2 PCL-PGA polymer surface preparation

Polymeric films were prepared using a melt-compression method. Briefly, a PCL-PGA series of polymers was processed at temperatures above their melting points on a Carver Press (M-11, Toms River, NJ, USA). The process temperature was summarized in Table 4.2. The melt compression was conducted using a Teflon mold to create films of 300 μm in thickness. Circular specimens, approximately 3mm in diameter, were cut with a polymer punch. The specimens were washed in deionized water and then dehydrated by dipping in isopropyl alcohol solution (70%) at room temperature. The alcohol dehydrated polymeric films were then dried in vacuum for 48 h at room temperature. All samples were stored in desiccators until used.

4.2.3 Polymeric surface characterization

4.2.3.1 Scanning electron microscopy (SEM)

The morphological structures of the films were studied by a JSM-5900 LV scanning electron microscope of JEOL, Tokyo, Japan. The dried film samples were mounted on a metal stub and sputtered with gold using a sputter coater (Desk-II, Denton vacuum Inc., Moorstown, NJ) in order to make the sample conductive, and the images were taken at an accelerating voltage of 10 kV and 4500-5000 x magnification.

4.2.3.2 Contact angle measurement (CA)

The static contact angles for PCL-PGA polymeric films were determined using a sessile drop method using a static Knuss drop shape analysis system (Knuss M 1020, Berlin, Germany). For each composition, three disks were used and five measurements were taken for mean and standard deviation calculation. Briefly, ultrapure water from Sigma Aldrich (St Louis, MO) was used to fill a 5 mL syringe. The film was mounted onto a microscope glass using double-sided tape. A 5 μ L drop of water was then placed on the test specimen film. The contact angle of each sample was measured five times, with mean of the readings reported. Wet films were exposed to water at room temperature for an hour, then patted dry on Kimwipes®. Contact angles were also measured on wet films to determine the effect of hydration on these materials.

4.2.3.3 Differential scanning calorimetry (DSC) analysis

Film samples (5 mg) were precisely weighed in aluminum pans and examined in a DSC analyzer (TA instruments Q200, New Castle, DE, USA) calibrated with indium. DSC

thermograms were recorded under nitrogen flow rate of 20 ml per minute and heating rate of 10°C per minute between the temperature range of -20 and 300 °C. Tests were done in triplicate. Films were submerged in 5mL of water for durations of 1h, 4h and 24h at room temperature. Then films were taken out and patted dry on Kimwipes®. These films were considered as “wet” films. DSC was performed on both dry and wet films using first heat cycle to truly reflect their crystallinity. For degree of crystallinity determination, samples were subjected to cooling cycle to -20°C to show the crystallinity exotherm.

4.2.3.4 Atomic force microscopy (AFM)

For AFM analyses, the PCL-PGA surfaces were rinsed first with PBS and then with highly purified water of conductivity not greater than 1 μ S. Then they were stored in a nitrogen oven for 1 h at room temperature, protected from light. The structural feature of the films was not expected to be substantially altered under our experimental conditions. All PCL-PGA surfaces were handled similarly prior to AFM measurements.

The films were examined without modification to reveal surface nanotopography. Phase angle images were recorded at ambient temperature by using a multimode nanoscope IV (Digital Instruments, Santa Barbara, CA, USA) operating in the tapping mode regime, in air, at room temperature. Microfabricated silicon cantilever tips coated with a gold layer for higher laser reflectivity (MPP-11100-10) with a resonance frequency of 299 KHz and a spring constant of 20-80 Nm^{-1} were used. The scan rate varied from 0.5 to 1 Hz. The

set point and gain were adjusted to obtain stable imaging conditions and a minimal noise. The scan size was either 100 nm x 100 nm or 20 nm x 20 nm. To obtain representative images and data, three or more different samples were scanned, each in three or more different surface areas.

Wsxm Image processing version software (beta 3.0) was used to determine diameters and the root mean squares average of height deviation (RMS) values for entire images. Thus only comparative analysis was performed to indicate existing relative differences. Direct comparison of surfaces was performed exclusively for the same scan size images.

Statistical Analyses

Student *T-test* and Microsoft Excel 2000 (Microsoft Corp., Redmond, WA, USA) was used for all statistical analyses. Differences were considered to be significant at $p < 0.05$.

4.2.4 Pre-osteoblast attachment and proliferation on PCL-PGA surfaces

Circular disc samples of 3mm in diameter which fit snugly into 96 well cell culture plates (96 well Corning Costar 3599) were placed into the plate. Films were sterilized by soaking in 70% isopropyl alcohol for 1 hr at room temperature, and rinsed in phosphate buffer saline (PBS) (Sigma Aldrich, St. Louis, MO) prior to cell adhesion studies. Studies were done on six different samples per material.

Human embryonic palatal mesenchymal pre-osteoblast cells (HEPM 1486) were obtained from ATCC (ATCC, Manassas, VA, USA) and used in the cell proliferation assay.

Briefly, HEPM 1486 were maintained and passaged in Eagle's minimum essential medium (EMEM) supplemented with Eagles' salts, L-glutamine (2mM), non-essential amine acids (0.1mM), sodium pyruvate (1mM), 10% fetal bovine serum, and 25µg/mL penicillin/streptomycin. In preparation for assay, cells were obtained for experiment by trypsinization from growing cultures. Cells were counted using Guava flow cytometry counter EasyCyte Plus (Guava Technologies, USA) and were plated out at a density of 3500 cell/cm² in 200 µl of culture medium in each well of a 96 well plate. Cells were allowed to grow for 24 hours at 37°C in a humidified 5% CO₂ atmosphere. After the medium was refreshed, cells were allowed to grow at 37 °C in a humidified 5% CO₂ atmosphere for 3-5 days. On the day of assay, cell proliferation was assessed using "CellTiter 96 Aqueous One Solution" from Promega Corporation (Madison, WI, USA) according to the manufacturer's instructions. The CellTiter 96[®] AQueous One Solution Cell Proliferation Assay is a colorimetric method for determining the number of viable cells in proliferation. The quantity of formazan product as measured by the amount of 490nm absorbance is directly proportional to the number of living cells in culture.

Briefly, in the 96 well plate with the cultured cell samples, 20 µl reagent containing color metric agents was pipetted into each well containing the 100 µl conditioned culture medium. The mixture was incubated for 4 hours at 37°C in a humidified, 5% CO₂ atmosphere. The absorbance of each sample, corresponding to cell number, was measured at 490nm using a 96-well plate reader. In each assay, a cell number standard

curve was generated as follows. From a stock of cell suspension with known cell concentration, aliquots of cells were plated out in quadruplicates at 0, 2500, 5000, 7500, 10000, 15000, 20000 cells per well. Cells were incubated at 37°C in a humidified, 5% CO₂ atmosphere. for 1-2 hours to allow for adherence to the bottom of each well. Quantification of cell number was done the same way as described above. The absorbance of each well was plotted against the corresponding seeded cell concentrations to give a standard curve of cell number and the cell number in each sample was obtained.

Osteoblast growth morphology was observed using a standard optical microscope (Leica Microsystems Wetzlar GmbH, Wetzlar, Germany).

4.2.5 Osteogenic gene expression

Preosteoblastic cell's (HEPM 1486, ATCC, Manassas, VA, USA) morphology, growth rate and phenotypic gene expression on these polymer matrices was studied. The osteoblastic expression of key phenotypic markers [142] such as osteocalcin, Runt Related gene 2 (Runx II) and collagen 1, at 3h, 24h, 1 week was examined .

Real-Time RT PCR

Cells cultured for 4h, 24h, 72h and 1 week were washed, and RNA was extracted for real-time reverse-transcription polymerase chain-reaction analysis. Primers and probes were designed for type I collagen, osteocalcin and Runx II with primer express software (Prism V 3.0). RNA extracts were analyzed in five duplicates by quantitative real-time multiplex

RT-PCR, with a TaqMan gold RT-PCR Kit (Perkin Elmer, Foster City, CA, USA). 18s ribosomal RNA was used as an endogenous control. The RNA was reverse transcribed into cDNA at 48°C for 30 min. Then, the Runx2 or osteocalcin, Collagen I target, and the endogenous rRNA control, were amplified by multiplex PCR with the thermal cycling parameters of 50 °C for 2 min, 95°C for 10min, 40 cycles of 95°C for 15 min and 60C for 1 min. The real-time PCR reactions were performed in 96-well Optical Reaction Plates (PerkinElmer) in an ABI Prism 7700 sequence Detection System (PerkinElmer). Steady-state mRNA levels of each isoform was normalized to 18s rRNA and calculated by the Comparative Method of Relative Quantification in Multiplex Reactions (PerkinElmer). Statistical analysis (N=5) of $\Delta\Delta$ Ct was performed using a one-way analysis of variance (ANOVA) with a student T-test to a confidence level of $p < 0.05$.

4.3 Crystallinity induced poly(L-lactide-*co*-glycolide) PLGA 85:15 and cellular responses

4.3.1 Materials and methods

Polymers: Poly(L-lactide-*co*-glycolide) (PLGA) 85:15 (batch DB 570EL) polymers were purchased from Purac Polymers, Inc. (Lincolnshire, IL, USA). All other polymer surface characterization instruments, cell culture supplies as well as osteogenic gene expression assays were the same as in section 4.2.1 in P 41-43.

4.3.1.1 Surface preparation: poly(L-lactide-*co*-glycolide) 85:15 polymer film preparation and crystallinity induction:

Copolymer films were prepared using a melt-compression method. Briefly, PLGA 85:15 was processed at 250 °C on a Carver Press (M 11, Toms River, NJ, USA) under nitrogen blanket. Specifically, PLGA 85:15 films were compressed using a Teflon mold to create films of 150 µm in thickness.

Crystallinity of PLGA 85:15 films were induced as following:

Polymeric films were stretched above their T_g (70 °C) in a water bath to induce microorientation of the polymeric chain. Briefly, polymer films were soaked in a water bath at 80 °C for 5 min. Then the film was held by tools and manually stretched beyond its original length by 2 folds, 3 folds and 3.3 folds. Films were pat dry with Kimwipes® and stored in dissicator until use.

4.3.1.2 Crystallinity-induced PLGA 85:15 surface characterization

4.3.1.2.1 Scanning electron microscopy (SEM)

The morphological structures of the films were studied by a JSM-5900 LV scanning electron microscope of JEOL, Tokyo, Japan. The dried film samples were mounted on a metal stub and sputtered with gold using a sputter coater (Desk-II, Denton vacuum Inc., Moorstown, NJ) in order to make the sample conductive, and the images were taken at an accelerating voltage of 10 kV and 4500-5000 x magnification.

Polymeric films were examined with scanning electron microscopy (SEM) (JEOL JSM-5900LV SEM) at 10Kv. The samples were coated with gold and the coating time was 200s.

4.3.1.2.2 X-ray diffraction (XRD)

The XRD analyses were performed on a Fillips instrument (X'Pert APD) which operated at 300w, 15kv and 20mA. Samples were attached to the aluminum sample platform with double-sided tape. The take-off angle was 30% with respect to sample plane. The pressure during analysis was maintained at about 10^9 torr. Survey spectra were obtained using a passing energy of 17.9 eV. Quantitative analyses were performed using angular range of 5-40(2 θ) with nickel-filtered CuK α radiation ($\lambda = 0.154$ nm) at a voltage of 40 kV and current of 30 mA.

4.3.1.2.3 Contact angle measurement (CA)

The static contact angles for PCL-PGA polymeric films were determined using a sessile drop method using a static Knuss drop shape analysis system (Knuss M 1020, Berlin, Germany). For each composition, three disks were used and measurements were repeated five times for mean and standard derivation calculation. Briefly, ultrapure water from Sigma Aldrich (St Louis, MO) was used to fill a 20 mL syringe. The film was mounted onto a microscope glass using double-sided tape. A 5 μ L drop of water was then placed on the test specimen film. The contact angle of each sample (triplicate) was measured five times, with mean of the readings reported. Contact angles were also measured on

films, which had been exposed to water at room temperature for an hour to determine the effect of hydration on these materials.

4.3.1.2.4 Mechanical tests

This test was carried out with reference to ASTM specifications. Films were cut, using a standard template, into dumbbell-shaped strips. At least five samples were prepared of each film. They were inspected carefully for any defects, cracks or air bubbles. Any sample containing any of these defects, was discarded. Thickness of film strips was measured, using digital micrometer (Mitutoyo CD-8, Tokyo, Japan), from a number of places to ensure uniformity. Each strip then was fixed into the flat-faced grips of the testing machine (Instron corporation, Lincoln, NE, USA), which was pulled apart at constant rate of 10 mm/min. Tensile strength at break, elongation at break and elastic modulus was recorded. Mean values of at least six readings were calculated.

4.3.1.3.5 Atomic force microscopy (AFM)

Atomic force microscopy (AFM) images were recorded under ambient conditions using a multimode nanoscope IV (Digital Instruments, Santa Barbara, CA, USA) operating in the tapping mode regime. Microfabricated silicon cantilever tips (MPP-11100-10) with a resonance frequency of 299 KHz and a spring constant of 20-80 Nm^{-1} were used. The scan rate varied from 0.5 to 1 Hz. Detailed AFM protocol was the same as listed in detail in P45.

Statistical Analyses

Standard student T test and Microsoft Excel 2000 (Microsoft Corp., Redmond, WA, USA) was used for all statistical analyses. Differences were considered to be significant at $p < 0.05$.

4.3.1.3 Pre-osteoblast attachment and proliferation

Pre-osteoblasts were seeded and quantified using the protocol described in section of 4.2.4 on P 47.

4.3.1.4 Osteogenic gene expression

Osteogenic gene expression experiments were conducted using the protocol described in detail in section 4.2.5 in P 48-49.

4.4 Results and discussions

4.4.1 PCL-PGA films: Physicochemical properties and cell responses

PCL and PGA films are homogenously white or ivory from naked eyes because of their crystalline structure. Intermediate copolymer compositions of PCL-PGA 25:75, 35:65 and 45:55 are increasingly transparent. PCL and PGA films are also quite rigid whereas PCL-PGA copolymeric composition films are increasingly flexible with increasing PGA component. PGA film is more rigid than the PCL film.

4.4.1.1 Thickness of PCL-PGA films

Thickness of the films was found to range from 190 to 480 μm (Table 4-3 and Fig.4-2).

4.4.1.2 Differential scanning calorimetry (DSC)

The DSC spectra and thermal properties of dry PCL-PGA films are shown in Figure 4-3 and Table 4-4. PCL films have an endothermic peak at around 62°C and the PGA films have an endothermic peak at around 224°C. PCL-PGA polymeric films had two distinct endothermic zones, indicating the contributions from each monomeric component. The endothermic peak around 54°C in the first run corresponds to the PCL, and appeared in all of the film samples. No obvious glass transition temperature (T_g) was observed for these films because the intermolecular forces between polymer chains and consequently overall cohesion is rather low. The heat of fusion (ΔH_m and ΔH_c), melting temperature (T_m), crystallization temperatures (T_c) are summarized in Table 4-4. The ΔH_m for PCL-PGA films are decreasing from 79 J/g for PCL to 13 J/g for PCL 45:55 progressively with increasing PGA component in the copolymer. The ΔH_c is 60 J/g for PCL and 56 J/g for PGA. The T_m for PCL-PGA copolymers showing contributions from PCL and PGA melting temperatures, ranges from 112° to 209 °C. In the elastomeric PCL-PGA 45:55, the onset of the melting peak was taken to show phase transition. The T_c determined in the cooling run was 126°C for PGA and 26°C for PCL. There was no crystallization peak for the intermediate PCL-PGA copolymeric compositions. The crystallinity of PCL-PGA,

x_c , was calculated using the equation of $x_c = \Delta H_c / \Delta H_m \times 100\%$. x_c was 79% for PGA and 76% for PCL whereas the elastomeric copolymeric compositions were amorphous.

To compare if crystallinity changes with hydration, DSC was performed on both dry and wet films. Representative crystallinity changes with PCL and PCL-PGA 35:65 (post hydration for 1h in RT) are shown in Figure 4-4 and post hydration crystallinity data is summarized in Table 4-4. There were no appreciable differences in the crystallinity for all the dry and wet PCL-PGA films (not shown).

4.4.1.3 SEM

SEMs of the surfaces of PCL-PGA copolymer films Figures 4-5. The copolymer films were found to be smooth and homogenous.

4.4.1.4 Contact angel measurement

Since the polymeric films that come into contact with the cell culture medium become hydrated, the effect of both wet and dry film surfaces was studied. In order to determine if hydration state influences the contact angles of the surfaces of compression molded polymeric films of PCL and PGA, dry and wet film contact angles were determined and are shown in Figure 4-6 and in Table 4-4. The water contact angles of this series of PCL-PGA polymeric films were determined using a static Knuss drop analysis system at 25° C, in which reagent-grade 1 water was used as the wetting medium. In all cases, at least five replicate determinations were performed. The static contact angle measurements

show that monomeric PCL and PGA materials are similarly hydrophilic as the copolymeric PCL-PGA films. Even with the noted differences, all materials studied possess generally hydrophobic surfaces. In the dry state, these films possess water contact angles of 95 ± 2 , 95 ± 1 , 98 ± 1.4 , 97 ± 1.2 and 98 ± 1 degrees for PCL, PGA, PCL-PGA 25:75, PCL-PGA 35:45 and PCL-PGA 45:55 respectively. In “wet” state, these films possess advancing water contact angles of 95 ± 1.2 , 98 ± 2 , 99 ± 2 , 98 ± 1 and 95 ± 2 degrees for PCL, PGA, PCL-PGA 25:75, PCL-PGA 35:45 and PCL-PGA 45:55 respectively. It appears that post-hydration, the film surfaces became slightly more hydrophilic, but overall no significant changes were observed by wetting the films.

4.4.1.5 Atomic force microscopy

Tapping-mode AFM images yielded information about the surface nanotopographic features of the various films. PCL and PGA as well as the copolymeric compositions PCL-PGA 25:75, 35:65 and 45:55 inherently contain “hard, rigid” crystalline and relatively “soft, flexible” amorphous segments, hence structural heterogeneity is directly responsible for micro-domain separated morphologies as shown in Figure 4-7. Although the compression molding processing condition was constant for all of the matrices, the PCL 35:65 and PCL 45:55 films had rougher terrains compared to the other films studied. Figure 4a shows the surface topography of PCL films exhibiting undulations with irregularly spaced features of various sizes ranging from 393 nm in height and few nanometers in width, corresponding to the intact and withered granular envelopes or

ghosts resulting from the fast crystallization of PCL. The surface of the PGA films (Figure 4-7b) was relatively smooth, homogeneous and had a continuous matrix with good structural integrity. They were flat and compact with very sparsely distributed small particles having peak heights of 170 nm without any phase separation. The AFM topographic images of the copolymeric films exhibited an intermediate character (Figure 4-7c, d and e) to that of the PCL and PGA films, with particles of peak heights between 87 and 313 nm and the uniformity in the distribution of particles reduced with the increasing monomer concentration of PCL. The respective PCL-PGA 25:75, PCL-PGA 35:65 and PCL-PGA 45:55 also demonstrated surface roughness, with 26 nm, 88 nm and 41 nm in roughness respectively. Both phase contrast and slight phase separation were observed in the phase images of copolymeric films (not shown). The RMS (root mean square roughness) values are tabulated in Table 4-5.

After hydrating the films in water for one hour at room temperature, the RMS was measured again using AFM. The RMS roughness pre and post hydration was shown in Fig. 4-8 and Table 4-5.

There was a decrease in roughness for the hydrated films for all of the polymeric compositions tested. However, PCL 35:65 demonstrated the largest reduction in roughness from 87.7 nm to 21.4 nm, a change of 66.3 nm. PCL 45:55 and PGA demonstrated the second largest reduction in roughness representing a change of 25.1 nm, respectively. There was little change for pre- and post- hydration roughness of the PCL

25:75 films. The pre- and post-hydration roughness is shown in Table II. However, one striking finding from these post-hydration films was that there is very little difference in surface roughness among the PCL-PGA polymer substrates, with PCL-PGA 45 possessing the lowest roughness of 16 nm and PCL the highest roughness of 23 nm.

4.4.1.6 Osteogenic gene expression

Initial osteoblasts attachment density to PCL-PGA polymeric films after 24h, 72h and 1 week culture is shown in Figure 4-9. The number of adherent cells per unit area at 72 h was significantly more on areas of moderate to low PCL concentration (PCL-PGA 25:75 (3723 cells/disc), PCL-PGA 45:55 (3582 cells/disc), with the peak of cell attachment for PCL-PGA 35:65 (5174 ± 27 cells/disc), and reaching the lowest cell density levels (~ 1098 cells/disc for PCL, and 1691 cells for PGA), respectively. This was comparable to an average cell density of 2030 ± 90 cells/disc observed on "positive" TCPS controls (not shown). Measurements of surface wettability of these series of copolymeric films showed average contact angles ranging from $95^\circ \pm 0.9^\circ$ and $100^\circ \pm 2.1^\circ$, respectively, suggesting that surface energy is not discriminating for these surfaces with regards to cell attachment on them. Either surface roughness or material rigidity, or both, as the only statistically significant factor ($p < 0.05$) that influenced initial cell adherence over the polymer series.

Osteoblast morphology on PCL-PGA surfaces is demonstrated in Figure 4-10. Representative optical microscopy images of osteoblast attachment at 24 hours post

seeding is shown in Figure 4-10 (a) for PCL-PGA 35:65, while Figure 4-10 (b) and (c) demonstrate attachment for 72 h and 168 h respectively. Cells were largely polygonal, with extended filopodia and exhibited an organized monolayer of interacting cells at 72 hours. By 168 hours in culture, the osteoblasts spread across the plate and become confluent, indicating that PCL-PGA 35:65 effectively supported osteoblast attachment and proliferation. Figure 4-10 (d) shows the co-existence of spread and rounded osteoblasts on the PCL surface at 24 hours post seeding, further indicating that osteoblasts did not attach and proliferate as well on PCL surfaces. Figure 4-10 (e) shows a representative case where the low-cell cluster Tissue Culture Plastic (TCP) dish did not fully support osteoblast growth in the current study.

Expression of FAK, Cbfa1 and collagen I were not promoted when pre-osteoblasts were cultured on PCL-PGA 35:65 and PCL films, for both 24 hr and 72 hr culture (Figure 4-11, 12 and 4-14). However, expression of osteocalcin was promoted at 24 hr and 72 hrs, especially when cultured on PCL-PGA 35:65 films (Figure 4-13). A maximal enhancement in the expression of osteocalcin (about 2 folds) occurred on the PCL-PGA 35:65 film at 72 hours in culture. On this surface, expression of Cbfa1 and type I collagen did not increase.

An osteogenic gene expression experiment was repeated at 72 hr and 2 weeks to look at longer effects of surfaces on osteogenic gene expression. At 72 hrs, up-regulation of osteocalcin expression was noted on PCL-PGA 35:65 (Figure 4-15); the rest of the gene

primers did not see an up-regulation (not shown). At 2 weeks in cell culture, none of the materials promoted osteogenic gene expression.

These results have correlated with the observation that osteoblast attachment and proliferation, as well as osteogenic gene expression is dependent on PCL-PGA polymer matrix crystallinity. Among the several factors for biomaterials capable of influencing cell responses including chemical, topological and mechanical [119], the present study demonstrates that crystallinity of the PCL-PGA substrate influences osteoblast and fibroblast responses.

Copolymers of two individually highly crystalline polymers, PCL and PGA, have many clinical applications due to their mechanical strength, degradability and biocompatibility[132, 135-136, 143]. They also represent a suitable model for evaluating the cellular behavior in response to varied crystallinity. Common methods for fabricating PCL films have been presented in recent publications including solvent casting of polymers onto a Petri dish or compression molding into thin films [41, 43]. Each method will produce large differences in terms of molecular conformation, surface chemistry/energy, topography and porosity. So far, a systematic comparison of different polymeric ratios of PCL-PGA and their effect with regards to cellular behavior has not been reported; nor have there been studies into such processes on copolymeric films made by compression molding.

PCL and PGA are biodegradable and biocompatible polymers. Copolymers of PCL and PGA can exhibit an array of degradation rates, with the larger the PCL components, the slower the degradation rate [72]. Of special note for this study, PCL and PGA are highly crystalline materials, whereas their copolymeric intermediate compositions of PCL-PGA (25:75, 35:65 and 45:55) are increasingly amorphous. This study aims to discern the cellular attachment and proliferation behavior on these materials with the intent of using these data to characterize their expected tissue response *in vivo*. PCL-PGA polymers are compression molded into thin films as a practical and simplified means to study surface interaction of the materials with cells, in this case, osteoblasts and fibroblasts. Since PCL and PGA lack specifically engineered cell binding domains, the observed cellular response could be attributed to the underlying material physicochemical properties. Particularly, we hypothesized that PCL-PGA crystallinity is the most important factor for cell responses, among several other substrate physicochemical properties, such as copolymeric composition, surface hydrophobicity, surface nano-topography (roughness).

Contact angle measurement demonstrated little variation for compression-molded films of varying copolymeric composition of PCL and PGA; all the copolymeric composition showed that they are hydrophobic surfaces (Figure 4-6). The contact angle of PCL was approximately 95° (93° by Tang et al from solution cast PCL film [144]). The processing method will influence the surface generated thus influencing the water contact angle. The hydration of the film was expected to alter the water contact angle, but results from the

present study showed that both wet and dry films are similarly hydrophobic. These results will exclude PCL-PGA polymer hydrophobicity as a major factor influencing subsequent cell responses differently.

PCL-PGA substrate crystallinity results have shown PGA and PCL are highly crystalline materials ($x_c=79\%$ for PGA and $x_c=76\%$ for PCL). This result correlates with the observation that PGA is the most opaque film whereas PCL films possess a slight transparency. PCL and PGA are also rigid materials, indicating the compactness of the polymer macromolecules and the difficulty with which they move. The ΔH_m for PCL (79 J/g) is greater than PGA (71 J/g), implying PGA is more rigid than PCL. PGA melts at 224 °C and PCL melts at 62 °C. PGA is the most rigid because PGA's T_g is around 30°C and T_g of PCL is -60°C, which also supports PCL as a more flexible material. The copolymeric films are amorphous, which implies that the crystallization of PCL and PGA segments might constrain each other in the copolymers. The PCL and PGA copolymers are quite flexible, exhibiting increasing rigidity with increasing PGA content. The three amorphous films of PCL-PGA (25:75, 35:65 and 45:55) also possess elasticity. The peak melting temperature of PGA decreases upon increasing PCL content within the block copolymers and with respect to neat PCL. As the content of PCL increases, the glass transition temperatures increases, indicating a degree of miscibility between the components. According to previous work [145] [146] PLLA- β -PCL block copolymers are either mixed in the melt or weakly segregated (i.e., they mostly crystallize from a mixed

melt except at compositions close to 50-50 when they can form well organized melt structures which are later destroyed or modified by the crystallization of each block). It is apparently the case with PCL-PGA that partial miscibility can also induce a diluting effect of the PCL block over the PGA block, depressing T_m of the PGA block. Crystallization of PGA block can be seen for all compositions in Figure 4-3, except for PCL-PGA 45/55, since this composition permits the two monomeric composition to form well organized melt structures. This is the reason that PCL-PGA 45:55 are the most flexible among all five of the polymeric compositions. The increase in crystallinity reflects differences in materials rigidity. While PCL and PGA are highly crystalline and rigid, the intermediate copolymeric compositions, such as PCL-PGA 25:75, 35:65 and 45:55 are increasingly flexible (less rigid) with increasing PGA composition. Crystallization kinetics of PCL is also significantly impaired due to the covalently bonded PGA block which crystallizes first during cooling. Because of this, PCL blocks remain virtually amorphous in the molded films when present in 25:75 and 35:65. The slowly drifting lower T_m of PGA is a clear sign for miscibility; this also correlates well with the fact that PCL-PGA 25:75 is more rigid than PCL-PGA 35:65.

DSC results for the hydrated PCL-PGA films showed that hydration did not alter their crystallinity (Fig 4-4 and Table 4-4). Wet PCL-PGA films remains highly crystalline for PCL and PGA and amorphous for the copolymeric compositions. Degirmenbasi [43] conducted similar hydration studies on polyester materials and found no significant

differences in the crystallinity for the hydrated samples as well. These findings suggest crystallinity and rigidity of PCL-PGA polymers might be a major contributor influencing cellular responses.

Compression molding allowed us to generate surfaces of PCL-PGA with a range of surface topographies as shown in Figure 4-7. Kabacova et al [120] found that surface roughness plays an important role in guiding cell proliferation and differentiation. In the current study, surface roughness was examined for both dry and wet surface films. The purpose for this was to determine hydration effects on PCL-PGA material nanotopography, because the wet films were used in the cellular studies. Despite the fact that melt processing produced varied surface topographical features for PCL-PGA films, post-hydration roughness for all PCL-PGA surfaces exhibited similar surface nanotopographic roughness (Fig 4-7 and Fig. 4-8). This is probably due to the fact that all surfaces are similarly hydrophilic, indicating that water molecules would approach all the surfaces of interest in the same manner. In addition, water serves as a flattening component to fill the nano-voids existing in the dry films, causing the post-hydration roughness of these surfaces to be essentially the same. The observed reduction in roughness for surfaces post hydration was consistent with other reports [133].

In vitro cellular response studies on different PCL-PGA polymeric films were conducted in terms of initial adhesion and subsequent proliferation. A preosteoblast cell line (HEPM 1486) was used for attachment and proliferation studies. Figure 4-9 indicates initial

osteoblast attachment density to PCL-PGA polymeric films follows the trend that osteoblasts attached and proliferated the least on rigid surfaces (PCL and PGA), and the most on flexible surfaces (PCL-PGA 35:65). Proliferation of osteoblasts follows the same trend. Similar observations have been reported by other investigators who correlated matrix rigidity with cell adhesion and migration [147-148]. Pelham has shown substrate flexibility affected cell focal adhesion and locomotion. Tzvetkova demonstrated that the combined effects of substrate rigidity and anisotropic structure impact cell motility. The attachment and proliferation of PCL-PGA surfaces indicated that there was an optimal copolymeric ratio of PCL-PGA for the expansion of osteoblast cells. This optimal copolymeric ratio again related to PCL-PGA crystallinity and rigidity. Washburn concluded that crystallinity can induce topographical changes and osteoblasts proliferated better on the smooth region than on the rough region as a function of varied crystallinity [125]. However, the present studies demonstrated that nanotopographical features of PCL-PGA substrates played only a minor role in influencing cellular responses. Representative osteoblast morphology is shown in Figure 4-10 and exhibited an organized monolayer. This observed cellular morphology is consistent with the results reported for osteoblast growth on TCP surfaces [42] [149]. It further demonstrates that osteoblasts prefer the PCL-PGA 35:65 surface, which is a flexible/amorphous surface.

Although osteoblastic activity can be assessed in terms of the above osteoblast response studies, studying gene expression by the osteoblasts will give more accurate and in-depth

information about cellular activity and will also disclose whether the cells are healthy and fully functional [150-152]. Differential gene expression of osteogenic cells can be defined by three principal biological stages: cellular proliferation, cell maturation and focal mineralization. Runx 2 is an important transcriptional determination of osteoblast differentiation and gene expression [153]. This in vitro study was based on the hypothesis that PCL-PGA series of polymers are different in terms of regulating a number of genes and proteins associated with differentiation and ECM deposition, due to their varied crystallinity. Osteogenic gene expression of key osteogenic gene markers: Runx 2 (Cbfa), Osteocalcin Collagen 1 and FAK, have shown similar responses for all the PCL-PGA surfaces at 24 hours, 72 hours and 1 week. However, cells grown on PCL-PGA 35:65 demonstrated upregulation of Osteocalcin mRNA at 72 hours by approximately two fold, compared with TCP (Figure 4-15). This was correlated with the cell attachment and proliferation studies that PCL-PGA 35:65 was the best surface for osteoblast growth and differentiation among the PCL-PGA surfaces.

It is understood that bulk and surface properties of polymers, such as wettability, chemistry, electric charge, surface energy, roughness and rigidity may influence biological responses [42, 117, 119-120, 122, 124, 135, 147]. Despite this knowledge, we are still far away from understanding the molecular basis and the relative importance of these features. There is contradicting information in the literature that indicates material crystallinity, morphology, and topography impact cellular responses [42-43, 120-121,

123-124, 129, 132-133, 147-148]. The present study results all point to the fact that the attachment and proliferation of osteoblasts on flexible/amorphous PCL-PGA 35:65 surfaces were more efficient, and were poor on highly rigid PCL and PGA surfaces. It appears counter-intuitive because osteoblasts (bone-forming cells) generally reside in hard tissue and might be expected to favor rigid/crystalline materials. Careful study design allowed us to compare among thermal properties (crystallinity and rigidity), nanotopography and surface hydrophobicity for PCL-PGA surfaces. Under these conditions, it seems that the most important feature is the material crystallinity/rigidity of the PCL-PGA films.

HEPM preosteoblastic cell attachment and proliferation can be understood in terms of substrate hydration, charge and rigidity. A few recent studies have investigated the effect of film rigidity altered via chemical crosslinking and how that influenced smooth muscle cell attachment and proliferation [154]. Mendelsohn et al. found the adhesion of murine fibroblasts to be increased on films with greater ionic cross-linking, and thus with a lower degree of hydration, as controlled through the formation pH [155]. Our studies have shown that a suitable combination of these factors might give rise to optimal pre-osteoblast attachment and proliferation, on PCL-PGA 35:65 surfaces. A combined effect of protein coated surfaces composition; an optimal surface toughness might promote pre-osteoblast attachment and proliferation, even differentiation. Osteogenic gene expression suggests that Osteocalcin, which is a differentiation marker, has been promoted at 72hrs by

PCL-PGA 35:65 which is an elastomeric material whose mechanical properties lie between the rigid extreme of PCL and PGA and the softer extreme of PCL-PGA 45:55.

4.4.2 Crystallinity-induced PLGA 85:15 films physicochemical properties and cellular responses

4.4.2.1 Thickness of PLGA 85:15 films

The stretched polymeric films physical parameters are given in Table 4-6 and Figure 4-16. The flexibility of the polymeric film is poor, probably due to the compactness of the polymer macromolecules, crystallinity and difficulty in their movement.

Film thickness was found to range from 285 to 580 μm (Table 4-6).

4.4.2.2 Mechanical strength

The tensile strength (TS) values of the PLGA 85:15 films with the different degree of stretching are shown in Figure 4-17. It was found that the TS values of the stretched films increased first with the 3x and 3.3x stretched films, with a maximum of 70 MPa at 3x and 75 Mpa at 3.3x stretched films, due to the formation of intermolecular polymeric chain alignment. The TS values decreased with 2x stretching with a maximum of 55 Mpa, which may be due to initial phase separation between the two main components.

The percentage elongation (*E*) values of the films are a measure of the flexibility of the film and were affected by the degree of stretching. A striking finding is that at 2x

stretching, the strain % increased to almost 75% (Figure 4-17). The increase in percentage elongation with 2x stretching is due to the reduction in the number of intermolecular cross-links and increase in the intermolecular distance. However, once additional stretching is enforced, the effect of increasing of E doesn't hold, which indicates that the entanglement of the polymeric chains behaves in a rather complicated way.

4.4.2.3 X-ray diffraction

X-ray diffractograms (XRDs) of PLGA 85:15 stretched films are shown in Figure 4-18 and 4-19. In Figure 4-18, as observed, the PLGA 85:15 film was in a crystalline state because two main diffraction peaks ($2\theta = 16$ and 32.02) were observed in its X-ray diffraction pattern. The intensity of the crystal peak at 16 (2θ) was higher than that at 32.02° . In the PLGA film, the intramolecular interactions between the monomeric components and hydroxyl groups in PLGA limited the molecular movement of the PLGA chain and reduced its crystallization. Therefore PLGA films prepared by melt compression were in semi-crystalline form owing to the presence of monomeric lactide and glycolide component, which might have hindered the formation of inter- and intramolecular hydrogen bonds in and around the hydroxyl groups thus resulting in less dense packing.

Upon stretching, the crystalline structure demonstrates a diffraction peak at around 16° (2θ) and a few small peaks at around 2θ of 15° , 20° , 22° and 24° (Figure 4-19). The

crystallinity in polymeric materials is generally dependent on the crystallization rate, which follows a bell-shaped curve between the temperatures T_g and T_m . Apparently in cases where stretching is increased to 2x, the polymeric chain alignment is increased compared to un-stretched materials but the overall crystallinity remains low. Upon stretching to 3x of its original length, the *E* type of crystallinity is found to rearrange into a more crystalline structure, whereas 3.3x stretching did not seem to impact the crystalline structure to a significant degree, compared to 3x stretching.

4.4.2.4 Contact angel measurement

The advancing and receding contact angles of PLGA 85:15 and stretched PLGA 85:15 films were determined using the sessile drop static contact analyzer at 25°, in which reagent-grade 1 water was used as the wetting medium. In all cases, at least five replicate determinations were performed.

The static contact angle measurement demonstrated that all PLGA films have the similar hydrophobicity, for both control and stretched films (Figure 4-20). In this study, contact angle measurements were carried out to determine whether there was a relationship between hydrophobic/hydrophilic property and protein adsorption and cellular responses. It is concluded that this physicochemical property does not appear to be a primary contributor to influencing the downstream responses because PLGA films keep their hydrophobicity essentially the same across the range of materials tested here.

4.4.2.5 DSC for dry and wet PLGA 85:15 films

DSC results on both hydrated PLGA films and dry PLGA films did not show appreciable changes for crystallinity (Figure 4-21).

4.4.2.6 AFM for hydrated films:

Surface roughness for the PLGA series of films which had been hydrated was measured using AFM and shown in Figure 4-22. The roughness of dry PLGA films are 20.3 ± 0.6 , 15.3 ± 4.1 , 5.9 ± 2.6 and 11.0 ± 2.5 nm for PLGA, 2x, 3x and 3.3x films respectively. The roughness for post hydration PLGA films are 29.8 ± 9.9 , 33.1 ± 10.8 , 20.3 ± 0.6 and 6.3 ± 1.8 nm for PLGA, 2x, 3x and 3.3x films respectively. There was an increase for all the post-hydration films, compared with their dry counterparts. This was contrary to the observation for PCL-PGA films.

AFM images for hydration film of PLGA 85:15 was shown in Figure 4-23.

4.4.2.7 Osteogenic cellular responses

Initial osteoblast attachment density to PLGA films after 24h, 72h and 1 week culture is shown in Figure 4-24. At 24 hours, the number of adherent cells per unit area was not significantly different on areas of stretched films compared to un-stretched films ($\phi \leq 800$); this was comparable to an average cell density of 807 cells/disc observed on "positive" TCPS controls. At ϕ_{control} cells adhered nearly uniformly along lines of constant composition, regardless of the varying surface morphology generated by the stretching.

At 72 hours, the number of adherent cells per unit area was not significantly different on areas of stretched films compared to un-stretched films ($\phi \leq 1100$), but the 2x stretched film demonstrated a two fold increase in the number of cells (2200 cells/disc) among the rest of the surfaces in the group. At 168h, cell number was the highest for the 2x films (>400 cells per disc) among the groups, where as the 3.3x stretched films supported the least cell proliferation (< 500 cells/disc). This suggested that there is a suitable range of stretching that will elicit favorable cell attachment and proliferation for this material. Either too little degree or too great degree of stretching will probably disturb the underlying polymeric chain distribution which became un-supportive to cell attachment and proliferation. Measurements of surface wettability of PLGA 85:15 films with different degree of stretching (data not shown) did not show differences, suggesting that cells attach preferentially to the higher stretched 2x, due to the fact that these films have microorientation which is of higher energy surface.

4.4.2.8 Osteogenic gene expression

Gene expression (Figure 4-25) of human collagen I, osteocalcin and human Runx 2 were investigated by real time RT-PCR to evaluate cell differentiation. Collagen I as an initial step of cell deposition onto surfaces, demonstrated no differences among all surface groups of PLGA films. The adhesion observed by osteoblasts on our PLGA films were similar or slightly better than the “positive” tissue culture plastic group (not shown). Similarly, the differentiated cell function of HPEM preosteoblasts was slightly influenced

with regards to collagen type I, osteocalcin and human Runx 2 gene expression, resulting in no difference at the early time point (3h). However, there was up-regulation of the gene expression at the later stage (24h, 72h and 168h) for 3 fold stretched films. Human Runx2, as a marker for a more differentiated cell type-produced an almost 1.5 fold increase (n=5) on 3 fold stretched surfaces at 72 hours of cultivation. At 168 hours, Runx2 mRNA levels were up-regulated to almost two fold for 3 fold stretched PLGA films.

4.5 Conclusions

PCL-PGA series of polymers were characterized for their physicochemical properties. They possessed similar hydrophobicity, surface morphology and differed significantly in nanotopography for the dry surfaces. However, their nanotopographical roughness became similar upon hydration. PCL-PGA films varied to a large extent in crystallinity, i.e. the PCL and PGA being the highly crystalline materials, and the copolymeric compositions of PCL-PGA 25:75, 35:65 and 45:55 being increasingly amorphous.

Pre-osteoblast attachment and proliferation, as well as osteogenic gene expression results on PCL-PGA polymeric surfaces indicated that amorphous PCL-PGA 35:65 was significantly better in supporting pre-osteoblast growth, whereas highly crystalline PCL and PGA surfaces didn't support pre-osteoblast growth.

To further test the hypothesis that crystallinity of the polymer substrate impacts osteoblast attachment and proliferation, PLGA 85:15 series of materials were employed to form substrates for cell responses studies. The induced crystallinity on PLGA 85:15 films indicated there was optimal crystallinity of the substrates supporting osteoblast cell attachment and proliferation most effectively.

Ostogenic gene expression study results have demonstrated that there was up-regulation of PCL-PGA 35:65 (amorphous and highly flexible) for osteocalcin on this surface and

upregulation of Runx 2 on PLGA 85:15 (3 fold stretched surfaces), indicating optimal material crystallinity governed optimal osteogenic gene expression.

4.6 Tables

Polymer	Melting Point (°C)	Glass-Transition Temp (°C)	Modulus (Gpa)	Degradation Time (months)
PLGA 85:15	225—230	35—40	7.0	6 to 12
PCL	173—178	60—65	2.7	>24
PGA	225-230	34-40	1	6-12
PCL-PGA 35:65	113-120	-4	0.4	12
PCL-PGA 25:75	130-140	<0	0.6	8-15
PCL-PGA 45:55	100-108	<0	0.3	6-15

Table 4- 1 Physicochemical properties of Poly (caprolactone-*co*-glycolide) (PCL-PGA) and PLGA 85:15 polymers

Polymers	Process Temp. (°C)	Circular Disc Diameter (mm) (n=5)
PCL	70	3.0 ± 0.04
PGA	220	2.9 ± 0.10
PCL-PGA 25	200	3.0 ± 0.07
PCL-PGA 35	185	3.1 ± 0.02
PCL-PGA 45	150	2.9 ± 0.12

Table 4- 2. Processing Temperatures for Compression Molding of PCL-PGA Films and Circular Disc Diameter Measurement.

	Thickness (μm)
Polyglycolide (PCL)	190 (0.2)
Polycaprolactone (PGA)	395 (41)
PCL-PGA 25:75	297 (26)
PCL-PGA 35:65	477 (32)
PCL-PGA 45:55	320 (13)

Table 4- 3. Thickness of Stretched PCL-PGA Polymeric Films (Mean value of six measurements on each film)

	Pre Hydration							Post Hydration (1h)							78
	θ_{H_2O} (deg) (n=5)	ΔH_m (J/g) (n=3)	T_m (°C)	ΔH_c (J/g) (n=3)	T_c (°C)	x_c		θ_{H_2O} (deg) (n=5)	ΔH_m (J/g) (n=3)	T_m (°C)	ΔH_c (J/g) (n=3)	T_c (°C)	x_c		
PCL	95.0 ± 2.1	79	62	60	26	76%		95.5 ± 1.2	80	62	60	27	75%		
PGA	95.2 ± 1.3	71	224	56	126	79%		97.5 ± 2.1	72	223	57	126	79%		
PCL-PGA 25:75	98.5 ± 1.4	34	209		-	-		98.5 ± 2.1	33	202	-	-	-		
PCL-PGA 35:65	97.0 ± 1.2	20	112	-	-	-		97.5 ± 1.0	21	112	-	-	-		
PCL-PGA 45:55	98.3 ± 0.6	13	34	-	-	-		95.5 ± 2.1	17	13	-	-	-		

Table 4- 4. Basic physicochemical properties: thermal properties of PCL-PGA films and hydrophobicity.

	Pre Hydration			Post Hydration				
	Surface Roughness RMS ± SD (nm) (n=6)	Mean Ht ± SD (nm) (n=6)		Surface Roughness RMS ± SD (nm) (n=6)	Mean Ht ± SD (nm) (n=6)		Roughness Changes RMS (nm)	Mean Height Change (nm)
PCL	37.79 ± 1.20	393.0 ± 43.2		23.49 ± 7.44	433.1 ± 32.1		15.3	40
PGA	41.33 ± 2.21	170.7 ± 24.6		16.29 ± 1.4	212.0 ± 30.2		25.05	42
PCL-PGA 25:75	25.47 ± 2.32	260.4 ± 46.7		22.48 ± 2.89	275.2 ± 22.1		2.99	15
PCL-PGA 35:65	87.70 ± 7.01	313.5 ± 35.4		21.39 ± 5.77	260.4 ± 21.5		66.31	53
PCL-PGA 45:55	40.93 ± 8.38	87.2 ± 10.3		15.77 ± 0.73	108.2 ± 14.2		25.16	21

Table 4- 5. Nanotopographic roughness for pre- and post-hydration PCL-PGA films. (Values presented are mean of three measurements and SD is standard deviations.)

PLGA 85:15 films	Thickness (μm) (S.D.)
Control	583 (35)
2x	275 (8)
3x	362 (12)
3.3x	357 (20)

Table 4- 6. Thickness of Stretched PLGA 85:15 Films. (Mean value of six measurements on each film)

4.7 Figures

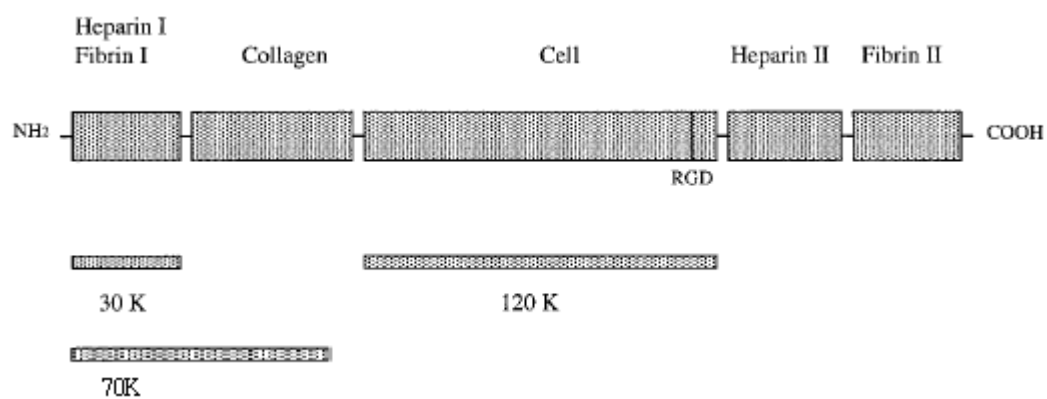


Fig. 4- 1 Schematic Model of Fn and Its Major Domains [156].

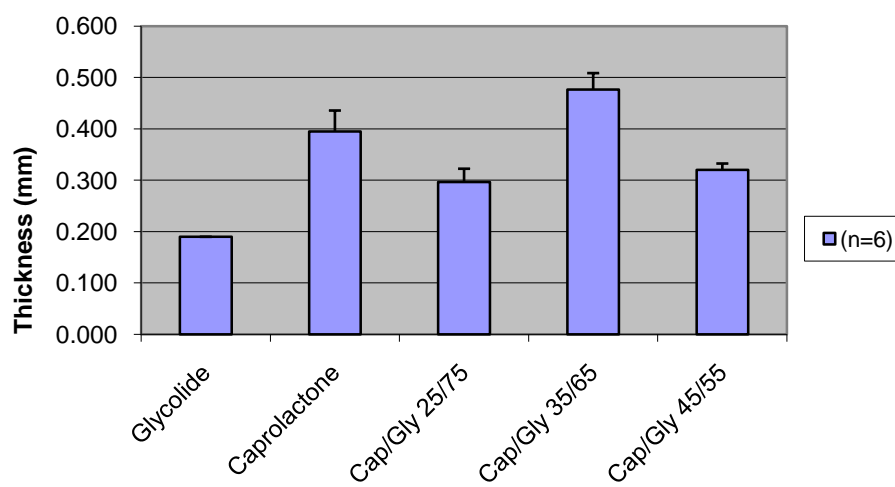


Fig. 4- 2 Thickness of PCL-PGA Films.

The PCL-PGA films are of equal thickness at around 400 μ m. Mean value of six measurements were reported.

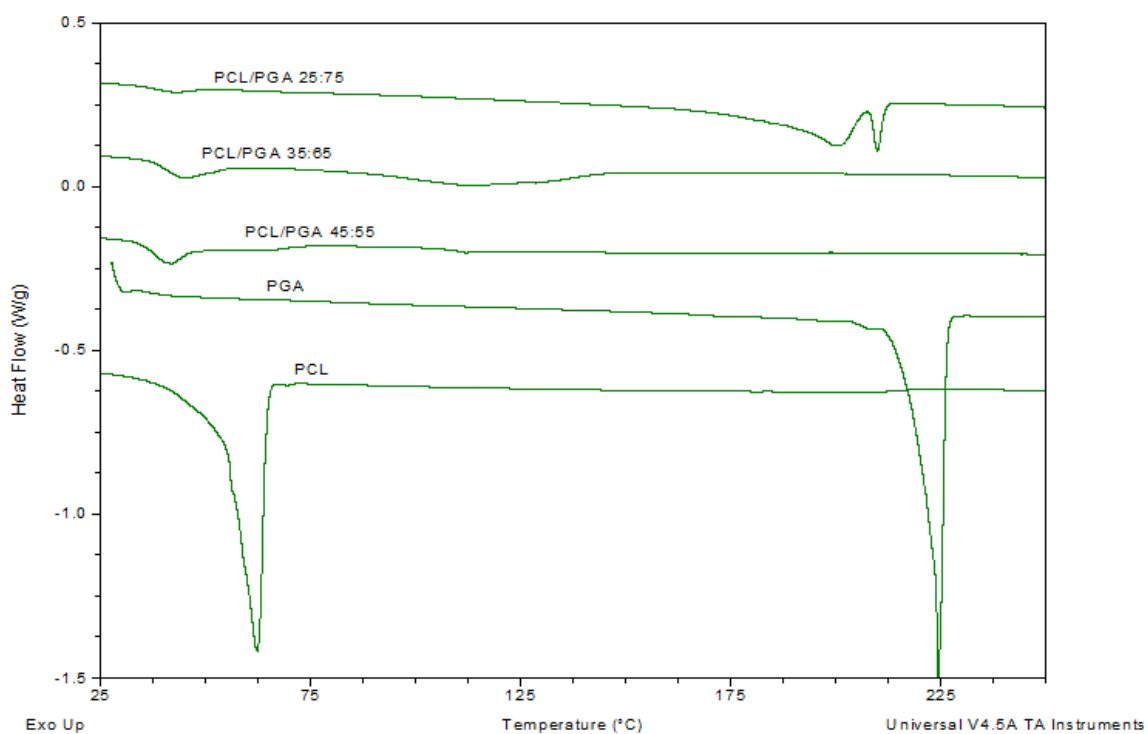


Fig. 4- 3 Differential Scanning Calorimetry thermograms of PCL-PGA Films. PCL: $T_m = 62.3\text{ }^{\circ}\text{C}$, PGA: $T_m = 225.8\text{ }^{\circ}\text{C}$, PCL 25: $T_m = 201.5\text{ }^{\circ}\text{C}$, PCL 35: $T_m = 112.8\text{ }^{\circ}\text{C}$ and PCL 45: $T_m = 41.7\text{ }^{\circ}\text{C}$. Mean \pm DSC of three determinations is reported.

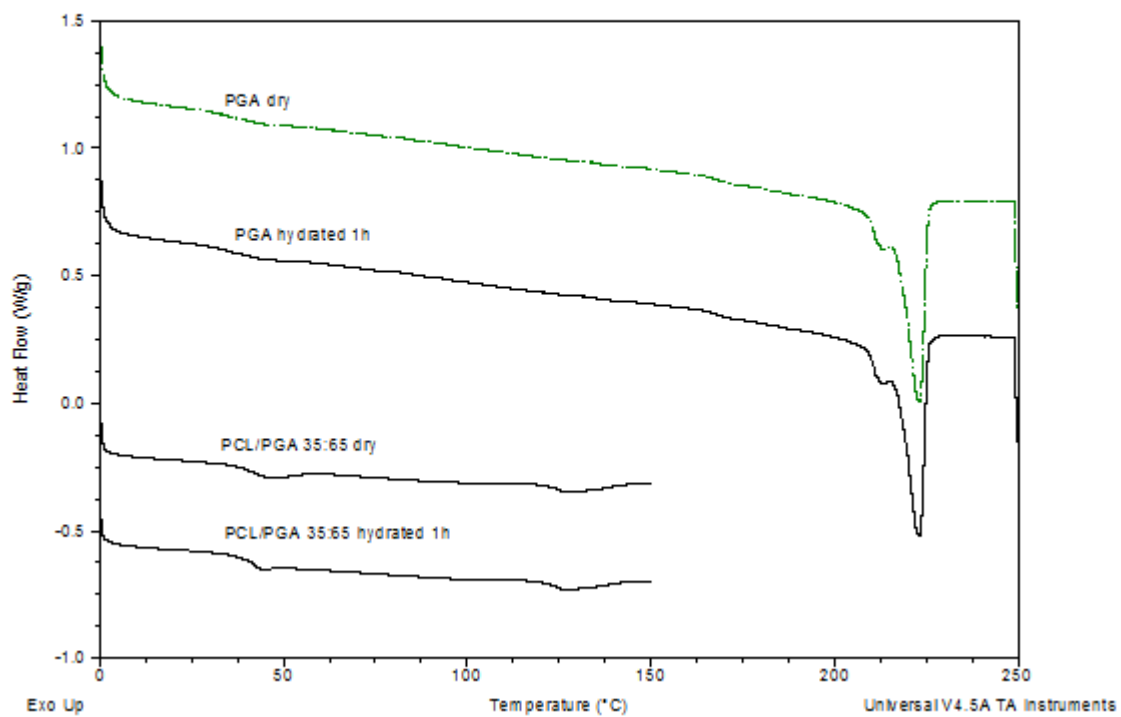


Fig. 4- 4 DSC Thermograms on Dry and Wet PCL-PGA 35:65 and PGA polymeric Films. (hydration time = 1h in water at room temperature). For each film, analysis was done in duplicates.

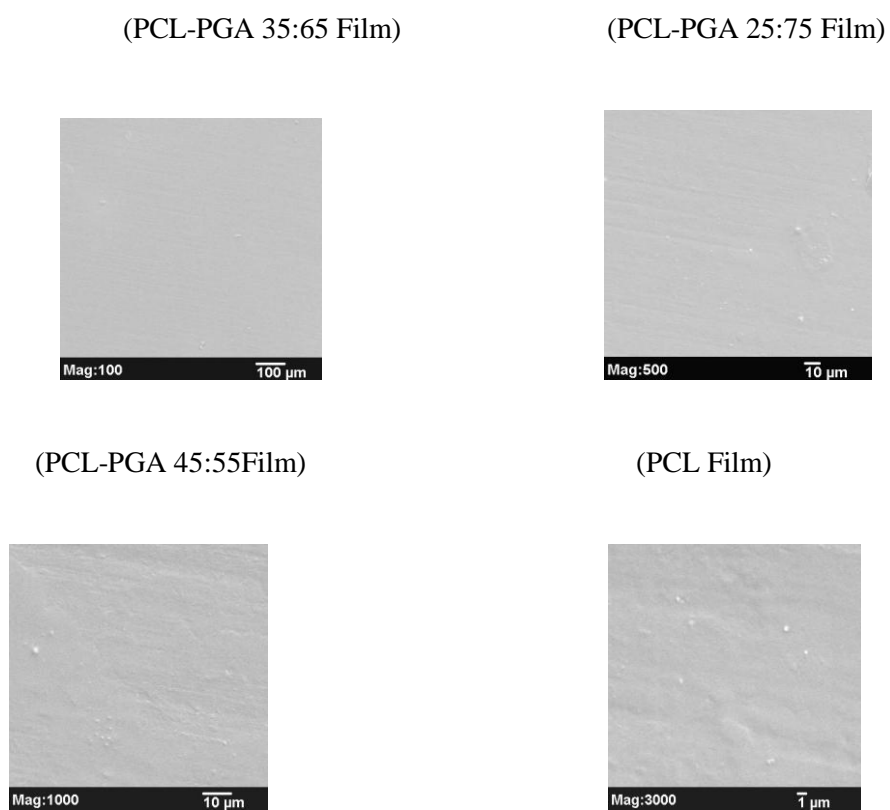


Fig. 4- 5 SEM Images of PCL-PGA Films. The films are homogenous with few surface defects.

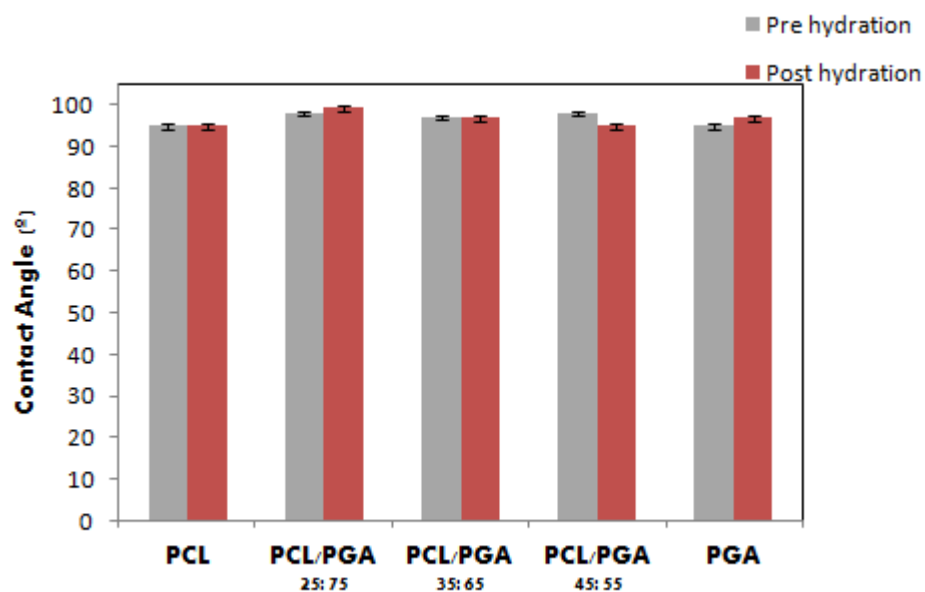


Fig. 4- 6 Contact Angle Measurement of PCL-PGA Films. **Values given in the figure represent five different measurements on three replicate samples per materials, the error bars are the standard deviations.** PCL-PGA films (both wet and dry) are similarly hydrophobic.

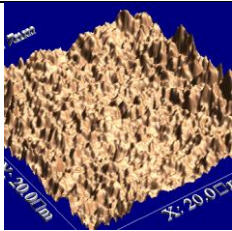
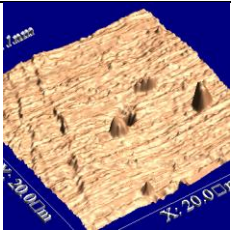
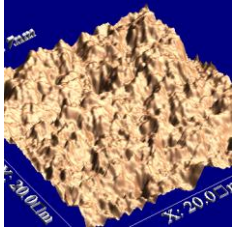
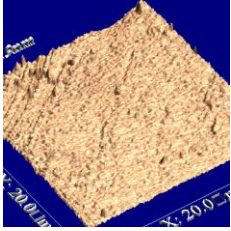
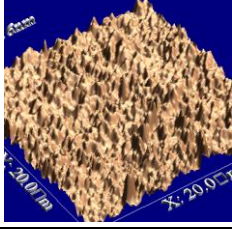
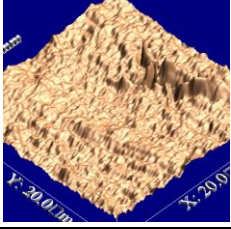
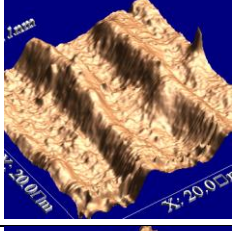
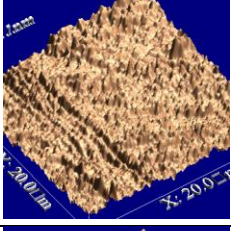
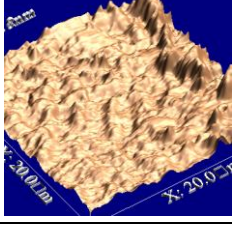
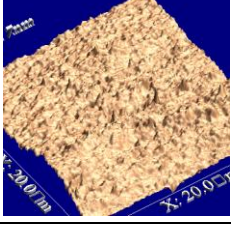
	nanotopography Pre-hydration		nanotopography Post-hydration	
A: PCL				
B:PGA				
C: PCL-PGA 25/75				
D:PCL-PGA 35/65				
E: PCL-PGA 45/55				

Fig. 4- 7 Representative AFM surface topographic features (Tapping mode) for PCL-PGA films. (A): PCL; (B): PGA; (C): PCL-PGA 25:75; (D): PCL-PGA 35:65; (E): PCL-PGA 45:55. Apparent smoothing of the post-hydrated surfaces can be clearly seen from these images. Scale bars represent 20 nm.

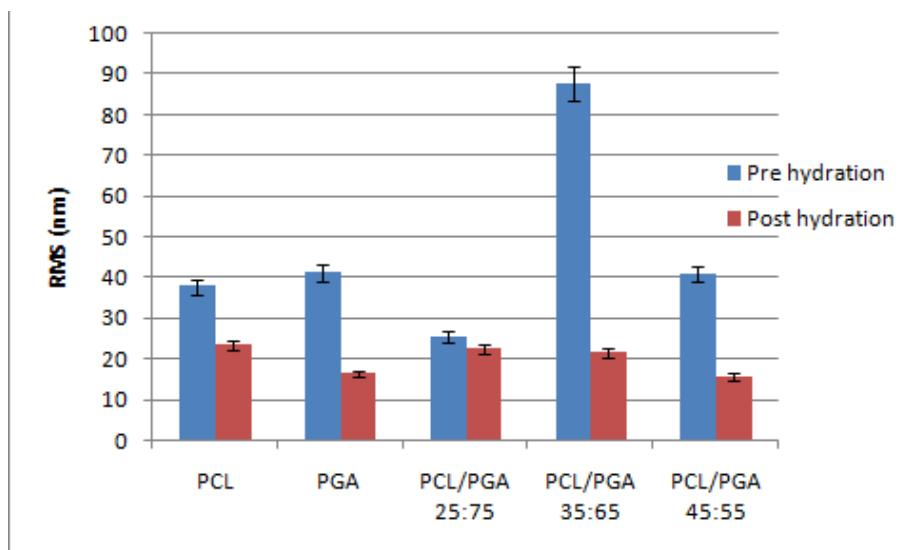


Fig. 4- 8 Roughness of PCL-PGA Films Comparison: Pre- and Post-Hydration. **There are significant drop in surfaces roughness for post-hydrated films. Measurements were done on five readings from each film specimen. Analysis were done using excel student *T-test* ($P < 0.05$)**

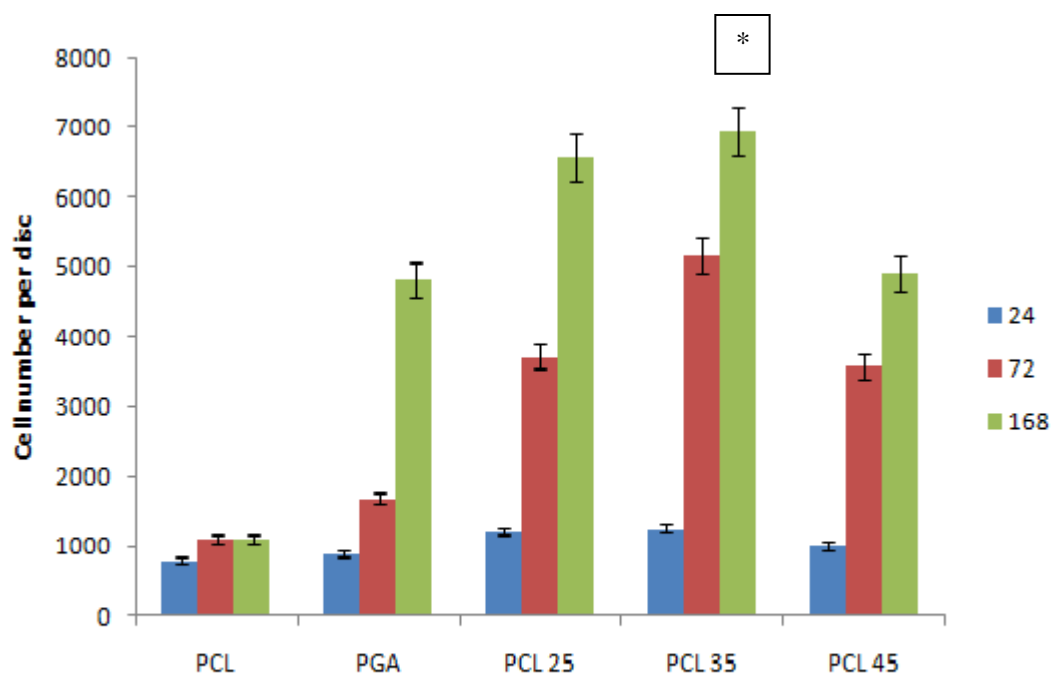
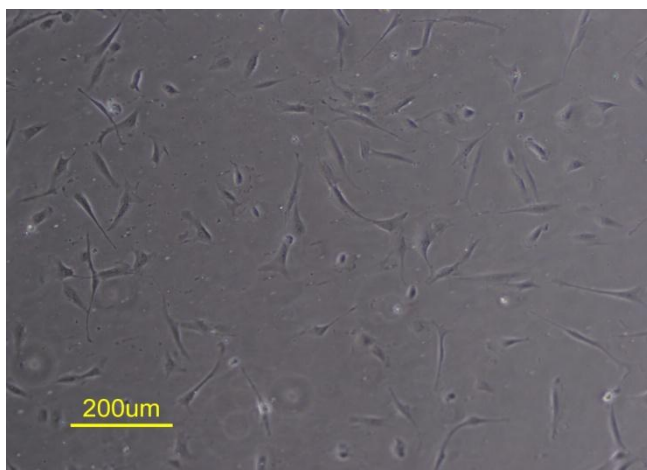
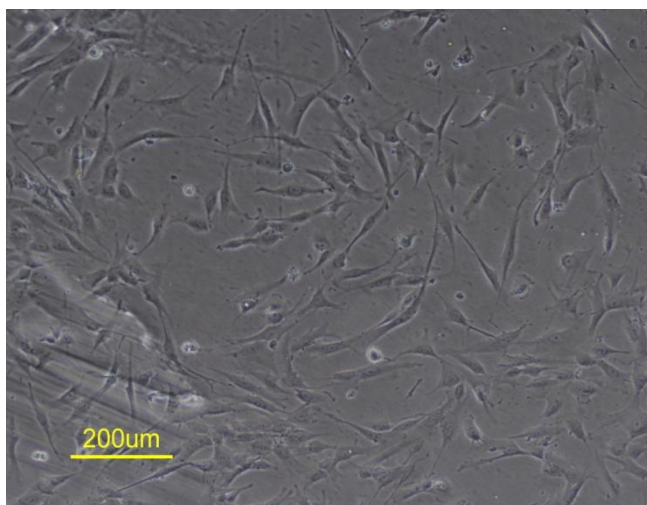


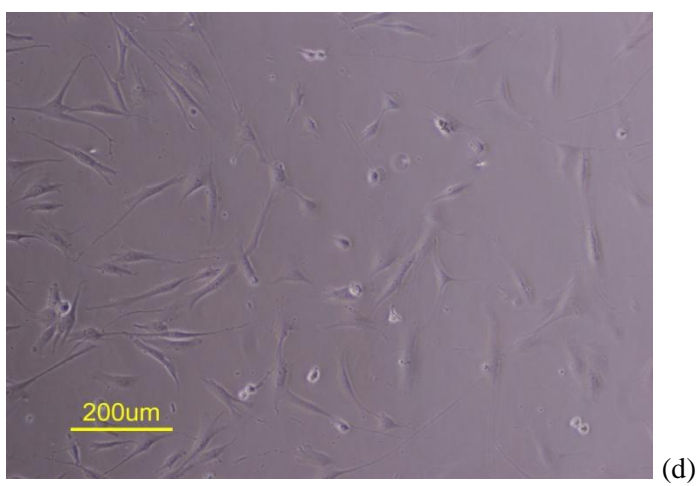
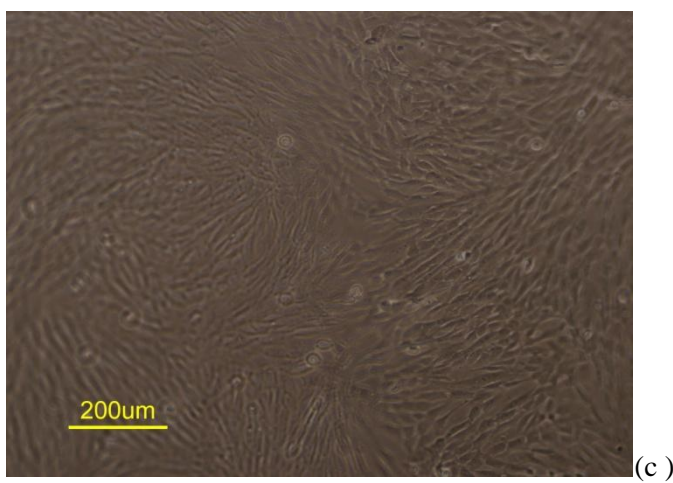
Fig. 4- 9. Roughness Pre-osteoblasts Attachment and Proliferation on PCL-PGA Copolymeric Films at 24, 72 and 168 hours. Cell seeding studies were done on five replicate films and mean of five readings were reported. The cell attachment and proliferation was significantly higher for PCL-35 surfaces, compared to PCL 25 and PCL 45. ($p < 0.05$).



(a)



(b)



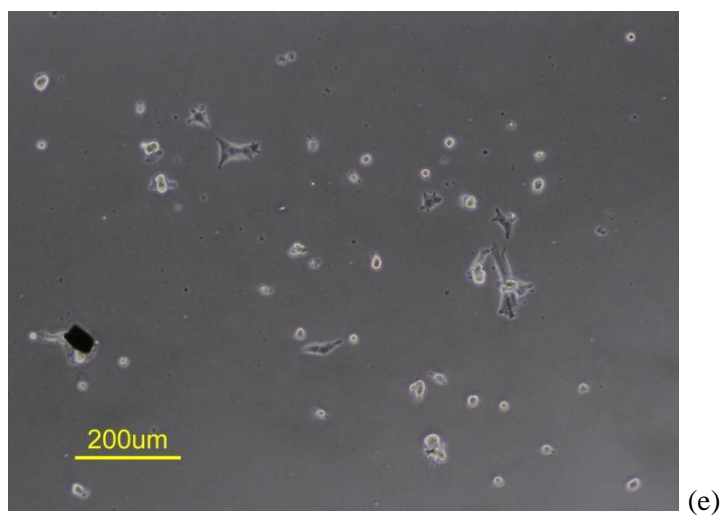
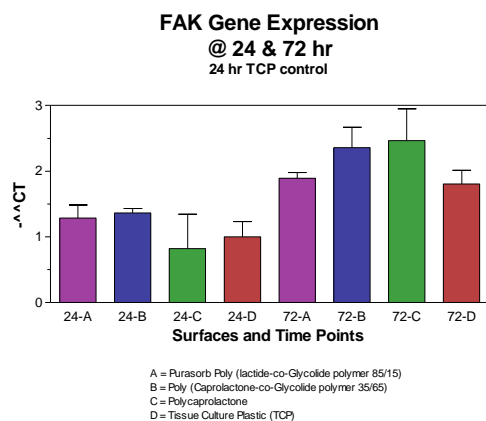


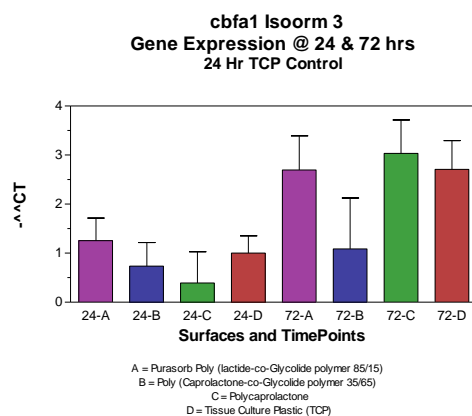
Fig. 4- 10. Osteoblasts morphology (optical microscopy) post seeding on PCL-PGA surface. (a) PCL-PGA 35/65 at 24h, (b) PCL-PGA 35/65 at 72h; (c) PCL-PGA 35/65 at 168h; (d) PCL film at 24h; (e) TCP at 24h



HEPM1486 cells were plated @ 3×10^5 cells/mL/well in two 24-well plates onto five different surfaces: three types of polymers, Healos Bone Graft material and TCP. Triplicate cultures were plated for each surface.

At each time point (24 and 72 hrs), unattached cells were quantitated with the Model Z1 Coulter Counter and RNA was isolated from cultures with RNeasy Kit (Qiagen). Real time PCR was done for comparative gene expression of four genes.

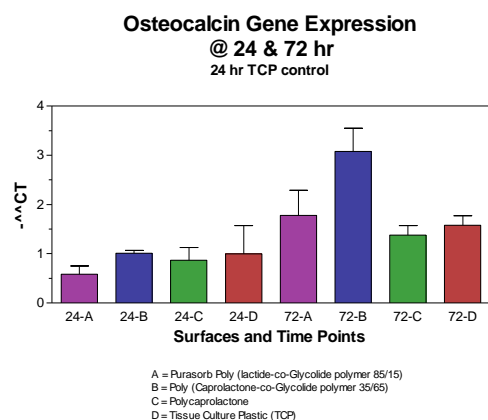
Fig. 4- 11. FAK Gene Expression on PCL and PCL-PGA 35:65 Films at 24 and 72 hours. Statistical analysis (N=5) of $\Delta\Delta$ Ct was performed using a one-way analysis of variance (ANOVA) with a student T-test to a confidence level of $p < 0.05$.



HEPM1486 cells were plated @ 3×10^5 cells/mL/well in two 24-well plates onto five different surfaces: three types of polymers, Healos Bone Graft material and TCP. Triplicate cultures were plated for each surface.

At each time point (24 and 72 hrs), unattached cells were quantitated with the Model Z1 Coulter Counter and RNA was isolated from cultures with RNeasy Kit (Qiagen). Real time PCR was done for comparative gene expression of four genes.

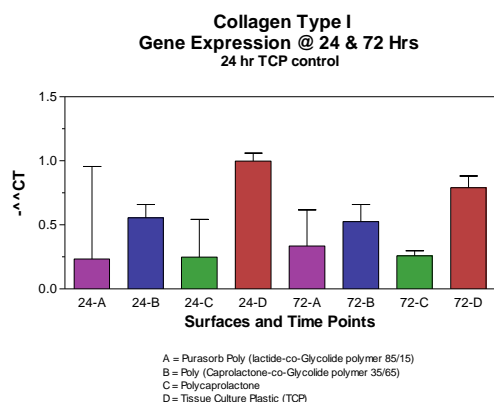
Fig. 4- 12. cbfa-1 Expression on PCL and PCL-PGA 35:65 Films at 24 and 72 hours. Statistical analysis (N=5) of $\Delta\Delta$ Ct was performed using a one-way analysis of variance (ANOVA) with a student T-test to a confidence level of $p < 0.05$.



HEPM 1486 cells were plated @ 3×10^5 cells/mL/well in two 24-well plates onto five different surfaces: three types of polymers, Healos Bone Graft material and TCP. Triplicate cultures were plated for each surface.

At each time point (24 and 72 hrs), unattached cells were quantitated with the Model Z1 Coulter Counter and RNA was isolated from cultures with RNeasy Kit (Qiagen). Real time PCR was done for comparative gene expression of four genes.

Fig. 4- 13. Osteocalcin Expression on PCL and PCL-PGA Films at 24 and 72 hours. There was up regulation of Osteocalcin on PCL 35 surface at both 24 and 72 hours. Statistical analysis (N=5) of $\Delta\Delta$ Ct was performed using a one-way analysis of variance (ANOVA) with a student T-test to a confidence level of $p < 0.05$.



HEPM 1486 cells were plated @ 3×10^5 cells/mL/well in two 24-well plates onto five different surfaces: three types of polymers, Healos Bone Graft material and TCP. Triplicate cultures were plated for each surface.

At each time point (24 and 72 hrs), unattached cells were quantitated with the Model Z1 Coulter Counter and RNA was isolated from cultures with RNeasy Kit (Qiagen). Real time PCR was done for comparative gene expression of four genes.

Fig. 4- 14. Collagen Type I gene expression on PCL and PCL-PGA 35:65 films at 24 and 72 hours. Statistical analysis (N=5) of $\Delta\Delta$ Ct was performed using a one-way analysis of variance (ANOVA) with a student T-test to a confidence level of $p < 0.05$.

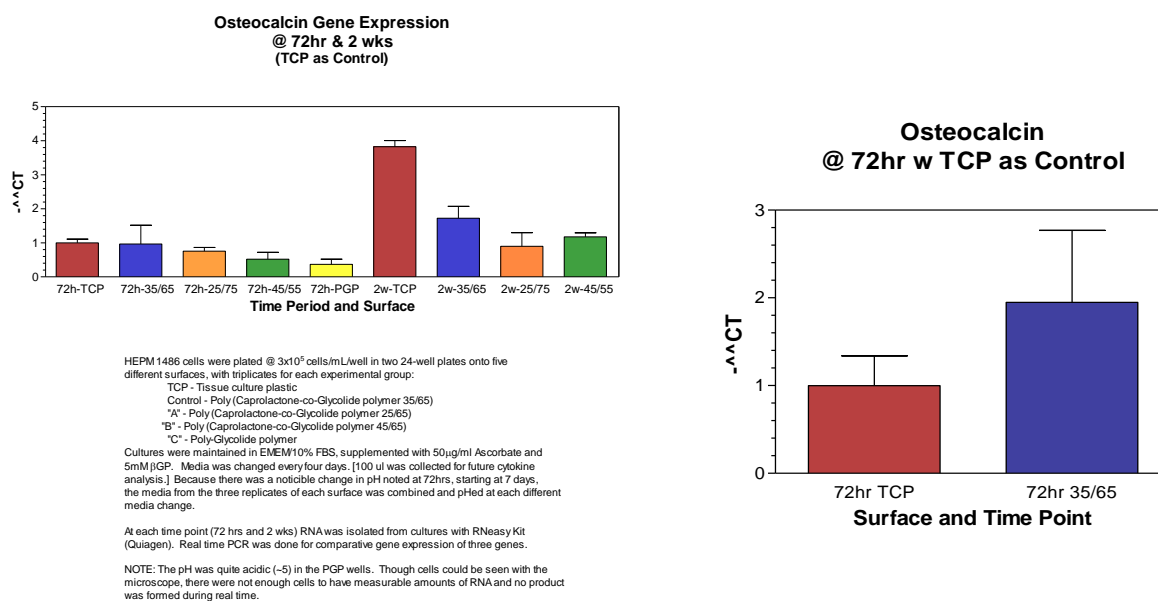


Fig. 4- 15. Osteocalcin Expression on PCL-PGA Series of Polymers at 72 hours and 1 week. There was no up regulation for all the PCL-PGA surfaces tested on any other gene markers, compared to TCP as control. Statistical analysis (N=5) of $\Delta\Delta$ Ct was performed using a one-way analysis of variance (ANOVA) with a student T-test to a confidence level of $p < 0.05$.

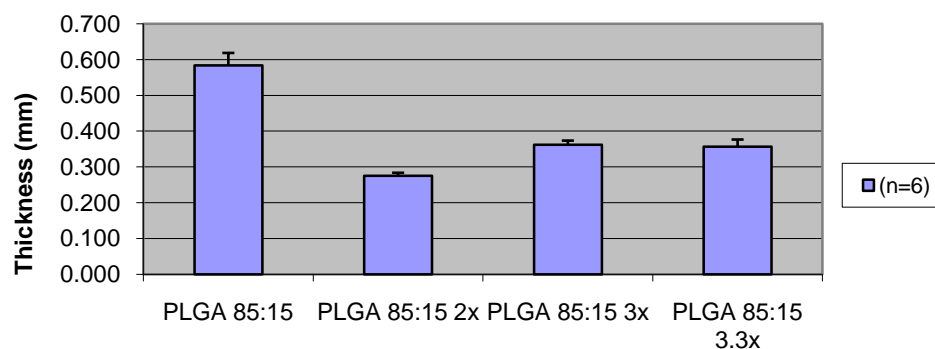


Fig. 4- 16. The Thickness of the PLGA 85:15 films. Mean value of six measurements on each specimen were reported.

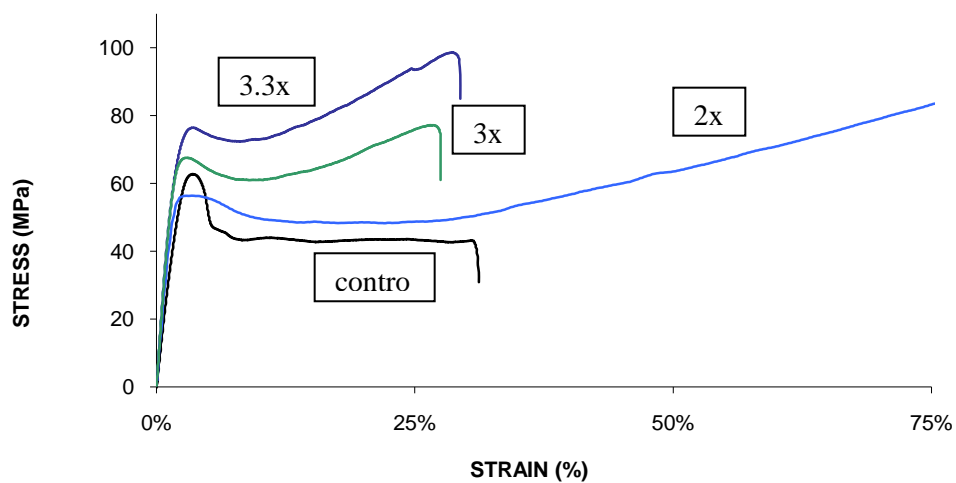


Fig. 4- 17. Effect of the Degree of Stretching on the Tensile Strength and Percentage Elongation of Poly (lactide-co-glycolide) 85:15 Films of Different Degree of Mechanical Stretching. Results are mean of six parallel measurements.

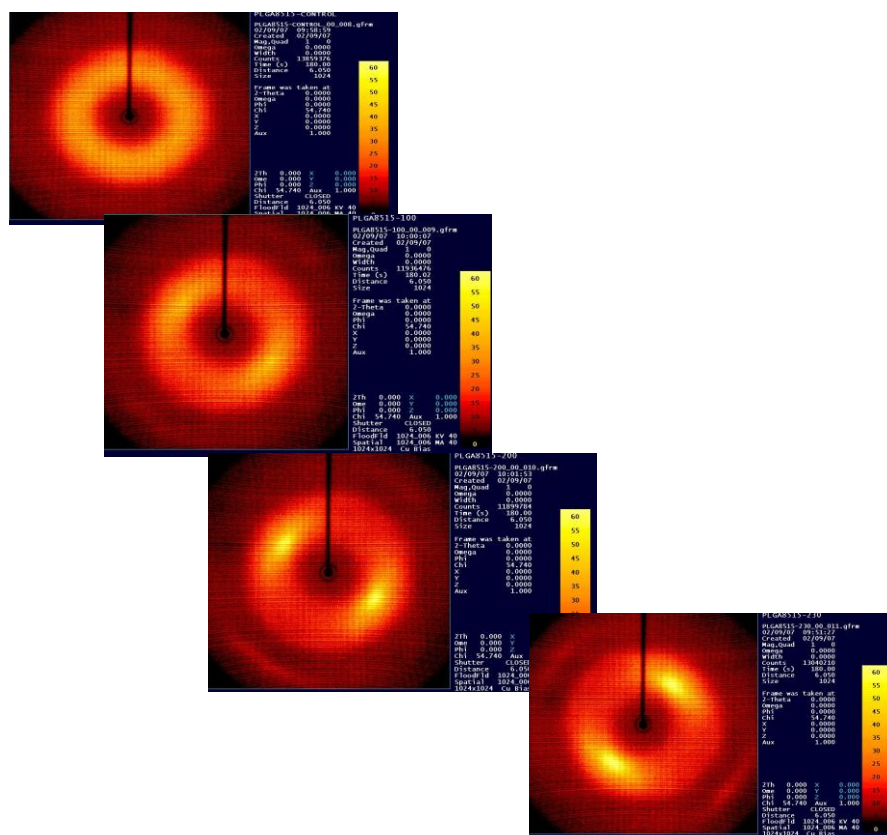


Fig. 4- 18. X-ray Scattered Plot of PLGA 85:15 Films. The intensity of the diffraction ring indicates degree of crystallinity. It is clear that PLGA 85:15 induces crystallinity as degree of stretching increases.

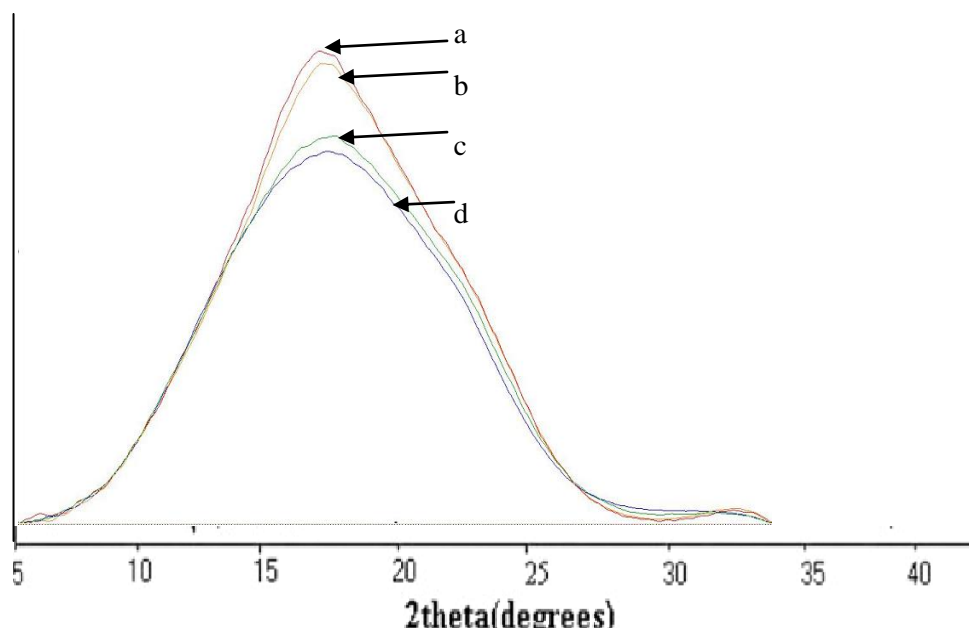


Fig. 4- 19. X-ray Diffraction for PLGA 85:15 Films. (a: 3.3x; b: 3x; c: 2x and d: control). Total area under the diffraction spectrum curve indicated total degree of crystallinity of the specimen. There was induced crystallinity as degree of stretching increases.

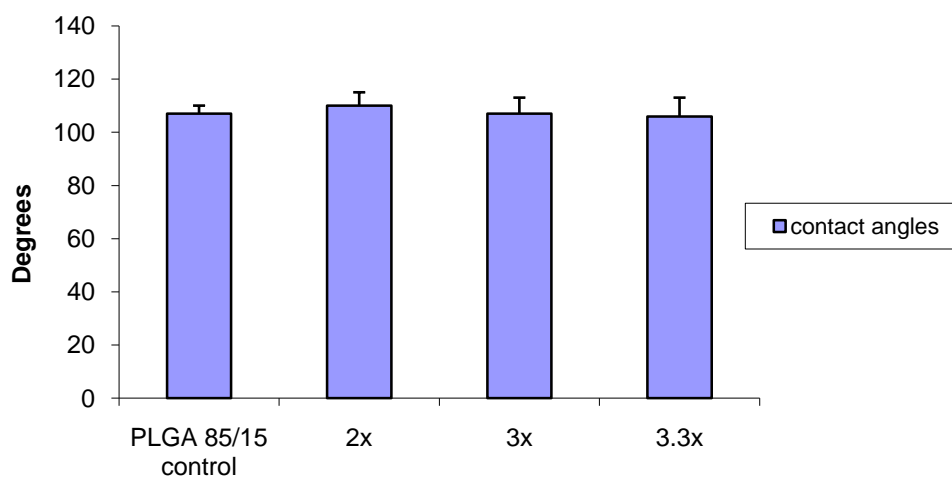
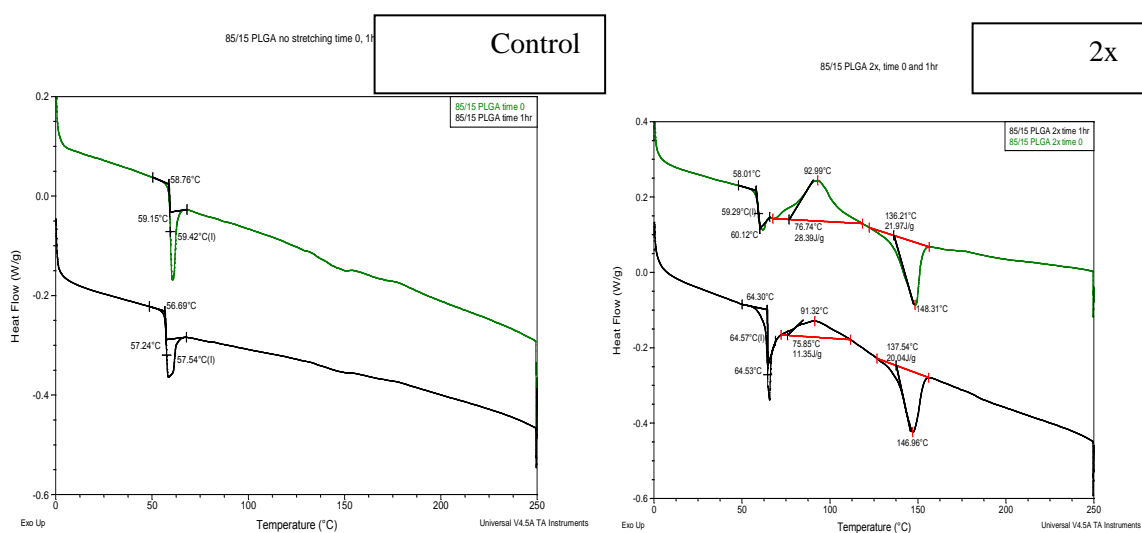


Fig. 4- 20. Contact Angle Measurement of PLGA 85/15 Films with Different Degree of Mechanical Stretching.

Mean value of six readings of advancing contact angles on each film was reported. These surfaces are very similar in terms of hydrophobicity.



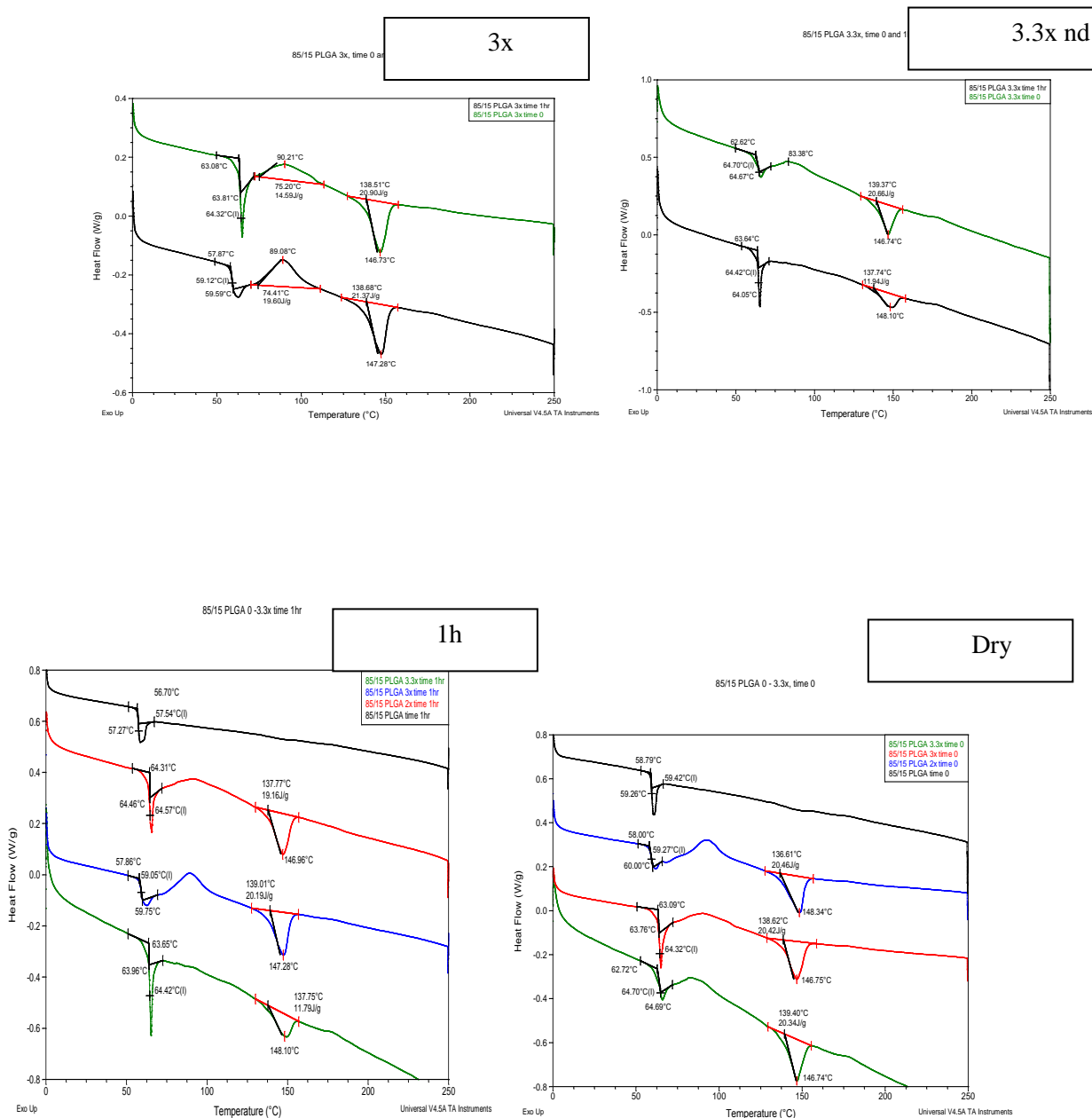


Fig. 4- 21. Kinetic DSC on Films without Hydration and Hydrated for 1h. There was no changes of crystallinity by being submerged in water for 1 hour for PLGA surfaces.

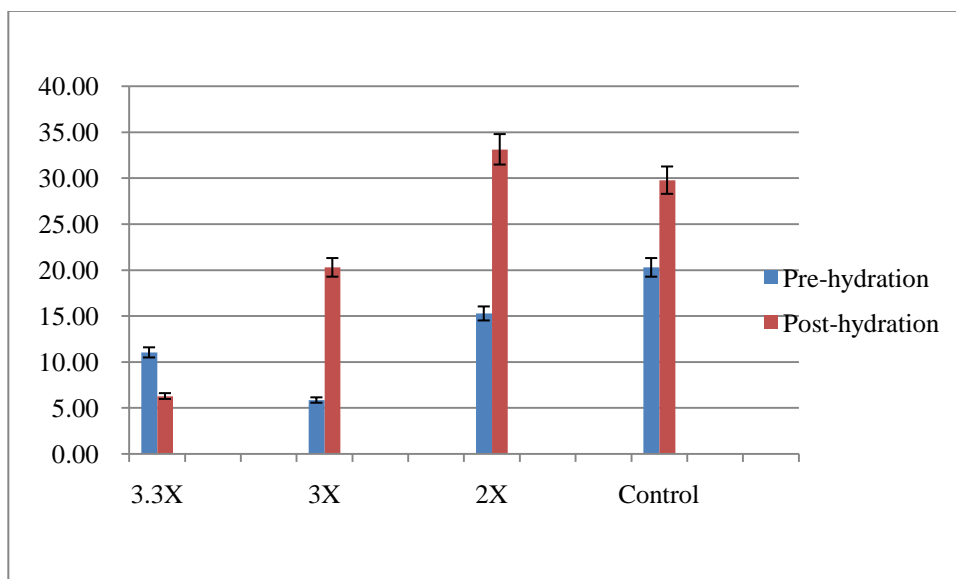


Fig. 4- 22. RMS Roughness for “dry” and “wet” PLGA 85:15 Films. Pre-hydration roughness for PLGA 85:15 is the lower, compared to the post-hydration roughness, except for the 3x films. Mean values are reported from measurements from three films for each material.

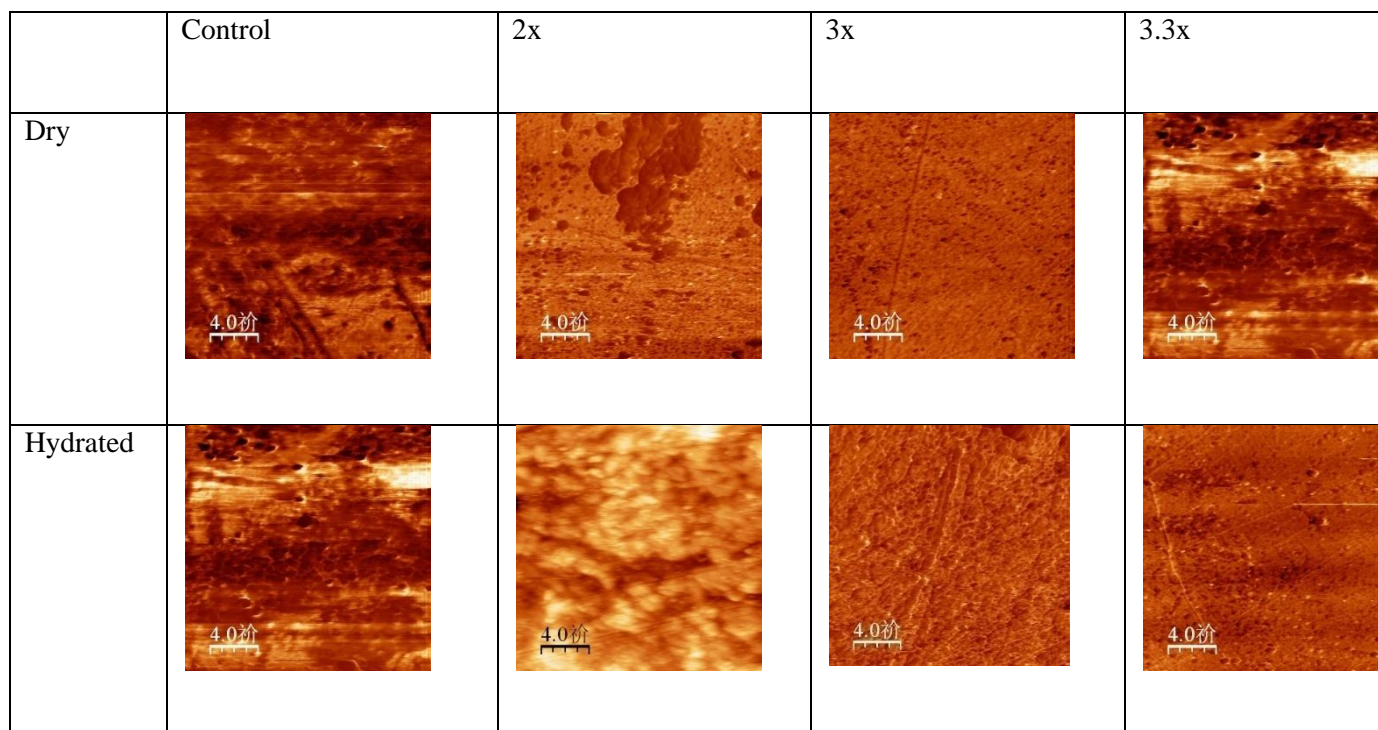


Fig. 4- 23. AFM Nanotopography Images of Dry and Wet PLGA 85:15 Films.

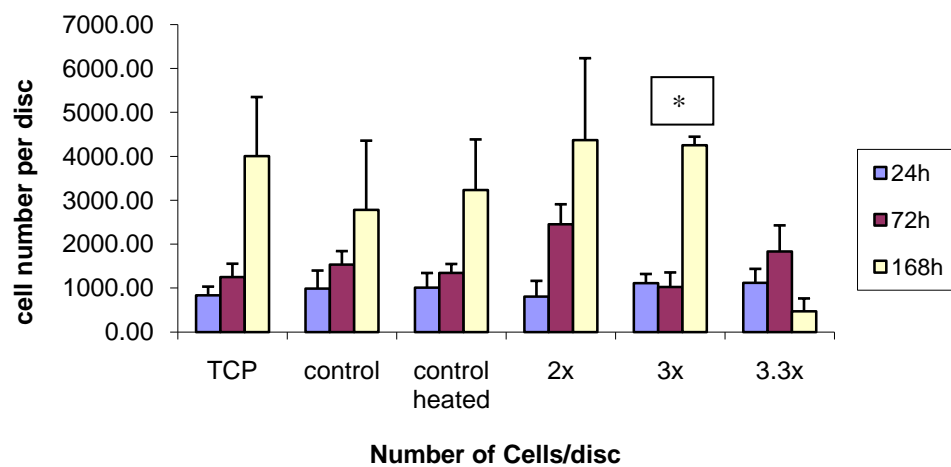


Fig. 4- 24. Pre-osteoblast Cell Attachment and Proliferation on Stretched PLGA 85:15 Films. PLGA 85:15 3x films were significantly better for cell attachment and proliferation at all time points (24h, 72h and 168 h, $P<0.05$).

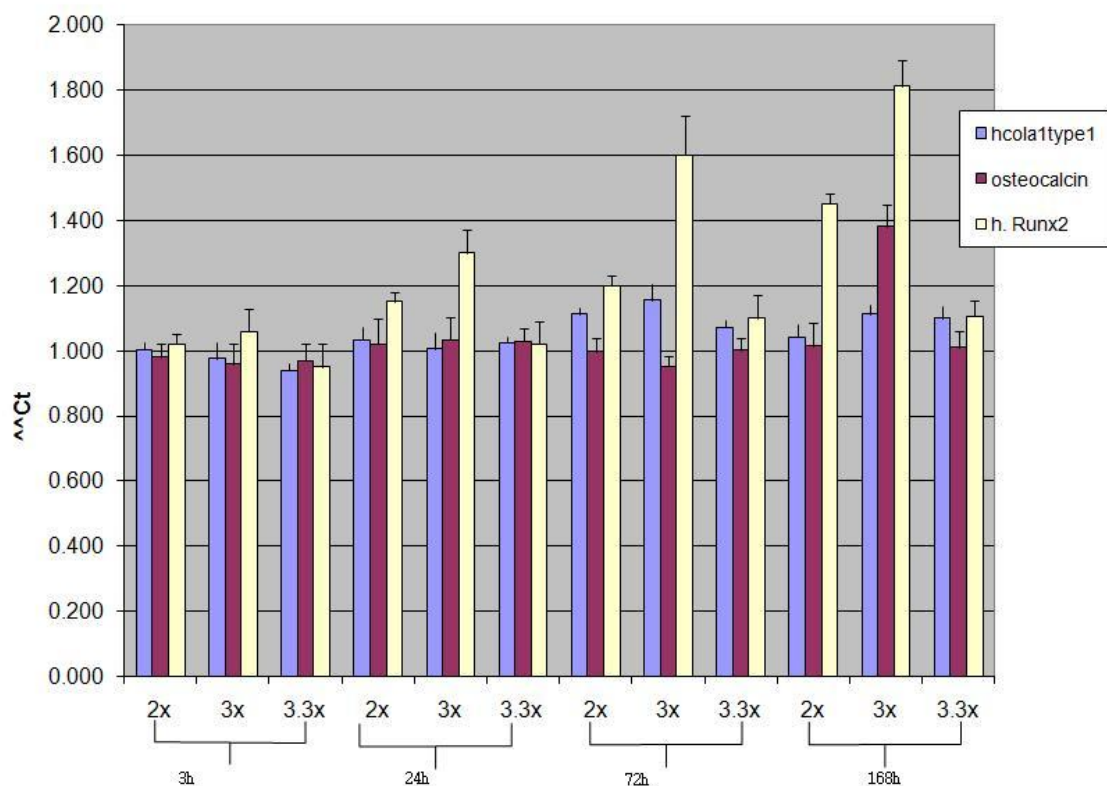


Fig. 4- 25. Osteogenic Gene Expression from PLGA 85:15 Films. PLGA 85:15 (3x film) up regulated Runx 2 at all time points (3h, 24h, 72h and 168 h). Statistical analysis (N=4) of $\Delta\Delta Ct$ was performed using a one-way analysis of variance (ANOVA) with a student T-test to a confidence level of $p < 0.05$.

5 rhGDF-5 ADSORPTION ON POLY(CAPROLACTONE-CO-GLYCOLIDE) SURFACES

5.1 Introduction

This part of the study constitutes part I for the investigation of biological actives interactions with PCL/PGA substrates.

Local delivery of GDF through a scaffold offers several advantages, because 1) it provides GDFs at a desirable concentration within their therapeutic window at the site where they are needed without eliciting potential toxicity associated with systemic delivery; 2) Carrier matrices also delay the otherwise rapid dispersion of the water-soluble, readily diffusible GDFs from the implant site without which, they, like other protein therapeutics, would likely have a short serum half life because of liver uptake and catabolism; and 3) the scaffold is a 3-D matrix suitable for permitting tissue ingrowth and regeneration.

Various materials, including inorganic materials [99-100], synthetic polymers [101-103], natural materials [104-105], and its combination [106] have been tested as promising GDF carriers. However, reproducible sourcing and processing, the possibility of contamination with adventitious agents, and the potential for immunogenicity associated with natural materials has moved the field in the direction of synthetic materials. Commonly used synthetic materials include calcium phosphates (such as hydroxyapatite,

tricalcium phosphate and cements), and synthetic polymers such as the poly α -hydroxyl acids (e.g. polylactide, polyglycolide and their copolymers). Many of these materials lack optimal biological properties, thus composites of them are also used. Many of the delivery systems designed for GDFs and other bone inducing factors were used as carriers for GDF as well as scaffolds for bone formation. The appropriate choice of the delivery system for a particular growth factor is essential to induce a specific biological effect, as demonstrated by several examples in the literature, where failure of bone repair was associated with the type of delivery device. For example, locally administered solutions of bFGF did not promote bone regeneration in rabbit skull defects in contrast to bFGF incorporated in gelatin hydrogels [107]. Failure of BMP in an insoluble bone matrix to induce bone growth around titanium implants was attributed to unsuitable carrier properties [108]. Finally, locally applied IGF-1 failed to induce bone repair when delivered by an osmotic pump directly into the osteotomy [109-110], but was successful when embedded in biodegradable microspheres to heal segmental long bone defects [111]. But there are few reports concerning the effect of the controlled release of GDFs from a carrier on bone formation in surrounding tissue, nor are there reports concerning the 3D structural conformation of the GDF, which usually translates into protein stability and bioactivity, after being incorporated into the scaffold.

rhGDF-5 is a human analogue of growth and differentiation factor-5 (GDF-5) which is a homodimer of two 119-amino acid residue monomers. rhGDF-5 is a disulphide cross linked homo-dimer with each monomer having seven (7) cysteine residues, which is common for other growth factors from the transforming growth factor beta (TGF- β) super family [157]. These seven cysteine residue in each monomer form three intra molecular (monomer) disulfide bonds and one intermolecular disulfide bond (Figure 2-1). The multiple cystine residuals, especially those that are located on the surface of the molecules, created multiple opportunities for the occurrence of disulphide exchange.

The adsorption isotherm is a function that relates the measured adsorbed amount of a protein (per unit area), Γ_p , to the solution concentration of protein, c_p . Typically, Γ_p increases sharply at low solution concentrations of protein and levels off at higher protein concentrations approaching a limiting Γ_p value. The existence of a Γ_p adsorption “plateau” has been interpreted as a sign that the adsorbing surface is “saturated” with protein molecules; any further increase in the solution protein concentration typically does not affect Γ_p . The amount of adsorbed protein at the “plateau” of the adsorption isotherm is often close to the amount that can fit into a closed-packed monolayer; hence, the notion of a saturating monolayer coverage is often applied to protein adsorption [69]. The adsorption of rhGDF-5 to PCL-PGA substrates for the present study was conducted using high protein concentrations (0.7 mg/mL) to allow the maximum adsorption to that particular surface. The study was under the assumption that adsorption isotherm was not

referring to the identical molecules, i.e. protein might encounter conformation changes upon adsorption. It reflects the competition between various protein conformations for a limited adsorption surface area [50, 69, 158].

The radioisotope of iodine (^{125}I) is selected as a probe for the quantitative determination of the amount of protein adsorbed to the PCL-PGA surfaces for the following reasons: elemental iodine is chemically reactive; it can be bonded covalently to protein; an iodine atom is relatively small, so it is expected to have minimal influence on protein properties; radiation from ^{125}I is detected easily; and handling of ^{125}I can be reasonable safe. ^{125}I emits strong γ -radiation with the energy of 35 KeV during its conversion to ^{125}Te . The half-life of the radioisotope (59.6 days) gives a good balance between the efficacy of radioactivity detection and safety [159].

Solution depletion, as one of the simplest methods to study protein adsorption, was used for our studies. Concentration changes in bulk solution prior to and after adsorption, ΔC_p . In the solution depletion technique, any protein concentration change is attributed to the adsorbed layer, i.e., $\Gamma_p = \Delta C_p V / A_{tot}$, where V is the total volume of protein solution and A_{tot} is the total area available for adsorption.

In this study, PCL-PGA substrates and PLGA 85:15 substrates were used. rhGDF-5 and reduced rhGDF-5 were adsorbed under non-competitive (single protein solution) conditions [160-161]. Their behavior was compared at different levels: adsorbed amount (radiolabelling), displacement (elution studies), and nanotopographic analysis (AFM).

The trend observed for rhGDF-5 adsorption was correlated with underlying materials' physicochemical properties.

5.2 Materials and methods

5.2.1 Materials

rhGDF-5 was obtained from Biopharm GmbH (Germany). HPLC Water (JT Baker Catalog no. 4219 or equivalent), Acetonitrile (JT Baker Catalog no. 9017 or equivalent), Trifluoroacetic Acid, Sequanal Grade (Pierce Catalog no. 28904), Urea (Sigma Catalog no. U5378 or equivalent), Tris Base (JT Baker Catalog no. 4109 or equivalent), Sodium Chloride (Sigma Catalog no. S-7653 or equivalent), 5 N HCl (JT Baker Catalog no. 5618 or equivalent), 2-mercaptoethanol (Biorad Catalog no. 161-0710), rhGDF-5 Reference Iodine monochloride, ICI (carrier free, 97%, Amersham Life Science, Cleveland, OH), PD-10 minicolumn (Pharmacia Piscataway, NJ), Standard Purified water from a Millipore "Milli-Q" Water Purification System were obtained as indicated. BCA protein assay kit was obtained from Thermo Scientific, Rockford, IL, USA. Trichloroacetic acid (TCA, Sigma, St. Louis, MO, USA) and a Minicentrifuge (Model 235A, Fisher) were used in these studies. An Agilent 5834 UV-Vis spectrophotometer was used for the BSA assays. An Agilent 1100 HPLC was used for the reduced protein identification assays where a Discovery C18, 2.5 mm X460 mm, 5 μ m column was used. The radioactivity of 125 I] GDF-5 was measured using a Wallac 1409 Liquid Scintillation Counter (LSC)

(Wallace Oy, Turku, Finland). All other reagents were obtained from Sigma-Aldrich (St. Louis, MO, USA) unless otherwise described.

5.2.2 rhGDF-5 adsorption to PCL-PGA surfaces

5.2.2.1 Radiolabelling rhGDF-5 using Iodine monochloride (ICL)

A protocol from McFarlane [162] was used for rhGDF-5 labeling. A 2-mL solution of 0.7 mg/mL rhGDF-5 solution in 0.1N HCL, freshly made 25 μ L of 1mM ICL in pH 8.5 glycine buffer, and 1mCi of Na¹²⁵I are mixed together. The iodination reaction takes place at 4° for 1 hr. The reaction mixture is eluted through a PD-10 minicolumn with 0.01 M PBS and a 2-mL fraction is collected after the first eluted 2.5 mL. The protein concentration was determined by measuring the UV absorption at 280 nm.

The degree of rhGDF-5 labelling is computed from the protein and protein-bound ¹²⁵I concentrations. Total ¹²⁵I in protein solution is determined by measuring solution radioactivity and comparing it with the ¹²⁵I standard. The amount of free ¹²⁵I present in ¹²⁵I-labeled rhGDF-5 solution is determined using protein precipitation in trichloroacetic acid (TCA, sigma, St. Louis, MO). The control sample is made of a mixture of 45 μ L of bovine serum albumin (BSA) solution (20mg/mL), 50 μ L of PBS, and 5 μ L of TCA (20% solution), and 5 μ L of ¹²⁵I-labeled rhGDF-5 solution. Both samples are centrifuged at 15,000 rpm in a minicentrifuge for 10 min. Five microliters of both the control sample and supernatant of the precipitated test sample are counted for γ -radiation using the γ -

counter. The ratio of radioactivity in the supernatant of the precipitated sample to that in the control should be less than 0.05, i.e., less than 5% total ^{125}I is free in solution.

5.2.2.2 rhGDF-5 adsorption to PCL-PGA films

An adsorption study was done by adding ^{125}I labeled rhGDF-5 in 10mM HCl, 10mM HCl (82 μl of conc. HCL into 100 ml distilled water) and mixed well into 2.0 ml Siliconized Eppendorf tubes. 3mm diameter disks of each type of polymer matrix were punched out by a polymer punch. Each disk was weighed and the approximate surface area measured. One disk of each matrix sample was placed into one 2ml siliconized tube. Two disks of each matrix sample were also placed into duplicate tubes, making sure that the disk or 2 disks (per duplicate tubes) stay in the bottom of the vial. The discs were pre-wetted with 0.5ml 10mM HCl for ten to fifteen minutes. The 10mM HCl was removed by pipetting. A pre-prepared 2.4 ml radioactive protein probe containing 0.7mg/ml rhGDF-5, 10mM HCl and about 8×10^8 dpm [^{125}I] labeled rhGDF-5 were made. The concentration of the rhGDF-5 protein is approximately 4.76×10^5 dpm/ μg or 2.1×10^{-6} μg /dpm. 200 μl of the radioactive protein solution (containing 140 μg of rhGDF-5 and 6.7×10^7 dpm) was aliquoted into the sample tube with matrix disk(s) added. The test sample tube was incubated at 37°C for 1 hour with occasional mixing.

At the end of the protein adsorption step, the films were washed with 1ml of 10mM HCl for 1 minute. The 10mM HCl were removed by pipetting. The washing step was repeated for a total of four times.

5.2.2.3 rhGDF-5 displacement (desorption)

The desorption/release medium was 0.25mL of 10mM HCL due to the solubility of the protein. 2 disk were placed into 2ml siliconized tubes containing 0.25ml of 10 mM HCl allowing the rhGDF-5 protein to desorb for 0.5 hours, 2 hours, 5 hours, 12 hours and 24 hours at a temperature of 37 °C, under gentle agitation.

The concentration was determined by reading the radioactivity in a γ -radiation counter.

5.2.2.4 AFM for rhGDF-5 modified PCL-PGA surfaces

AFM nanostructure imaging on rhGDF-5 modified surfaces used the same protocol as explained in section 4.2.3.4 on P 45.

5.2.3 Reduced rhGDF-5 adsorption to PCL-PGA surfaces

5.2.3.1 Reduction of rhGDF-5 and characterization

rhGDF-5 is dried down and reconstituted in 8 M urea buffer adjusted to pH 8.0 with 5 N Sodium Hydroxide (NaOH). The sample is reduced using β -mercaptoethanol, and incubated for approximately 1 hour at 37°C.

The rhGDF-5 sample is analyzed using RP-HPLC. The identity, purity and percent oxidation of each sample is determined against a reference standard using the peak area and retention time.

5.2.3.2 Adsorption of reduced rhGDF-5 on PCL-PGA surfaces

The adsorption protocol was the same as in section 5.2.2.2 on P108.

5.2.3.3 AFM for reduced rhGDF-5 adsorbed surfaces

The AFM was done using the same protocol as described in section 4.2.3.4 on P45.

5.2.4 PLGA 85:15 interaction with rhGDF-5 and reduced rhGDF-5

5.2.4.1 Adsorption

The adsorption study was done using the same protocol as in section 5.2.2.2. on P108.

5.2.4.2 AFM

The AFM was done using the same protocol as described in section 4.2.3.4 on P 45.

5.3 Results and discussions

5.3.1 rhGDF-5 adsorption and desorption from PCL-PGA substrates

The rhGDF-5 adsorbed onto PCL-PGA were 117.2 ± 9.6 (N=3), 35.9 ± 5.7 (N=3), 29.8 ± 3.3 , 20.7 ± 3.0 ng and 16.8 ± 4.8 ng of rhGDF-5 per film for the samples of PCL, PCL-PGA 45:55, PCL-PGA 35:65, PCL-PGA 25:75 and PGA films, respectively (Figure 5-1). This superficial adsorption onto the pre-formed discs at $700 \mu\text{g/mL}$ rhGDF-5 resulted in significantly lower protein adsorption, compared with the starting rhGDF-5 solution concentrations. It has shown that the most rigid material, PGA, adsorbed the least amount of rhGDF-5, whereas the softest material among this series of copolymers, PCL-PGA

45:55, adsorbed the highest amount of rhGDF-5. However, the most amount of rhGDF-5 was adsorbed to PCL, which possesses the optimal balance of softness and rigidity.

For all PCL-PGA films, there is a trend that demonstrated that there is a similar rate of protein desorption from these surfaces. In addition, the more protein adsorbed onto the films, the greater percentage of the protein desorbed from the surfaces (Figure 5-2). However, the majority of the protein stayed with the surface after 24 hours in the in vitro release studies (greater than 50%).

5.3.2 Reduced rhGDF-5 adsorption to PCL-PGA films

Reduction of rhGDF-5:

rhGDF-5 solution (2mL) was reduced using 100 μ L of β -mercaptoethanol, and incubated for approximately 1 hour at 37°C. The rhGDF-5 sample was analyzed using RP-HPLC (Agilent 1100, San Francisco, USA). The identity, purity and percent oxidation of each sample was determined against a reference standard using the peak area and retention time.

A rhGDF-5 reduction protocol was followed and protein was fully reduced as indicated by the HPLC results shown in Figure 5-3.

rhGDF-5 was adsorbed to PCL-PGA series of films such that the higher the the higher the PGA content, the less rhGDF-5 adsorption. There was 117.2 ± 9.6 , 35.8 ± 5.6 , $29.8 \pm$

3.3, 20.7 ± 3.9 and 16.8 ± 4.8 ng/ bound per disc on PCL, PCL-PGA 45:55, PCL-PGA 35:65, PCL-PGA 25:75 and PGA respectively. A greater amount of reduced rhGDF-5 adsorbed on all these surfaces. There was 222.2 ± 14.2 , 71.7 ± 3.7 , 35.4 ± 5.9 , 37.4 ± 3.9 and 40.4 ± 4.2 ng reduced rhGDF-5 bound per disc on PCL, PCL-PGA 45:55, PCL-PGA 35:65, PCL-PGA 25:75 and PGA respectively. For each PCL-PGA material studied, a greater amount of reduced rhGDF-5 adsorbed on that surface than seen with neat rhGDF-5. But the same trend governs both rhGDF-5 adsorption and reduced form adsorption across all the PCL-PGA surfaces studied, namely the more PGA composition in the polymer, the less rhGDF-5 adsorption.

5.3.3 AFM for rhGDF-5 and reduced rhGDF-5 adsorbed PCL-PGA substrates

Surface roughness for all reduced rhGDF-5 adsorbed PCL-PGA surfaces decreased, except PCL 35:65. The RMS roughness for rhGDF-5 adsorption was 67.8 ± 15 , 44.9 ± 15 , 44.9 ± 20.7 , 68.8 ± 4.4 and 45.5 ± 5.6 nm for PCL, PCL 25, PCL 35, PCL 45 and PGA surfaces, respectively (Figure 5-5 and Figure 5-6). The RMS roughness for reduced rhGDF-5 adsorption was 45.2 ± 7.0 , 27.8 ± 10.6 , 77.1 ± 16.5 , 32.3 ± 6.3 and 40.6 ± 2.5 nm for PCL, PCL 25, PCL 35, PCL 45 and PGA surfaces, respectively (Figure 5-7). Because reduced protein is much more flexible than the neat protein, they adsorbed to surfaces in a unfolding state and exhibited more smooth surface nanotopography, than their rigid “neat” GDF-5 counterpart. The exception is PCL 35 on which the reduced

protein surfaces is rougher than rhGDF-5 coated surface. The surface nanotopography images are shown in Figure 5-8.

5.3.4 rhGDF-5 adsorption and desorption from PLGA 85:15 substrates

rhGDF-5 was adsorbed to PLGA 85:15 series of films in a way that the greater the degree of induced crystallinity, the more rhGDF-5 adsorption on that PLGA surface. There was 61.8 ± 7.9 , 80.6 ± 6.1 , 92.8 ± 3.4 and 100.9 ± 12.9 ng rhGDF-5 per disc on PLGA 85:15, 2x stretching, 3x stretching and 3.3 x stretching films respectively. Greater amount of reduced rhGDF-5 adsorbed on all these surfaces. There was 277.5 ± 25.3 , 252.9 ± 34.7 , 269.1 ± 22.1 , and 386.5 ± 19.6 ng reduced rhGDF-5 per disc on PLGA 85:15, 2x stretching, 3x stretching and 3.3 x stretching films respectively (Figure 5-9). For each PLGA 85:15 materials studied, greater amount of reduced rhGDF-5 adsorbed on that surface than the neat rhGDF-5 adsorbed. This superficial adsorption onto the pre-formed discs at 700 μ g/mL rhGDF-5 resulted in significantly lower protein adsorption, compared with the starting rhGDF-5 solution concentrations. But the same trend governs both rhGDF-5 adsorption and reduced form adsorption across all the PLGA surfaces studied, namely the higher the degree of the induced crystallinity of the PLGA 85:15 polymers, the more rhGDF-5 adsorption.

For all PLGA 85:15 films, there is a trend which demonstrated that the tighter the protein adsorbed onto the films, the slower the release was (Figure 5-10). In increasing order of rhGDF-5 adsorption onto PLGA 85:15, 2x stretched, 3x stretched and 3.3x stretched, the

release is in decreasing order from these surfaces. However, the majority of the protein stayed with the surface after 24 hours in the in vitro release studies.

5.3.5 AFM for rhGDF-5 and reduced rhGDF-5 adsorbed PLGA 85:15 substrates

Surface roughness for all reduced rhGDF-5 adsorbed PLGA surfaces decreased, except PLGA 3x stretched surfaces. The RMS roughness for rhGDF-5 adsorption was 26.8 ± 12.1 , 21.7 ± 14.6 , 28.9 ± 7.4 and 28.8 ± 6.4 nm for PLGA 3.3x, 3x, 2x stretched and PLGA control surfaces respectively. The RMS roughness for reduced rhGDF-5 adsorption was 21.6 ± 14.7 , 27.1 ± 2.7 , 12.8 ± 3.2 and 9.2 ± 2.0 nm for PLGA 3.3x, 3x, 2x stretched and PLGA control surfaces respectively (Figure 5-11). Because the cysteine knot was opened upon reduction, rhGDF-5 (reduced form) possessed a much more flexible form than the neat protein. The reduced protein adsorbed to surfaces in an unfolded state and exhibited more smooth surface nanotopography, than the rigid “neat” GDF-5 counterpart. The exception is PLGA 3x stretched surface on which the reduced protein surfaces is rougher than rhGDF-5 coated surface. The surface nanotopography images are shown in Figure 5-12.

Studies have shown rhGDF-5 can modulate various cell types towards collagenous soft tissue when applied to a 3D polymeric tissue engineering scaffold. It is known that interfacial reaction occurring when a material contacts a biological environment are modulated by the surface and the biomolecules, such as proteins. The effect of surface properties on the adsorption of proteins was examined with the goal of creating

biomimetic surfaces to improve surface recognition by cells. However, no mechanistic studies have been performed to investigate how rhGDF-5 interacts with polymeric materials. In this study, the capacity of rigidity induced materials to influence protein adsorption and cellular responses was assessed. The degree of binding of two model proteins (rhGDF-5 and Fn) were carried out using an indirect method using a colorimetric protein (BCA) assay and radio-labeling assay as previously described. Our protein adsorption/desorption studies have shown that rhGDF-5 adsorption was maximized on PCL surfaces, while adsorption was minimized on PGA surfaces. The relation between protein adsorption and contact angle/surface energy/morphology/nanotopography is controversial in the literature; it has been shown that decreasing surface hydrophilicity leads to lower protein adsorption and in contrast, it has also been reported that increasing surface energy leads to lower adsorption. In our studies, surface hydrophobicity didn't play a significant role in protein adsorption. It was previously discovered by researchers that rigidity of the materials also contributed to protein adsorption and cell spreading. Nanotopography did not play a significant role in altering protein deposition onto surfaces, due to similar nanotopography for all hydrated PCL-PGA surfaces. In our studies, we believe that the underlying reason for rhGDF-5 adsorption being maximized on PCL surface could be due to an effect of crystallinity. rhGDF-5 is a rather rigid protein due to the presence of seven di-sulfide bonds, six intramolecular di-sulfide bonds and one inter-molecular di-sulfide bond. The protein will remain in its native structure (dimers) while approaching the material surfaces. The PGA surface also carries a neutral charge.

There was the least amount of rhGDF-5 adsorbed to PGA surfaces which might be due to the surface topography. Since PGA surfaces post hydration possessed the highest surface roughness, rhGDF-5 might be least efficient in covering this rough surface and aligning themselves. While PCL surfaces possess the most level surface (least nano-voids), suggesting that rhGDF-5 will be able to exert its maximum surface coverage on a very smooth surface. On the other hand, for surfaces which have a lot of nano-voids, rhGDF-5 will have difficulty finding a “landing spot” so that it can cover the surface.

Reduction of rhGDF-5 resulted in a higher amount of adsorption onto PCL-PGA surfaces. This again correlates with the fact that more flexible and more hydrophilic proteins will be able to absorb themselves in an unfolded state onto the substrates. The trend of adsorption of both reduced rhGDF-5 and unreduced rhGDF-5 on PCL-PGA surfaces indicated that material properties play a minor role in determining how protein interact with surfaces. In addition, the more flexible reduced form of rhGDF-5 will exert much higher number of contact points with the underlying substrates, in correlation with other researchers' findings [163-166]. The reduced rhGDF-5 adheres to the surfaces in a monolayer fashion, which is why the post-adsorption roughness is much lower for all the PCL-PGA surfaces (Fig. 5-7 and Fig. 5-8).

As in the case of PCL-PGA 35:65, 25:75 and PCL-PGA 45:55, once rhGDF-5 adsorbs onto the surfaces, desorption occurs at a similar rate, suggesting the desorption from all

PCL-PGA films involves a common factor, probably in that hydrophobicity plays its unifying role in detaching proteins from these surfaces.

5.4 Conclusions

rhGDF-5 adsorption studies demonstrated that rhGDF-5 adsorbed to a high extent to PCL surfaces and least on PGA surfaces. rhGDF-5 adsorption on PLGA 85:15 with variable induced-crystallinity demonstrated slight changes in the amount of protein adsorption to these substrates. Collectively, these results indicated a slight impact of substrate crystallinity of surfaces on rhGDF-5 adsorption, as shown from both PCL-PGA and PLGA systems.

However, when a reduced-form of rhGDF-5, a more hydrophilic and flexible molecule, was used in adsorption studies on both PCL-PGA and PLGA systems, the amount of adsorbed protein was significantly increased (doubled for PCL-PGA polymers and tripled for PLGA polymers) on all surfaces. These results demonstrated that the conformation and hydrophobicity of rhGDF-5 played a major role in its adsorption to PCL-PGA surfaces.

5.5 Figures

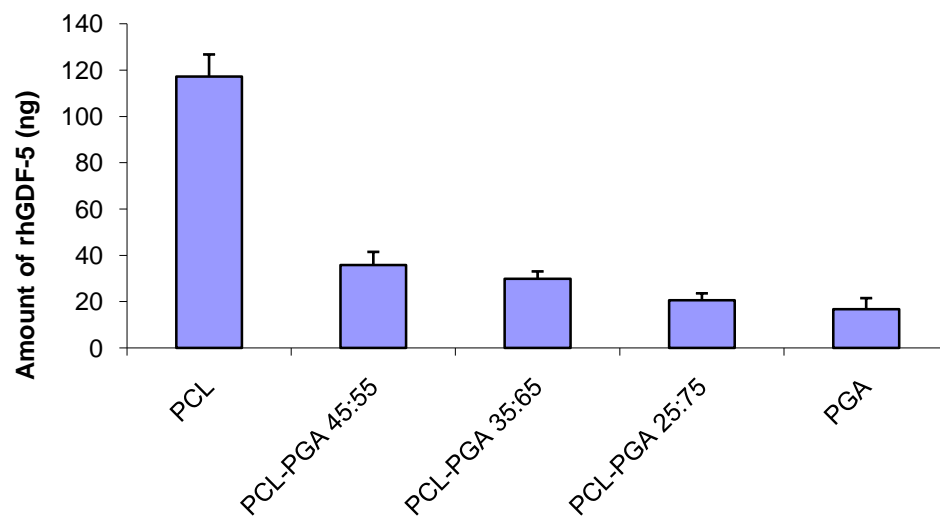


Fig. 5- 1 rhGDF-5 Adsorption onto PCL-PGA Films. The more PGA content in the substrate, the less amount of rhGDF-5 adsorbed to that material. There are six-folds of the amount of rhGDF-5 adsorbed to PCL (maximum amount of adsorption) than to PGA (least amount of adsorption). Adsorption studies were done on three replicate films for each material.

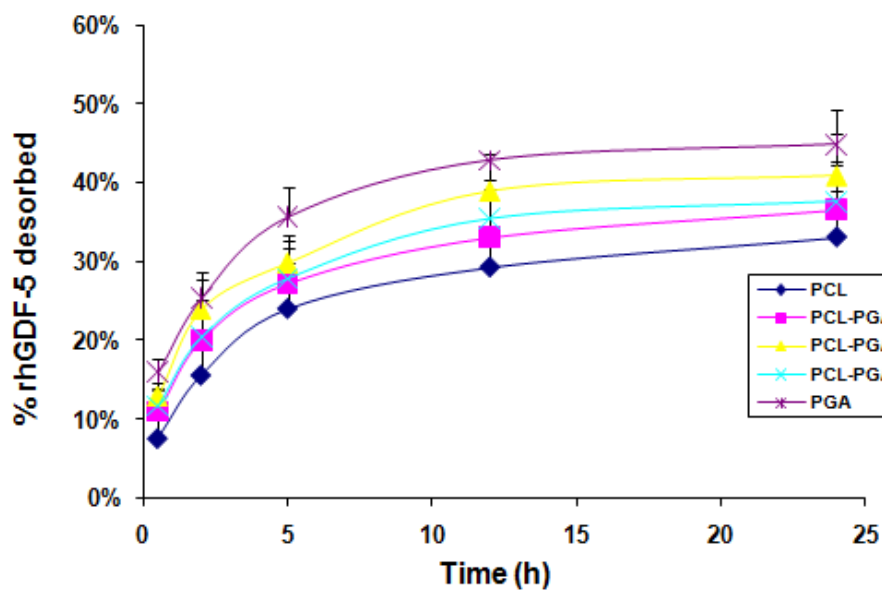


Fig. 5- 2 rhGDF-5 Desorption from PCL-PGA Films over the course of 24 h. **rhGDF-5 desorbed in similar rate from all PCL-PGA films. Retention of rhGDF-5 on these films was 70% approximately.**

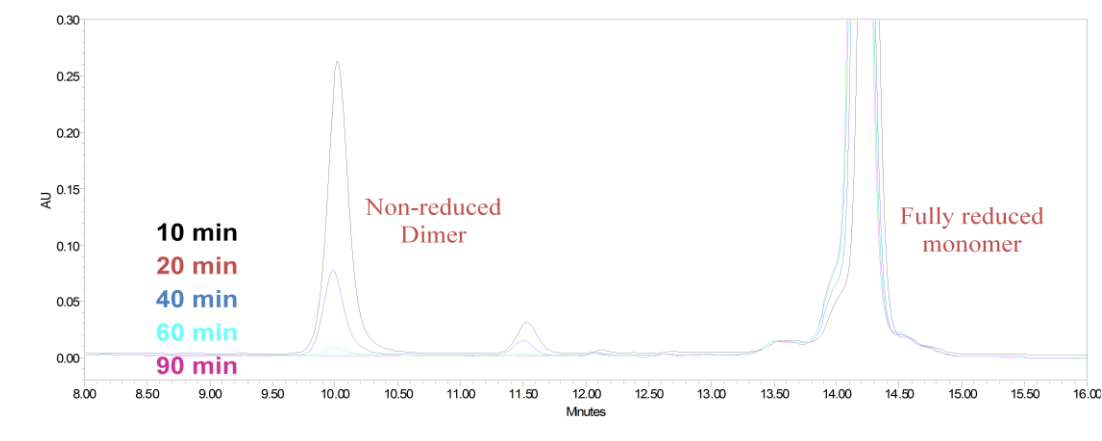


Fig. 5- 3 Chromatographic figure of rhGDF-5 which underwent Kinetic reduction of rhGDF-5. The fully reduced monomer of rhGDF-5 elutes at 12.45 min and the non-reduced dimer elutes at 10.2 min.

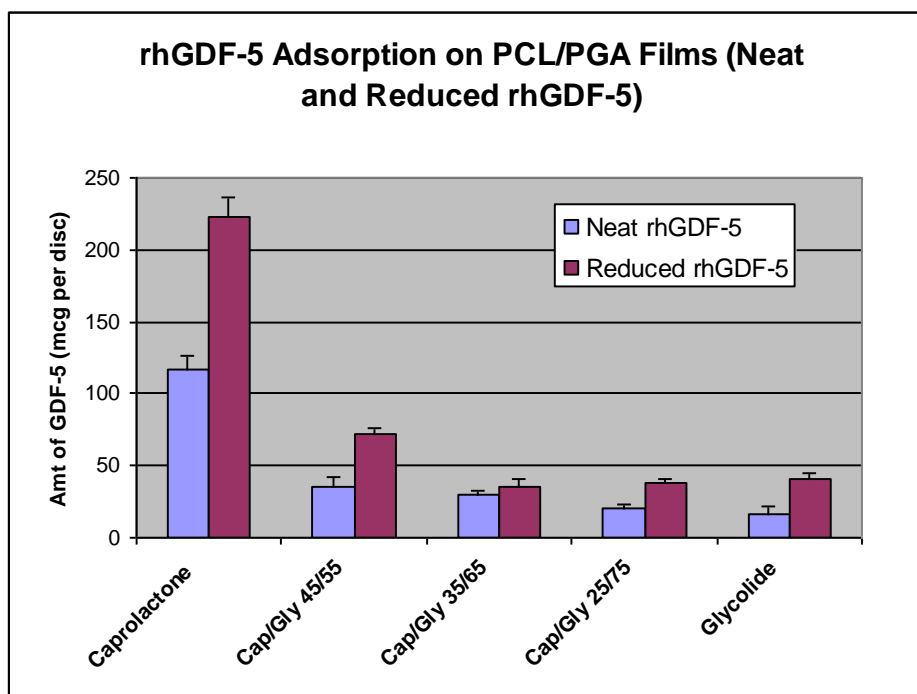


Fig. 5- 4 Amount of rhGDF-5 and Reduced rhGDF-5 Adsorption on PCL-PGA Surfaces. Both forms of rhGDF-5 adsorbed in similar manner to PCL-PGA surfaces. Reduced rhGDF-5 adsorbed in a greater amount, two folds more approximately, to PCL-PGA films, than rhGDF-5.

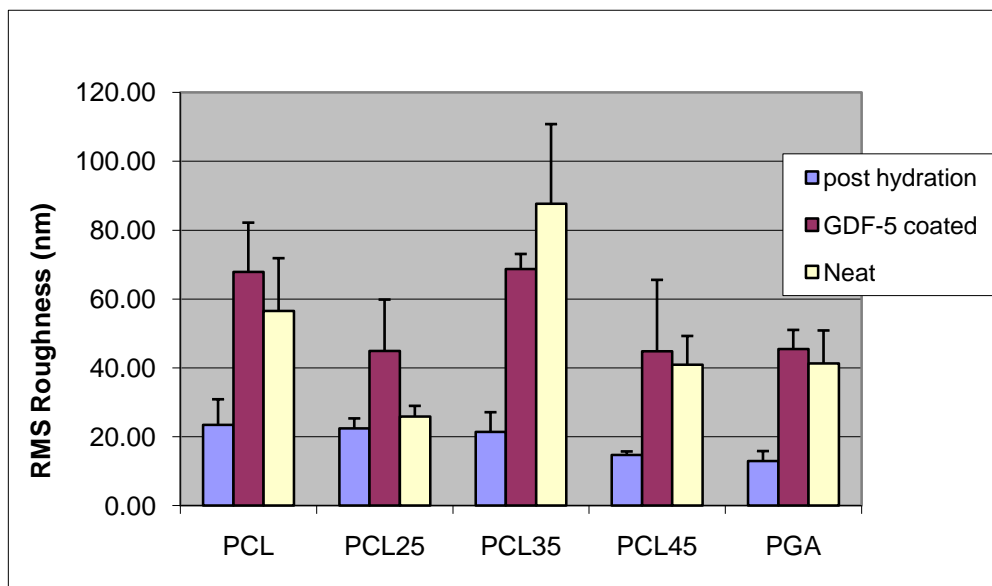


Fig. 5- 5 Surface Roughness of rhGDF-5 Adsorbed PCL-PGA. rhGDF-5 adsorbed surfaces post higher surface roughness for all PCL-PGA surfaces. Roughness mean values are of three measurements for each specimen.

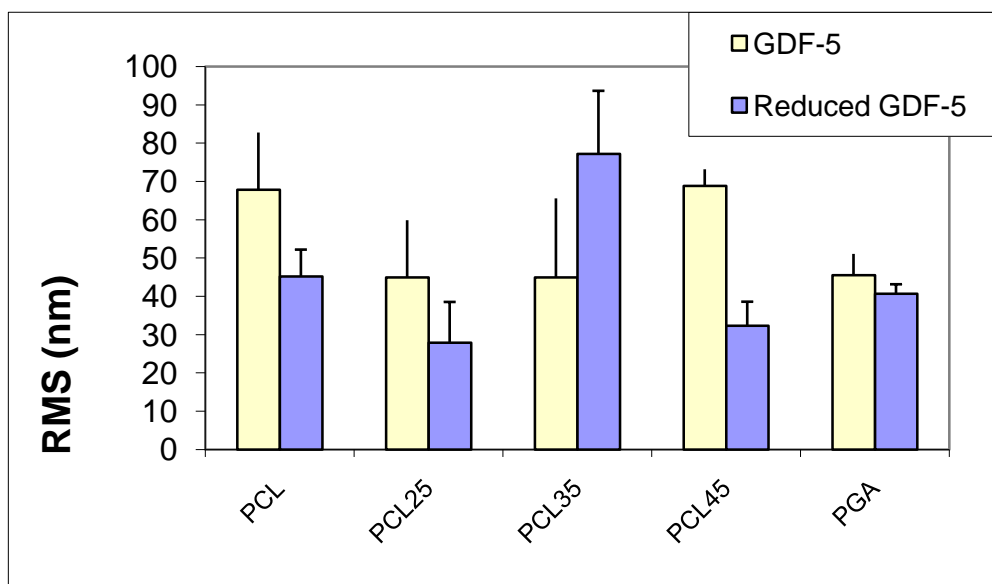


Fig. 5- 6. Surface Roughness of RhGDF-5 and Reduced rhGDF-5 Adsorbed PCL-PGA Films. Reduced rhGDF-5 adsorbed surfaces post lower surface roughness, except for PCL 35. Roughness mean values are of three measurements for each specimen.

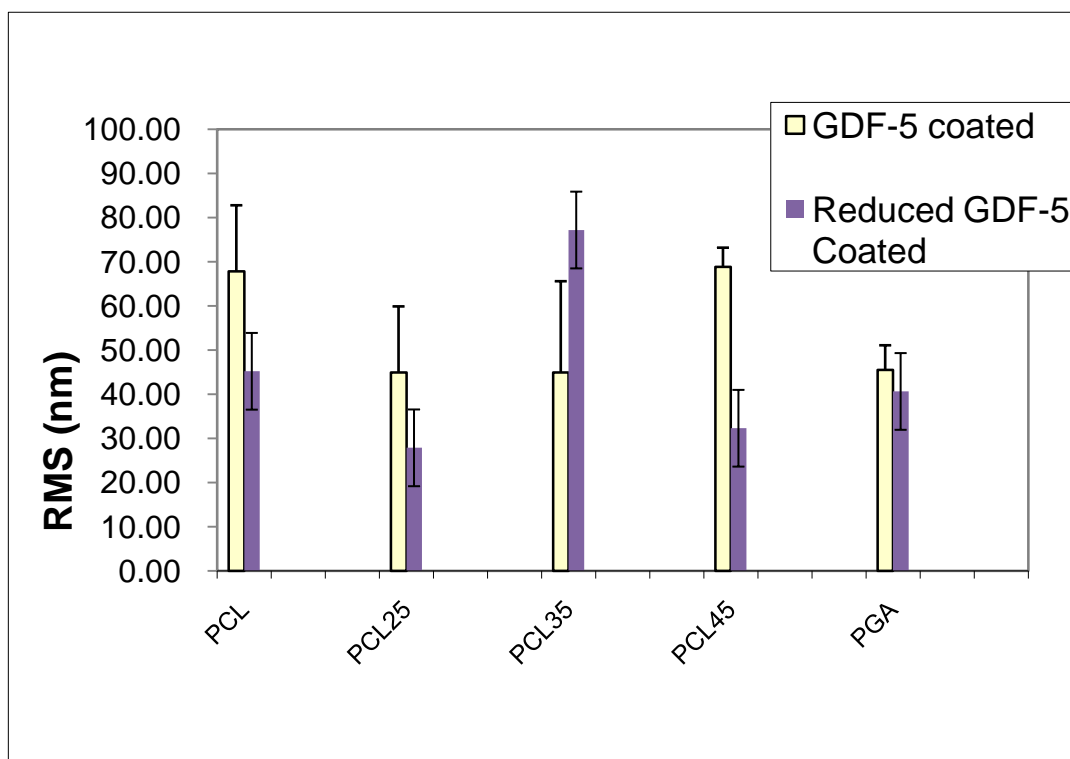
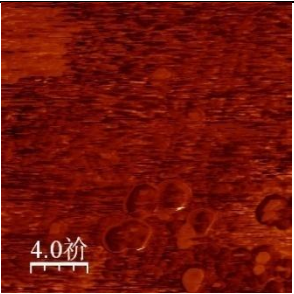
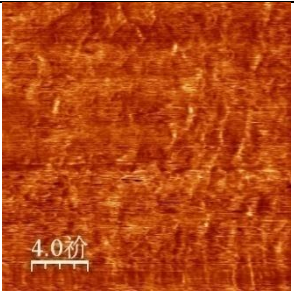
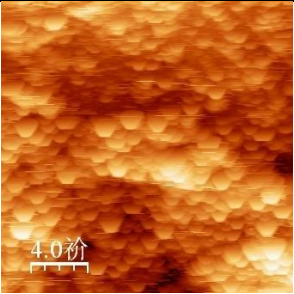
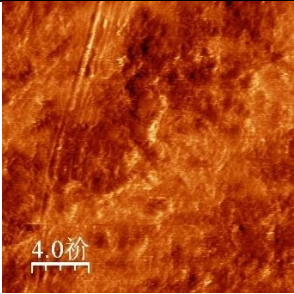
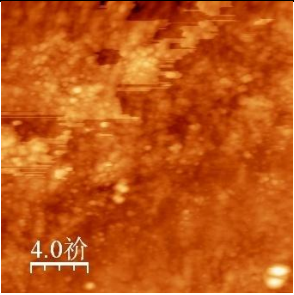
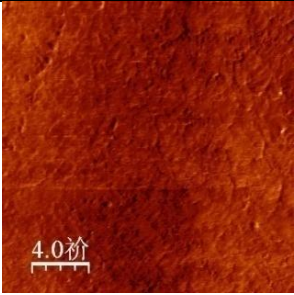
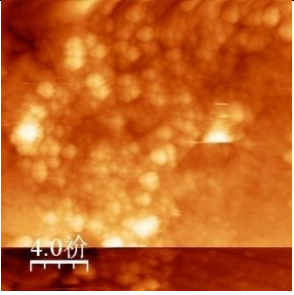
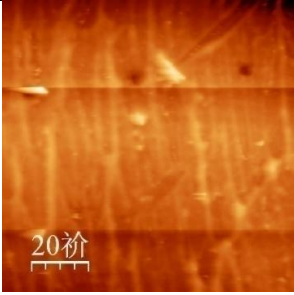


Fig. 5- 7 Roughness of rhGDF-5 and Reduced rhGDF-5 Adsorbed PCL-PGA Films. rhGDF-5 adsorbed surfaces post higher surface roughness than the reduced protein adsorbed surfaces, except for PCL 35. Roughness mean values are of three measurements for each specimen.

	GDF-5 Adsorbed	Reduced GDF-5 Adsorbed
PCL		
PGA		
PCL-PGA 25		
PCL-PGA 35		

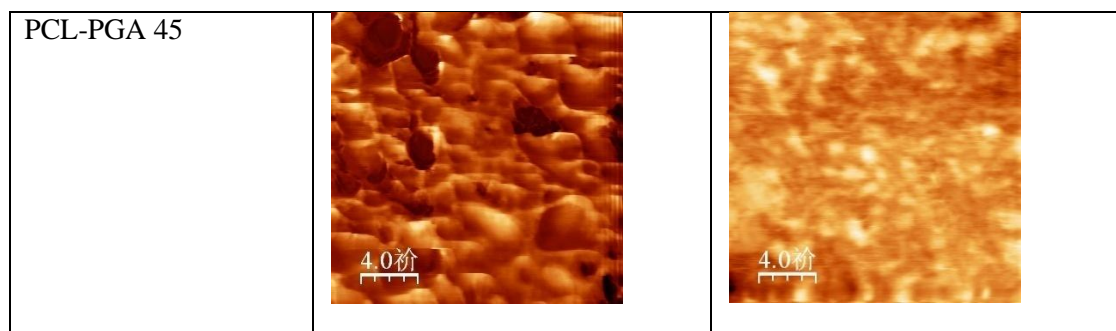


Fig. 5- 8 AFM Nanotopography Images of rhGDF-5 and Reduced rhGDF-5 Adsorbed PCL-PGA Surfaces. Reduced GDF-5 adsorbed surfaces post lower surface roughness, clearly indicative of a more extended feather for the reduced protein, compared to the native rhGDF-5.

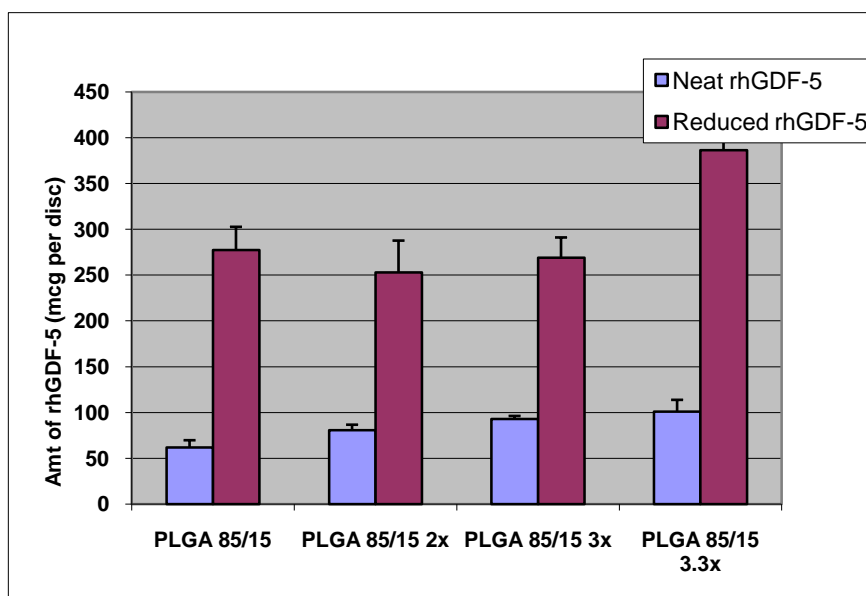


Fig. 5- 9 Amount of rhGDF-5 and Reduced rhGDF-5 Adsorption on PLGA 85:15 Films. The reduced rhGDF-5 adsorbed in greater amount to PLGA 85:15 films, compared to the native rhGDF-5. There is five folds increase of the amount of rhGDF-5 adsorption to the PLGA 85:15, compared with the amount of native rhGDF-5.

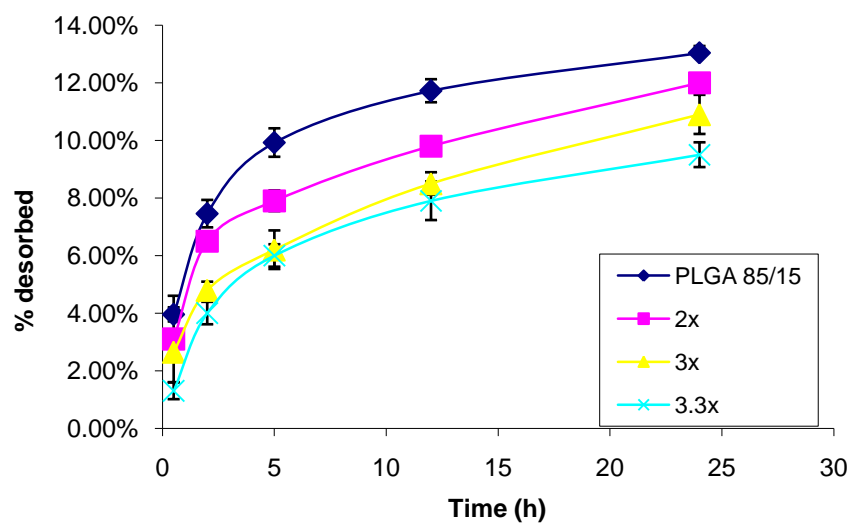


Fig. 5- 10. rhGDF-5 Desorption from Stretched PLGA 85:15 Films. rhGDF-5 desorbed in a similar rate from PLGA 85:15 surfaces, indicative similar affinity of rhGDF-5 to all PLGA 85:15 surfaces.

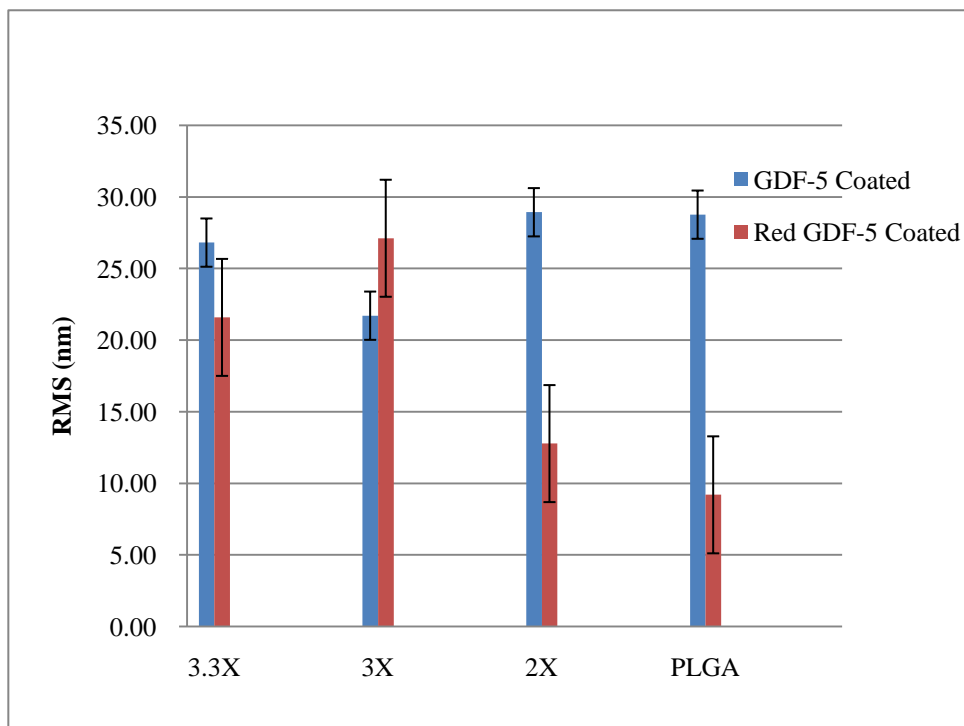


Fig. 5- 11. rhGDF-5 and Reduced rhGDF-5 Adsorbed Surface Roughness for PCL-PGA Films. Reduced protein adsorbed surfaces post lower surface roughness, except for PLGA 85:15 (3x stretched). Mean roughness value is of three measurements for each material specimen.

	rhGDF-5 Adsorbed	Reduced rhGDF-5 Adsorbed
Control	<p>4.0 μm</p>	<p>4.0 μm</p>
2x	<p>4.0 μm</p>	<p>4.0 μm</p>
3x	<p>4.0 μm</p>	<p>4.0 μm</p>
3.3x	<p>4.0 μm</p>	<p>4.0 μm</p>

Fig. 5- 12 AFM Nanotopography Images of rhGDF-5 and Reduced rhGDF-5 Adsorbed PLGA Surfaces. Reduced rhGDF-5 adsorbed surfaces exhibited flatter surfaces, compared to the native rhGDF-5 adsorbed surfaces.

6 FIBRONECTIN AND ITS FRAGMENTS ADSORPTION ON PCL-PGA SURFACES

6.1 Introduction

This study consists of part II of the investigation of biological active interaction with PCL-PGA substrates.

Fn is a high-molecular-weight glycoprotein containing about 5% carbohydrate, that binds to receptor proteins that span the cell's membrane, called integrins [114]. In addition to integrins, they also bind extracellular matrix components such as collagen, fibrin and heparin. Fn sometimes serves as a general cell adhesion molecule by anchoring cells to collagen or proteoglycan substrates. Fn also can serve to organize cellular interaction with the ECM by binding to different components of the extracellular matrix and to membrane-bound Fn receptors on cell surfaces. The importance of Fn in cell migration events during embryogenesis has been documented in several contexts, e.g.: 1) mesodermal cell migration during gastrulating can be blocked by injection of Arg-Gly-Asp (RGD) tripeptides that block cellular FN receptors (integrins); 2) injection of anti-Fn antibodies into chick embryos blocks migration of precardiac cells to the embryonic midline, and; 3) the patterns of Fn deposition in developing vertebrate limbs determines the patterns of precartilaginous cell adhesion to the ECM, thereby specifying limb-specific patterns of chondrogenesis.

Using proteolytic fragments of Fn, several domains with different binding activities have been mapped within the molecule [167-168] (Fig. 4.1). The major cell binding site, containing a crucial Arg-Gly-Asp sequence, is located within the 120-kDa fragment in the central part of the Fn molecule. The collagen-binding activity is located within the 40- to 45-kDa domain near the amino terminus, and the amino-terminal domain (30 kDa) contains multiple ligand binding activities with affinities to, e.g., heparin and fibrin. Fn contains a second heparin-binding domain in the carboxyl-terminal part of the molecule. Both domains interact with heparin and heparin sulfate proteoglycans. Heparin-binding activity has been shown to enhance cell adhesion to Fn. Fragments containing the assembly domain, such as the 70 kDa N-terminal fragment, can inhibit fibrillogenesis without affecting Fn-integrin interactions[169-171].

An adsorbent surface can compete for the hydrophobic interactions among the native structure of the protein side chains. [50], by unfolding the protein structure. Elements of the secondary structure of the protein (α helix and β sheet) together with the supersecondary motifs form a compact globular domain. Fn are built from more than one domain[115]. It is possible that one domain will dominate the adsorption property of the whole macromolecule at a particular type of interface [172].

The hypothesis of the present study is Fn fragments will dominate the adsorption property of Fn to PCL/PGA surfaces.

In this study, PCL-PGA substrates and PLGA 85:15 substrates were used. Fn and its fragments: 30 kDa, 70 kDa and 120 kDa were adsorbed under non-competitive (single protein solution) conditions [160-161] using concentrations which are above their adsorption isotherm. Their behavior was compared at different levels: adsorbed amount (radiolabelling), displacement (elution studies), and nanotopographic analysis (AFM).

The trend observed for Fn and fragments adsorption on PCL-PGA substrates was correlated with underlying materials' physicochemical properties.

6.2 Materials and methods

6.2.1 Materials

Fn and a Bicinchoninic acid (BCA) assay kit were purchased from Sigma-Aldrich (St. Louis, MO). Fn 30 kDa, 70 kDa and 120 kDa were obtained from Chemicon, Inc. (Danvers, MA, USA). Disks of 3mm in diameter of each type of polymer matrix were punched out by a polymer punch. HPLC Water (JT Baker Catalog no. 4219 or equivalent), Acetonitrile (JT Baker Catalog no. 9017 or equivalent), Trifluoroacetic Acid, Sequanal Grade (Pierce Catalog no. 28904), and an Agilent 5834 UV-Vis spectrophotometer were used for the BSA assays. AFM were recorded at ambient temperature by using a multimode nanoscope IV (Digital Instruments, Santa Barbara, CA, USA). All other chemicals were obtained from Sigma-Aldrich (St. Louis, MO)

unless otherwise specified. Each disk was weighed and the approximate surface area measured. Test specimen preparation was listed in detail in section 4.2.2 on P43.

6.2.2 Fn adsorption and desorption from PCL-PGA surfaces and PLGA 85:15 surfaces

6.2.2.1 Protein adsorption:

We utilized a solution depletion method[69] to study Fn adsorption. Briefly, a concentration change in bulk solution prior to and after adsorption was measured. One disk of each matrix sample was placed into one 2ml siliconized tube. Two disks of each matrix sample were also placed into duplicate tubes making sure the disk or 2 disks (per duplicate tubes) stayed in the bottom of the vial. The discs were pre-wetted with PBS for ten to fifteen minutes. The PBS was removed by pipetting. A 2.4mL Fn solution of 40 μ g/mL was added into the sample tube with matrix disk(s). The test sample tube was incubated at 37 °C for 1 hour with occasional mixing.

At the end of the protein adsorption step, the films were washed with 1ml of PBS for 1 minute. The PBS was removed by pipetting. The washing step was repeated for a total of four times.

6.2.2.1 Protein desorption:

The desorption/release medium was 0.25 mL of PBS due to the solubility the protein. 2 disk(s) were placed into siliconized microcentrifuge tubes containing 0.25ml of PBS and

allowed the Fn to desorb for 0.5 hours, 2 hours, 5 hours, 12 hours and 24 hours at a temperature of 37 °C.

It is generally accepted that protein concentration can be analyzed using various spectrophotometric methods[158]. Fn concentration determination was done using a Bicinchoninic acid (BCA) assay. This assay relies on the formation of a Cu^{2+} -protein complex under alkaline conditions, followed by reduction of the Cu^{2+} to Cu^{1+} . The amount of reduction is proportional to the protein present. Briefly, protein solution was mixed with BCA working reagent in a 20:1 ratio. Then the mixed solution was assayed by reading the absorbance at 562nm and protein concentration was determined by comparison to a standard curve.

6.2.2.3 AFM

The AFM protocol was followed as described in detail in section 4.2.3.4 on P45.

6.3 Results and discussion

6.3.1 Fn adsorption on PCL-PGA surfaces

The Fn contents adsorbed onto PCL-PGA films were 223.6 ± 3.3 (N=3), 189.6 ± 29.3 (N=3), 126.4 ± 35.5 , 110.8 ± 34.1 and 2.84 ± 1.4 ng/cm² Fn per PCL, PCL 25, PCL 35, PCL 45 and PGA film, respectively (Figure 6-1). This superficial adsorption onto the pre-formed discs at 40µg/mL Fn resulted in similar levels of protein concentration as compared with the starting Fn solution concentrations.

Fn adsorbed to the most crystalline PCL in the greatest amount and PGA the least amount. The desorption study results indicated that PCL desorbed 35% of the bound Fn in 4 hours, meaning Fibronectin adsorption on this surfaces is a reversible process. For all other PCL-PGA films, only ~10% of the bound Fn desorbed (Figure 6-2), while the majority of the protein was retained onto these surfaces, indicating an irreversible process.

6.3.2 Fn fragments adsorption on PCL-PGA surfaces

The Fn 30 kDa fragment adsorbed onto PCL-PGA films at 223.6 ± 3.3 (N=5), 189.6 ± 29.3 (N=5), 126.4 ± 35.5 , 110.8 ± 34.1 and 2.84 ± 1.4 ng/cm² Fn per PCL, PCL 25, PCL 35, PCL 45 and PGA film, respectively (Figure 6-3). This superficial adsorption onto the pre-formed discs at 40µg/mL Fn resulted in opposite trends as compared to full-length Fn adsorption. For example, for PCL surface which adsorbed the greatest amount of Fn, adsorbed the least amount of Fn 30 KDa; for PGA which adsorbed the least amount of Fn, it adsorbed the greatest amount of Fn 30 kDa fragment. It appeared that 30 kDa fragments adsorbed to intermediate PGA compositions the best (PCL-PGA 45:55).

The Fn 70 kDa fragment adsorbed onto PCL-PGA films at 248.5 ± 30.3 (N=5), 170.4 ± 20.1 (N=5), 92.3 ± 10.1 , 160.8 ± 40.1 and 11.84 ± 10.4 ng/cm² Fn per PCL, PCL 25, PCL 35, PCL 45 and PGA film, respectively (Figure 6-4). This superficial adsorption of Fn 70 kDa fragments correlates similarly with the amount of full-length Fn adsorption onto the pre-formed discs.

The Fn 120 kDa fragment adsorbed onto PCL-PGA films at 437.1 ± 61.3 (N=5), 414.4 ± 41.1 (N=5), 440.2 ± 10.1 , 400.4 ± 19.8 and 438.8 ± 22.4 ng/cm² Fn 120 kDa fragments per PCL, PCL 25, PCL 35, PCL 45 and PGA film, respectively (Figure 4-5). This superficial adsorption of Fn 120 kDa fragments was equal for all the PCL-PGA surfaces tested in the present study.

In the case of Fn, the surface charge, nano-topography and crystallinity/rigidity play combinative role. In contrary to rhGDF-5, Fn is a flexible protein which will unfold itself while approaching surfaces [173-176]. We believe the dominant factor for Fn adsorption on surfaces is crystallinity/rigidity, because PCL-PGA system varied to a significant degree in crystallinity (Chapter 4 in this thesis). This flexible protein will be able to fill the nano-voids of surfaces and merely see the nano-voids as more surface area. The adsorption is minimized on stiffer surfaces (crystalline surfaces) such as PCL and PGA, whereas the amount of adsorption onto elastmeric polymers such as PCL-PGA 35:65, 45:55 and 25:75 is greater. This is also probably due to the substrate flexibility that PCL-PGA copolymers possess. The desorption of Fn from these surfaces occurs at a nearly identical rate, suggesting there was common affinity for Fn towards these substrates.

6.3.3 AFM results of Fn and its fragments adsorbed on PCL-PGA surfaces

Roughness for Fn adsorbed PCL-PGA surfaces and hydrated surfaces is shown in Figure 6-6. 30 KDa fragments and Fn adsorbed surface roughness is shown in Figure 6-7. There

was a slight drop in surface roughness for all 30 KDa fragments adsorbed surfaces, except PCL 35.

Surface roughness for Fn adsorbed PCL-PGA films is summarized in Fig 4-6. Post hydration surface roughness is similar for all PCL-PGA surfaces. However, once Fn adsorbed to these surfaces, there was slight change for surface roughness for all surfaces except PCL 35. There was a significant increase in surface roughness. This can be seen from the AFM images that there were ridges of protein on surfaces, causing a rough surface for PCL 35 (Figure 6-7).

30 KDa fragments did not alter PCL-PGA surface roughness significantly except for PGA. There was a slight increase in roughness for all surfaces, but the increase in roughness was very dramatic for PGA (from 17.4 ± 0.9 nm to 189.7 ± 4.7 nm) (Figure 6-7). This was probably because that 30 kDa fragments adsorbed in combinative conformation of compact and extended forms. This drastic increase in surface roughness on PGA surfaces was due to the fact that adsorption of 30 kDa fragments on PGA was quite high, the adsorbed Fn 30 kDa was likely a combination of both compact and extended forms. There was also the possibility that the coverage on this surface was not very uniform across all the surfaces (Figure 6-10).

Surface roughness for 70 kDa fragments adsorbed PCL-PGA surfaces was higher than the “wet” PCL-PGA surfaces, namely 22.9 ± 6.3 , 21.2 ± 2.9 , 35.1 ± 3.7 , 32 ± 7.5 and 12.5

± 1.9 nm for PCL, PCL 25, PCL 35, PCL 45 and PGA surfaces respectively (Figure 6-8). Compared with Fn adsorbed surfaces, 70 kDa adsorbed surfaces for PCL, PCL 25 and PGA did not post significant changes. However, 70 kDa adsorbed onto PCL 35 surfaces was significantly more smooth than Fn adsorbed PCL 35, indicating a more uniform coverage by Fn 70 kDa fragment on this surface. In addition, the PCL 45 Fn coated surface was more smooth than 70 kDa adsorbed surfaces, which indicated that Fn covered PCL 45 surfaces more uniformly than Fn 70 kDa. In addition, AFM images (Figure 6-10) indicate that the 70 kDa fragment adsorbed in a highly flexible “rod” like conformation, which caused the high surface roughness.

There was slight increase in roughness for the 120 kDa fragments adsorbed onto PCL, PCL35, PCL45 and PGA surfaces, compared with both Fn adsorbed or “ wet” polymer surfaces. Namely the roughness for 120 kDa fragment adsorbed surfaces was 26.6 ± 4.5 , 15.5 ± 0.5 , 59.5 ± 4.9 , 26.8 ± 2.6 and 20.1 ± 8.1 nm for PCL, PCL 25, PCL 35, PCL 45 and PGA surfaces respectively (Figure 6-9). The slight increase for 120 KDa adsorbed surfaces than the Fn adsorbed surfaces was due probably to two reasons: 1) There was a significantly greater amount of Fn 120 kDa fragments adsorbed on all the surfaces than Fn adsorption, and 2) Fn 120 kDa fragments exists in compact and extended forms which contribute to the greater roughness.

6.3.4 Adsorption of Fn and fragments on crystallinity-induced PLGA 85:15 surfaces

6.3.4.1 Fn adsorption/desorption on PLGA 85:15 surfaces

Fn adsorbed on PLGA 85:15 film at about 40 µg/piece and on the crystallinity-induced films. The amount of Fn adsorbed onto PLGA 85:15 was 92.3 ± 10.8 (N=3), 7.0 ± 3.6 (N=3), 17.8 ± 2.1 and 54.2 ± 4.9 ng/cm² Fn per PLGA film for the samples of PLGA 85:15 control, 2x, 3x and 3.3x stretched films, respectively (Figure 6-11). This superficial adsorption onto the pre-formed discs in 40µg/mL Fn resulted in similar levels of protein concentration as compared with what has been published by other researchers [173-176].

For all PLGA 85:15 films, there is a trend which demonstrated that the tighter the protein adsorbed onto the films, the slower the release was (Figure 6-12). In increasing order of Fn adsorption onto PLGA 85:15, 2x stretched, 3x stretched and 3.3x stretched, the release is in decreasing order from these surfaces. However, a majority of the protein stayed with the surface after only two hours in the in vitro release studies. There was the initial burst phase which released around 8% of the Fn, followed by a much slower release phase which reached a plateau after two hours in the release studies.

6.3.4.2 Fibronectin fragments adsorption on PLGA 85:15 Surfaces

The Fn 30 KDa fragment adsorption onto PLGA 85:15 was 194.1 ± 10.4 (N=3), 345.10 ± 73.6 (N=3), 146.7 ± 21.1 and 9.2 ± 4.9 ng/cm² Fn 30 KDa fragment per PLGA film for the samples of PLGA 85:15 control, 2x, 3x and 3.3x stretched films, respectively (Figure

6-13). This superficial adsorption onto the pre-formed discs in 40 μ g/mL Fn resulted in similar levels of protein concentration as compared with what has been published by other researchers [173-176]. The greatest amount of Fn 30 kDa fragment adsorbed on PLGA 2x surfaces; As crystallinity increases, the amount of Fn 30 KDa decreases, reaching the lowest on PLGA 3.3x surfaces.

The amount of Fn 70 KDa fragment adsorbed onto PLGA 85:15 was 4.71 ± 1.1 (N=3), 94.10 ± 23.6 (N=3), 440.7 ± 31.1 and 222.2 ± 54.9 ng/cm² Fn 70 KDa fragment per PLGA film for the samples of PLGA 85:15 control, 2x, 3x and 3.3x stretched films, respectively (Figure 6-14). This superficial adsorption onto the pre-formed discs in 40 μ g/mL Fn resulted in similar levels of protein concentration as compared with what has been published by other researchers. The lowest amount adsorbed was on PLGA surfaces; As crystallinity of the substrate increases, the amount of adsorbed Fn 70 kDa fragment increases, reaching the maximum amount of Fn 70 kDa fragment adsorbed on PLGA 3x surfaces. Then as crystallinity further increases, the amount of Fn 30 kDa decreases.

The amount of Fn 120 KDa fragment adsorbed onto PLGA 85:15 was 30.71 ± 2.1 (N=5), 26.2 ± 1.7 (N=5), 29.7 ± 3.1 and 28.2 ± 1.9 ng/cm² Fn 120 KDa fragment (N=5) per PLGA film for the samples of PLGA 85:15 control, 2x, 3x and 3.3x stretched films, respectively (Figure 6-15). This superficial adsorption onto the pre-formed discs in 40 μ g/mL Fn resulted in similar levels of protein concentration as compared with what

has been published by other researchers. An interesting finding is that Fn 120 KDa fragments adsorbed to all PLGA surfaces equally.

6.3.4.2 AFM results on Fn adsorbed PLGA 85:15 surfaces.

The roughness for 30 kDa fragment adsorbed surfaces are 15.7 ± 3.1 , 21 ± 4.5 , 16.5 ± 7.9 and 7.4 ± 2.5 nm for PLGA, PLGA 2x, PLGA 3x and PLGA 3.3x films respectively. The roughness dropped for 30 K fragment adsorbed surfaces, compared with the “wet” surfaces.

The roughness for 70 kDa fragment adsorbed surfaces are 23.9 ± 0.6 , 10 ± 2.3 , 25.3 ± 1.7 and 14.4 ± 7.5 nm for PLGA, PLGA 2x, PLGA 3x and PLGA 3.3x films respectively (Figure 6-18). The roughness dropped for 70 K fragment adsorbed surfaces, compared with the “wet” surfaces. However, the surface roughness for 70 kDa fragment adsorbed PLGA surfaces are smoother than the Fn adsorbed surfaces.

The roughness for 120 kDa fragment adsorbed surfaces are 28.9 ± 5.6 , 28 ± 2.3 , 31.3 ± 10.7 and 26.8 ± 2.9 nm for PLGA, PLGA 2x, PLGA 3x and PLGA 3.3x films respectively (Figure 6-19). The roughness increased slightly for 120 K fragment adsorbed surfaces, compared with the “wet” surfaces.

The AFM images were summarized in the following table (Table 6-1) ; more striking findings are that 120 KDa fragments exist on the surface in a extended form that likely explains why it is equally adsorbed to all PLGA surfaces. Fn 70kDa fragments are in

compact form on PLGA surfaces, and much more extended form on PLGA 2x, 3x and 3.3x. This observation correlates well with the idea that extended form of Fn adsorbed more on these surfaces.

6.4 Discussion

The most fundamental cell-substrate interaction involves cellular recognition of appropriate surface sites and subsequent cell attachment to the substrate surface. As a cell approaches a substrate, it senses both chemical and physical characteristics of that substrate surface, which includes the protein layer deposited onto these surfaces. Influences of surface chemistry and topography on osteoblast adhesion are known and even slight changes in chemistry can have a marked effect on preosteoblast cell attachment and spreading.

Due to the hydrophobic nature of Fn, the Fn coated biomaterials surfaces might have different hydrophobicity as the uncoated surfaces. For example, Harnet et al. [11] found significant increases in surface hydrophobicity after coating various biomaterials with Fn.

This study was intended to probe firstly how materials physicochemical properties, e.g. hydrophobicity, nanotopography and crystallinity impact a cell adhesion proteins (Fn) adsorption and secondly, how the biological binding motif of Fn influence the adsorption process on PCL-PGA series of polymers.

Protein-surface interaction are influenced by the physical state of both the absorbent and the solution environment. The important factors, including surface energy, its polar and nonpolar contributions, surface charge, and surface roughness all have to be considered in defining the role of solid-solution interface. In most cases, dehydration of the hydrophobic surface of an absorbent alone may tip the adsorption-free energy balance in favor of strong adsorption. We previously demonstrated that the series of PCL-PGA copolymer surfaces have, on a microscopic level, fairly uniform surface characteristics. Once they were hydrated, both PCL and PGA films retained their surface roughness, under hydrated conditions, with its roughness unchanged, compared with dry surfaces, probably due to the increased crystallinity of these two materials and reduced water penetration. We have also demonstrated that the most striking difference in physicochemical properties of this series of PCL-PGA polymers is their differences in crystallinity, despite the fact that they have similar hydrophobicity and surface nanotopography.

Hydrophobicity of these films was measured using contact angle measurement and showed that the PCL films were the most hydrophilic, and PGA films the least hydrophilic, with the copolymer PCL-PGA (25:75; 35:65 and 45:55) of increasing hydrophilicity with increasing caprolactone content. But overall, polyester films are all thermodynamically unfavorable, meaning they are all rather hydrophobic. In the subsequent protein adsorption/desorption studies and cellular responses studies, we

hypothesized that surface hydrophobicity is unlikely the determining factor in these biological events since all films were similarly hydrophobic.

Fn adsorbed to PCL surfaces the most and on PGA surfaces the least. The adsorbed amount of Fn and its fragments was in correlation with other researcher's findings [177-179].

It is well known that protein interaction, both altered protein conformation [163], and type of protein adsorption are very important in mediating subsequent cellular adhesion [164-165]. Quantified analysis correlating implant surface properties (Such as surface chemistry and roughness) and protein adsorption is of paramount importance for determining cellular responses and longer term tissue growth [166, 173, 176, 180].

Fn binding to biological molecules have been well documented. There are fewer observations on how Fn's fragments adsorbed to biomaterials. Our results indicated that, due to its apparent hydrophobicity, differences among different fragments [160, 181] exerted a major impact on how Fn and its fragments adsorbed to biomaterial surfaces. The most hydrophilic 120 KDa fragments equally adsorbed to all the matrices investigated in the present study, including the PCL-PGA series of polymers and the PLGA 85:15 polymers. The most hydrophobic 70 KDa fragments adsorbed in a similar fashion on PCL-PGA series of polymers as Fn itself did, while a highly hydrophobic 30 KDa fragment adsorbed on PCL-PGA surfaces in a trend which was opposite to what Fn

did. This correlates well with previous findings that highly hydrophilic proteins will be able to unfold themselves on hydrophobic surfaces, allowing more contact points for adsorption [180]. Compared to the effects of Fn fragments to adsorption on matrix, the physicochemical properties of materials played minor impact on this adsorption process.

6.5 Conclusions

Fn's biological binding motifs (fragments) display varied hydrophobicity and molecular size. The protein adsorption study results indicated that Fn fragments properties played a major role in determining how they adsorbed to PCL-PGA surfaces.

Fn 70 kDa fragments (heparin and collagen binding fragments) and Fn are similarly hydrophobic and adsorbed in similar amounts on all PCL-PGA surfaces. In terms of the amount of protein adsorbed, more hydrophilic Fn 30 kDa fragments adsorbed in an opposite trend on PCL-PGA surfaces as Fn did on these substrates. 120 kDa fragments adsorbed to all PCL-PGA equally, probably due to its hydrophilic nature.

There were subtle differences in the amount of adsorption of Fn and its fragments on PCL-PGA and PLGA surfaces due to the variable substrate crystallinity.

6.6 Tables

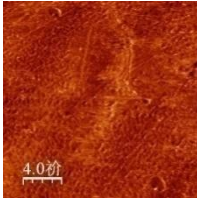
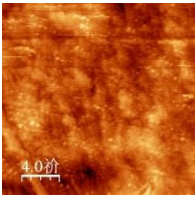
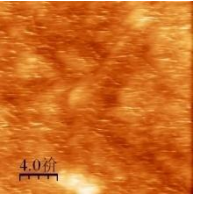
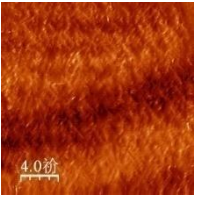
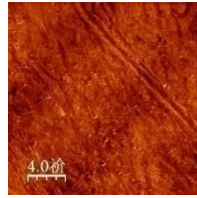
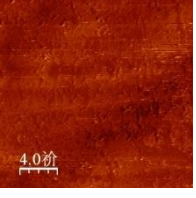
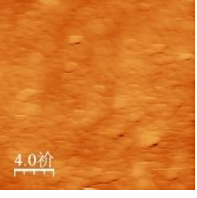
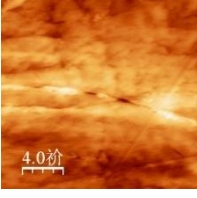

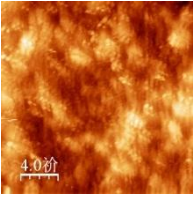
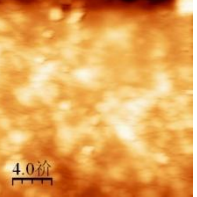
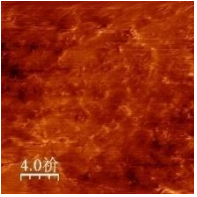
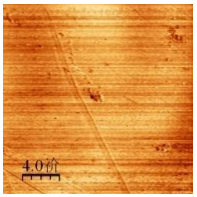
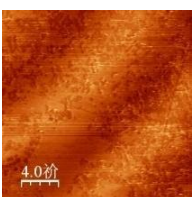
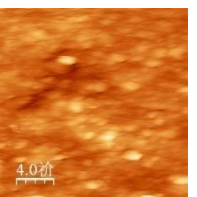
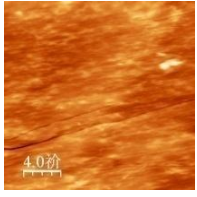
	Fn 30K	Fn 70K	Fn 120K	Fn
PLGA				
PLGA 2x				
PLGA 3x				
PLGA 3.3x				

Table 6- 1 AFM Nanotopography Images of Fn, Fn 30 KDa, Fn 70 KDa and Fn 120 KDa Adsorbed PLGA Surfaces.

6.7 Figures

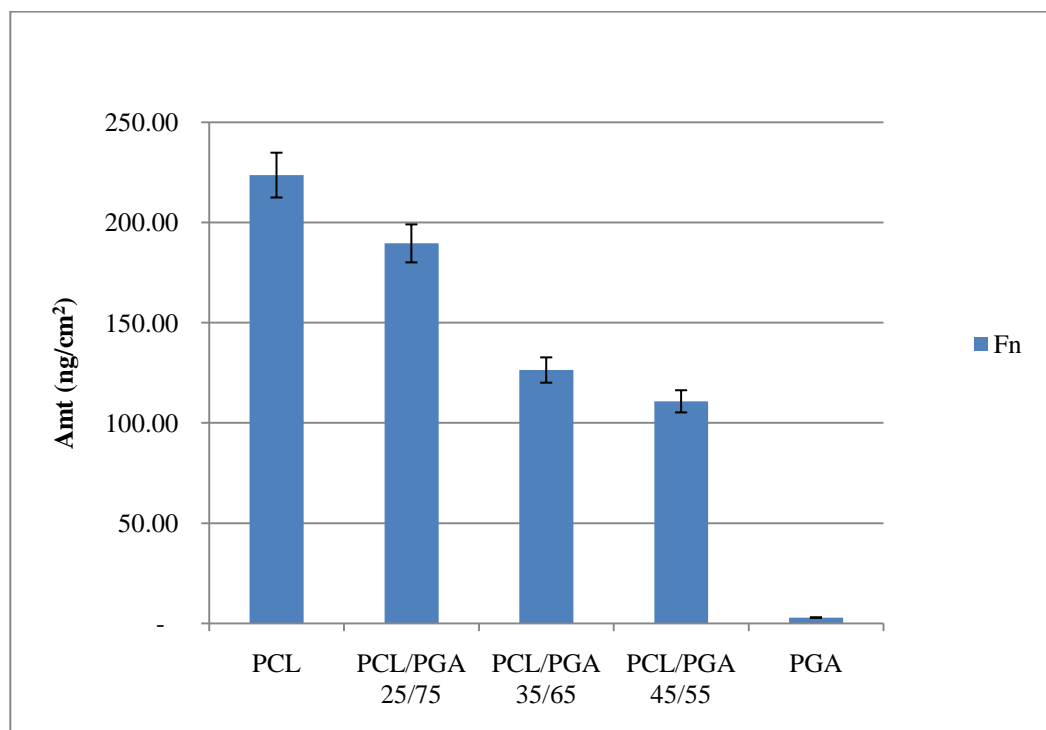


Fig. 6- 1 Fn Adsorption onto PCL-PGA Films. Fn adsorbed in greatest amount (223.65 ng/cm²) on PCL surface, and least amount on PGA (2.84 ng/cm²). In the intermediate polymer composition films, Fn adsorbed more on films with less PGA content.

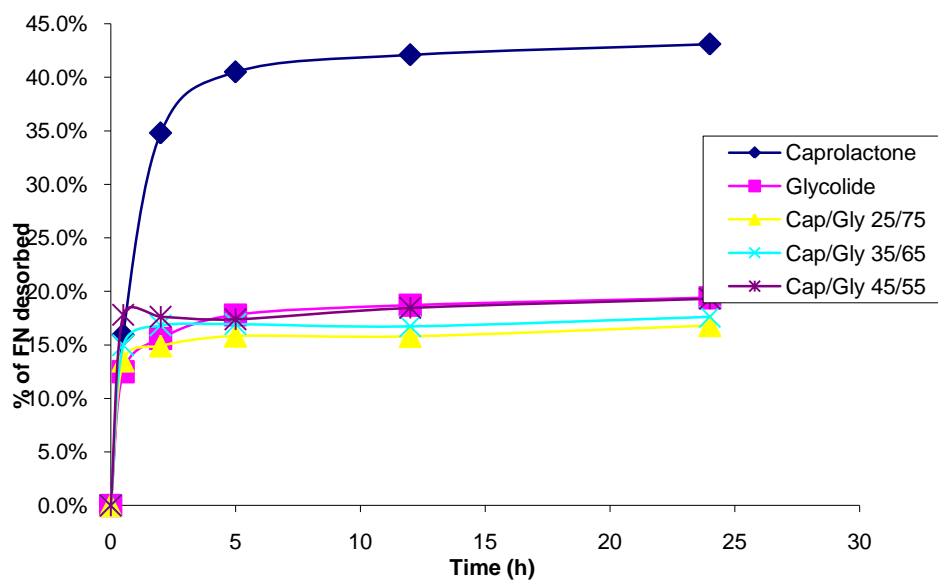


Fig. 6- 2 Fn Desorption from PCL-PGA Films. All PCL-PGA surfaces retained 85% of Fn, whereas PCL only retained 60% of Fn adsorbed, a clear indication Fn was adsorbed on PCL in more reversible form than on any other PCL-PGA films.

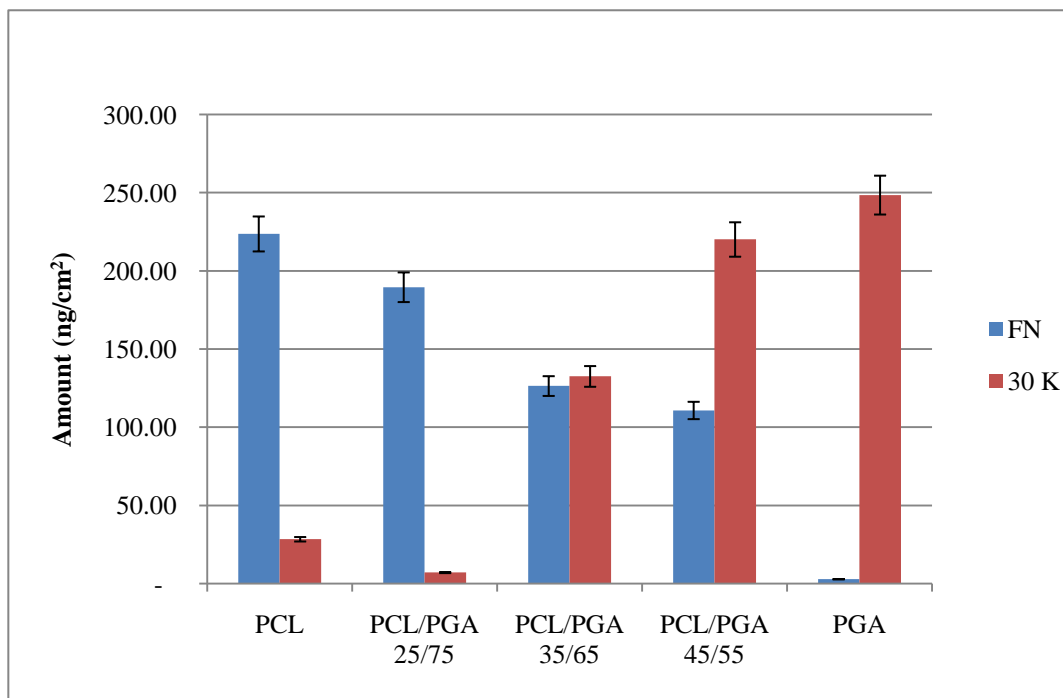


Fig. 6- 3. Fn 30 kDa Fragments and Fn Adsorption on PCL-PGA Surfaces. Fn 30 kDa fragments, in terms of adsorbed amount, demonstrated a opposite trend as Fn itself. Mean value of three replicates were reported.

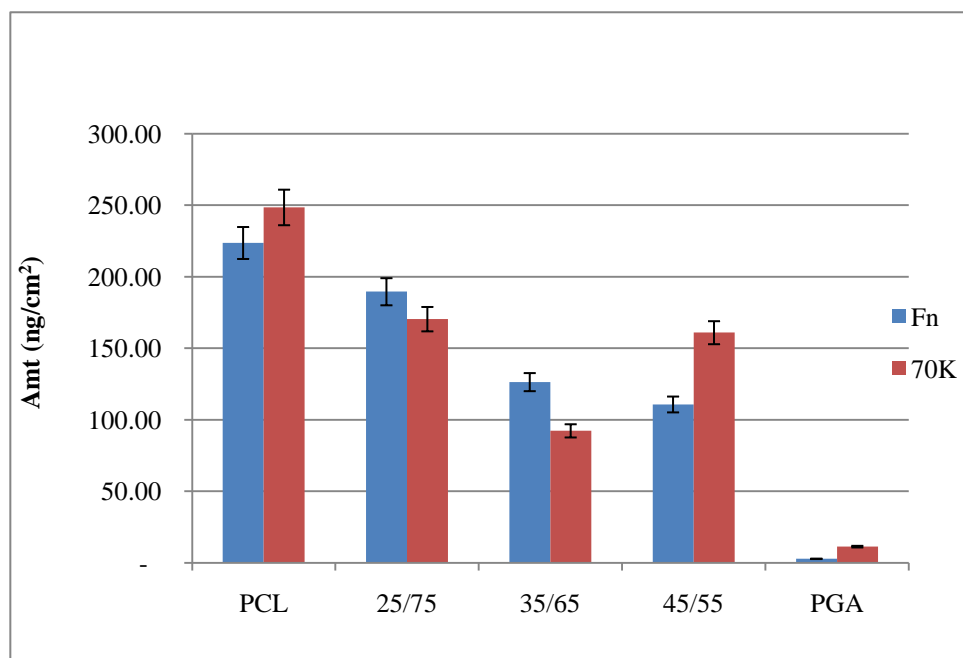


Fig. 6- 4. Fn 70 kDa Fragments and Fn Adsorption on PCL-PGA Films. Fn 70 kDa fragments, in terms of adsorbed amount, demonstrate same trends as Fn itself. Mean value of three replicates were reported.

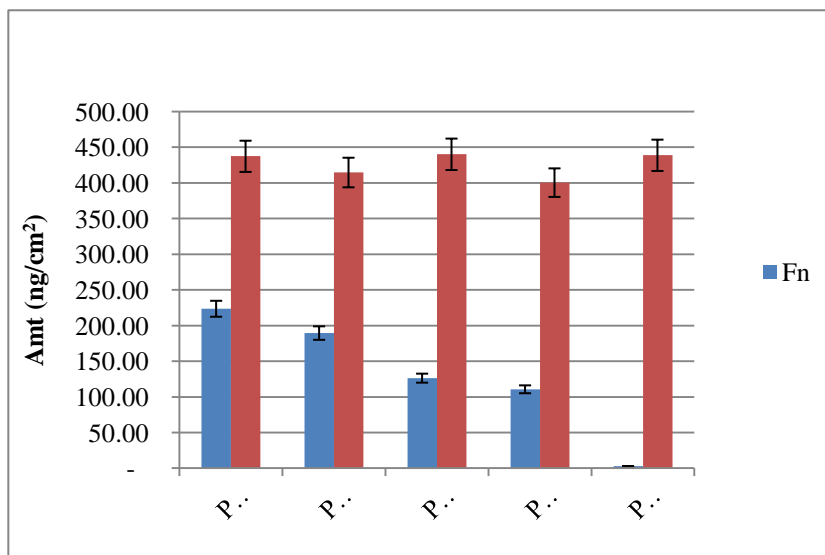


Fig. 6- 5. Fn 120 kDa and Fn Adsorption on PCL-PGA Films. Fn 120 kDa fragments adsorbed similar amount to all PCL-PGA surfaces. Mean value of three replicates were reported.

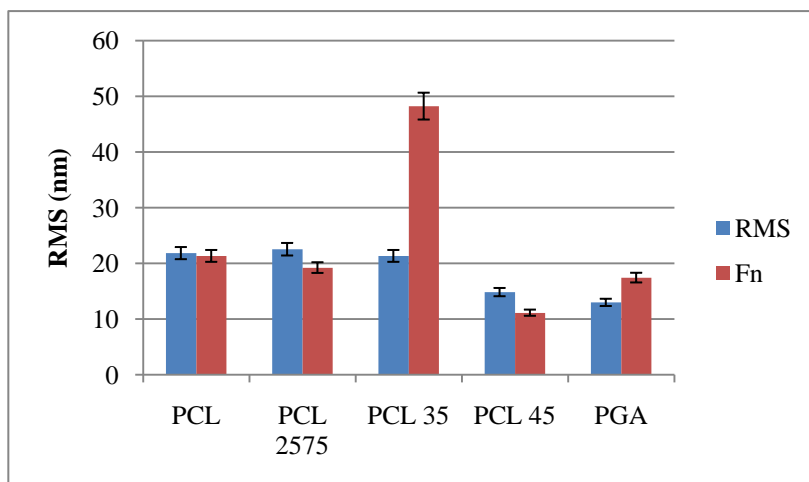


Fig. 6- 6. RMS roughness for Fn Adsorbed PCL-PGA Surfaces. Fn adsorbed PCL 35(two fold increase in roughness) and PGA surfaces (10 folds increase in roughness) become more rough and, all other PCL-PGA surfaces' roughness remain unchanged.

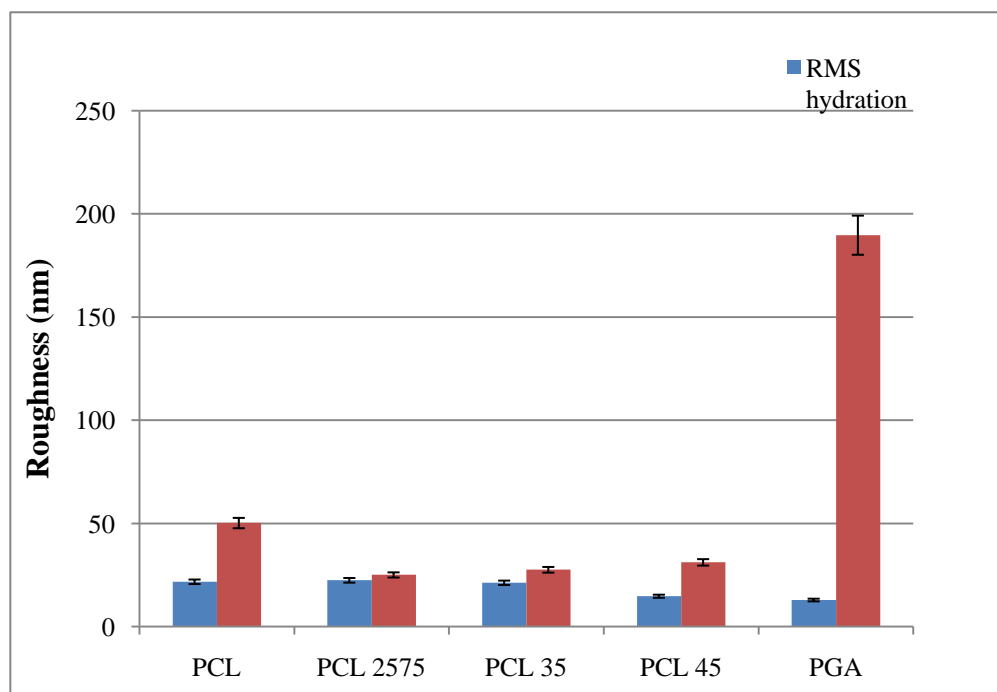


Fig. 6- 7. Roughness for Fn 30 KDa Fragment Adsorbed PCL-PGA Surfaces. 30 kDa fragment adsorbed PGA and PCL surfaces, the two most crystalline surfaces, become rougher. The copolymeric intermediate composition surfaces remain the same roughness post Fn 30 kDa fragment adsorption.

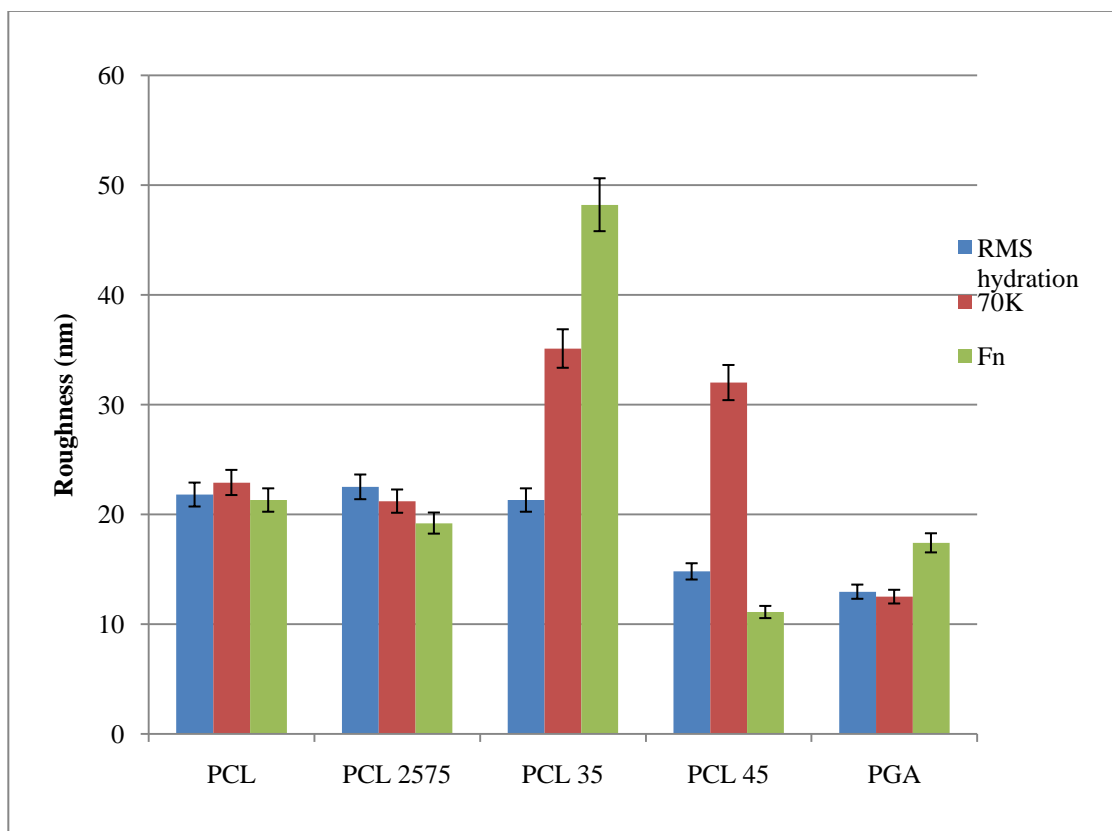


Fig. 6- 8. Roughness for 70K Fn Fragment and Fn. Fn 70 kDa fragment adsorbed PCL 35 and PCL 45, the two most amorphous surfaces, post apparent increase in surface roughness. The other PCL-PGA surfaces did not post changes for surface roughness, after Fn 70 kDa adsorption.

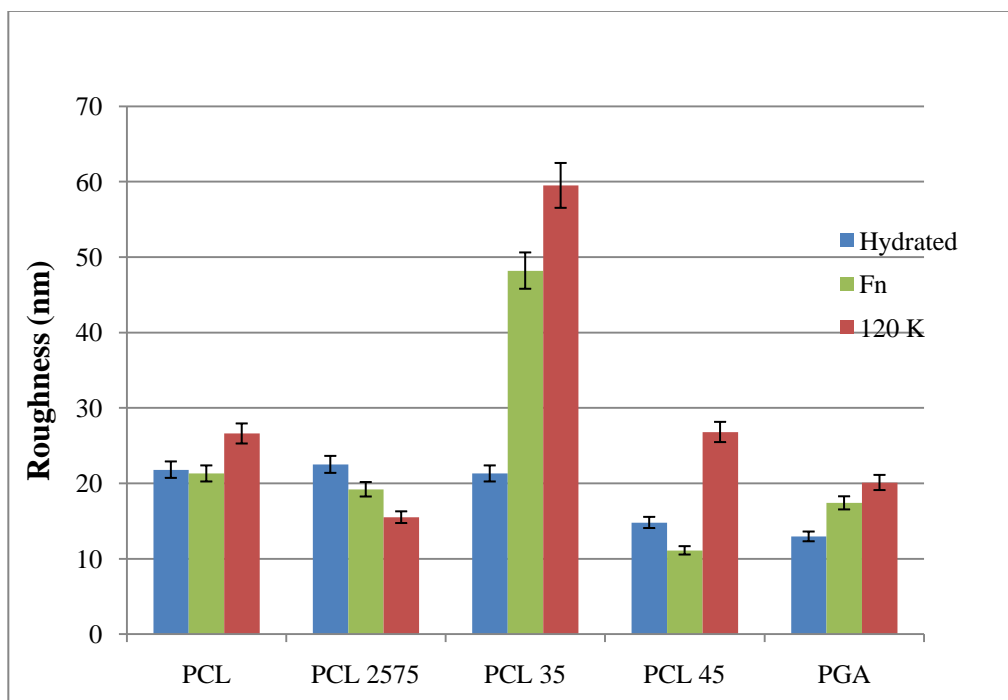


Fig. 6- 9. Surface Roughness for 120K Fn Fragments. Only PCL 35 post significant surface roughness increase (approximately two folds) post Fn and Fn 120 kDa fragment adsorption.

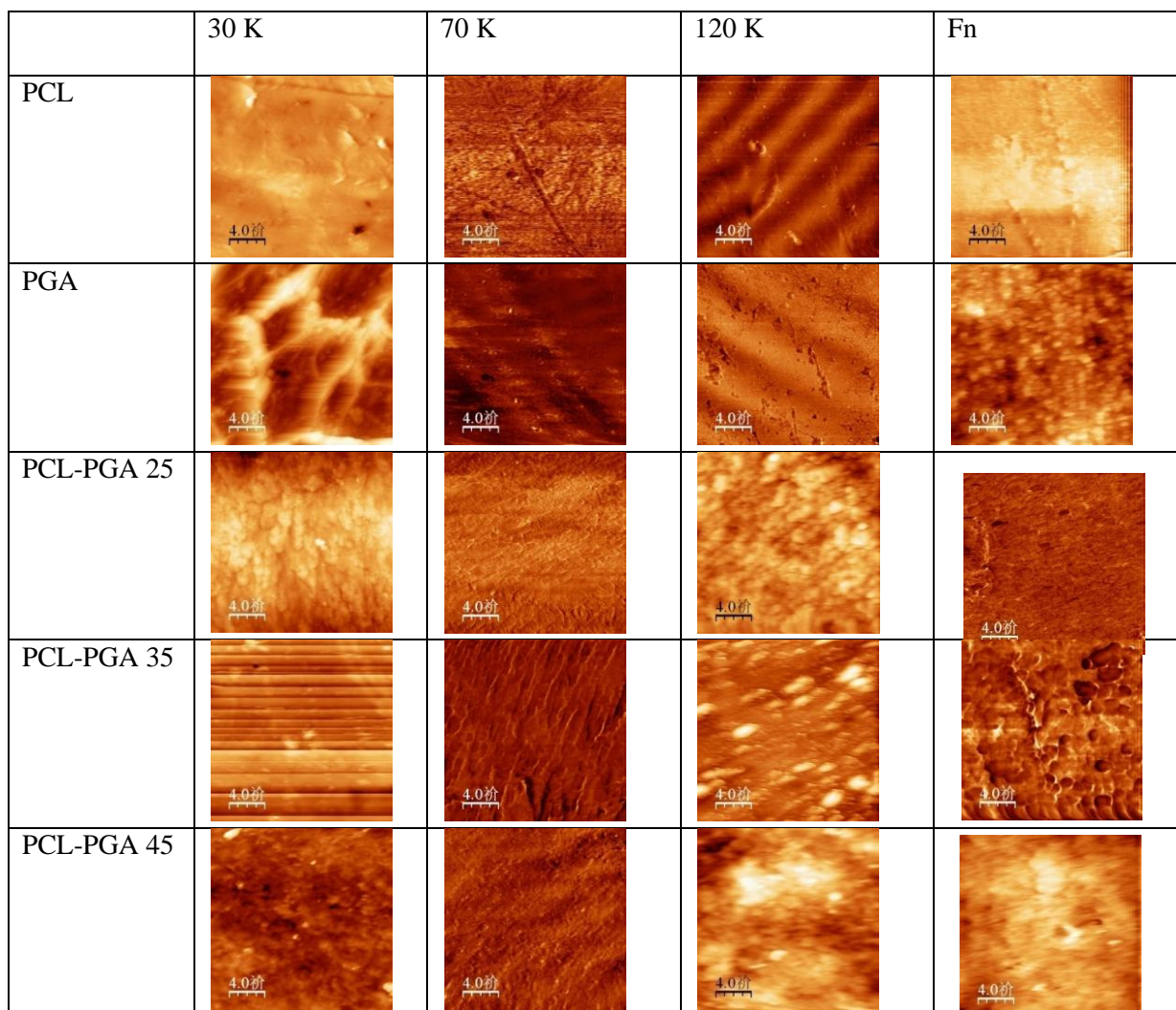


Fig. 6-10. AFM nanotopography Images of Fn, Fn 30 KDa, Fn 70 KDa and Fn 120 KDa Fragment Adsorbed PCL-PGA Surfaces. On PCL 35, distinct rod-like Fn and fragments indicated an extended conformation. On PCL 45, all Fn and fragments were in protein “clusters”.

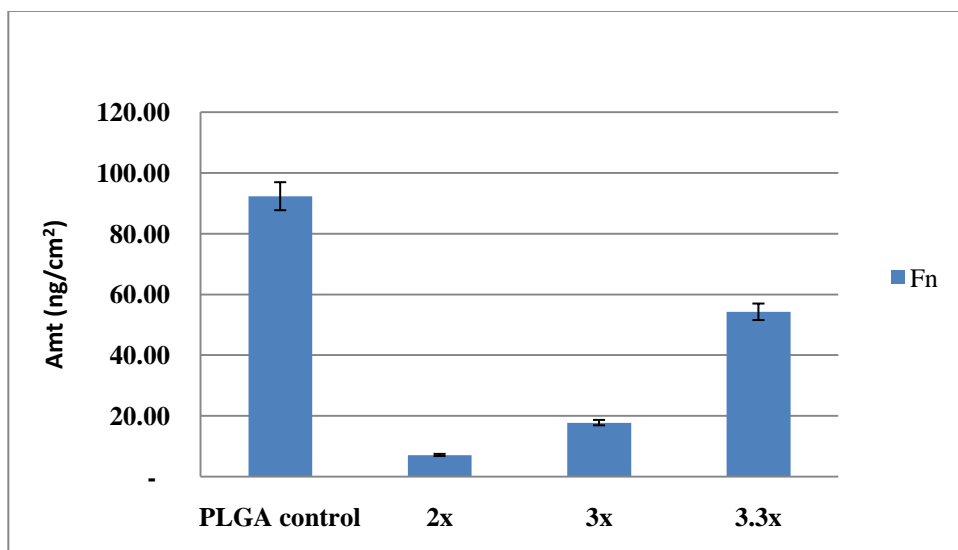


Fig. 6- 11. Fn Adsorption on PLGA Surfaces. Fn adsorbed in increasing amount on films undergone more degree of stretching (more crystalline films). Compared with PLGA control, stretched film adsorbed less Fn. Mean value are of three film replicates.

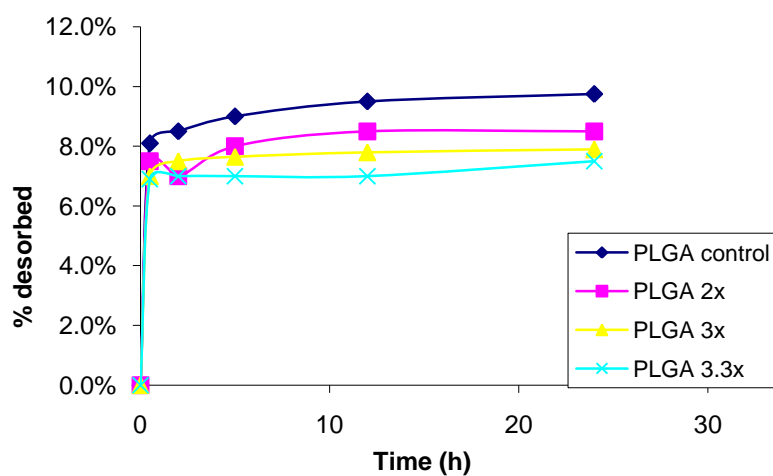


Fig. 6- 12 Fn Desorption from PLGA Films with Different Degree of Mechanical Stretching. Fn desorbed in similar rate from all PLGA films. Mean value are of three film replicates.

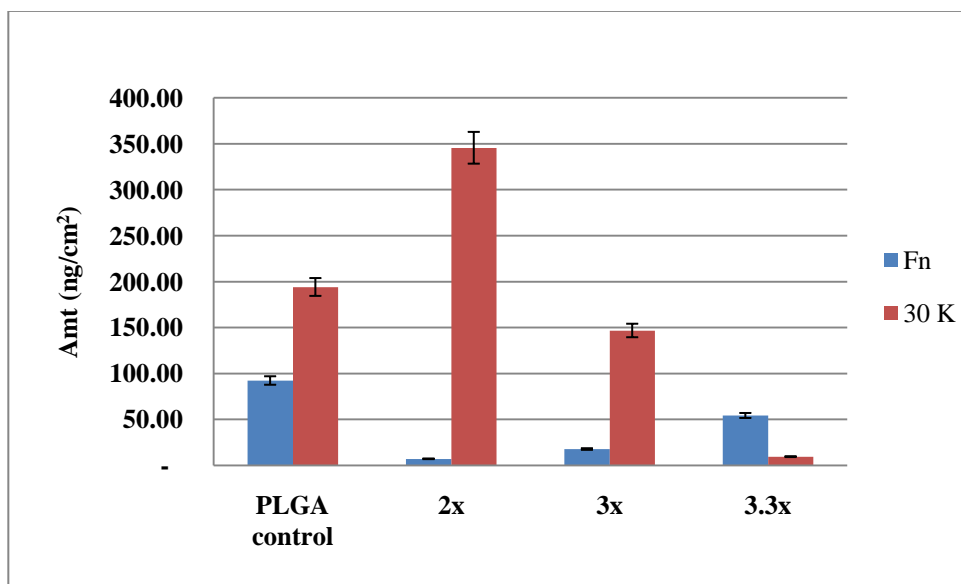


Fig. 6- 13. Fn and Fn 30 kDa Fragment Adsorption on PLGA Surfaces. 30 kDa fragments adsorbed the greatest amounts on films (2x stretched). There is optimal degree of stretching (crystallinity) which adsorbed the most Fn 30 kDa.

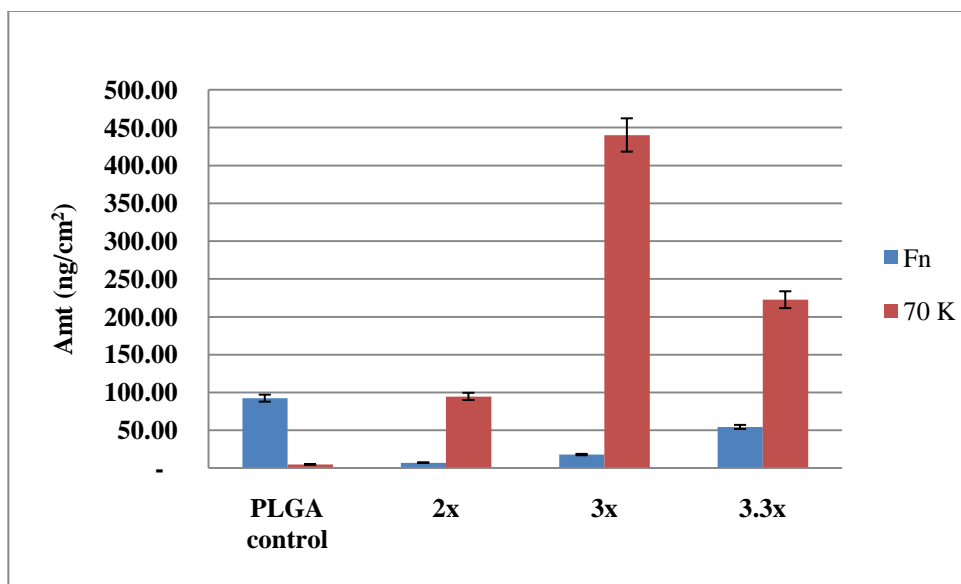


Fig. 6- 14. Fn and Fn 70 kDa Fragment Adsorption on PLGA Surfaces. Optimal crystallinity (3x stretched films) adsorbed the greatest amount of 70 kDa fragment.

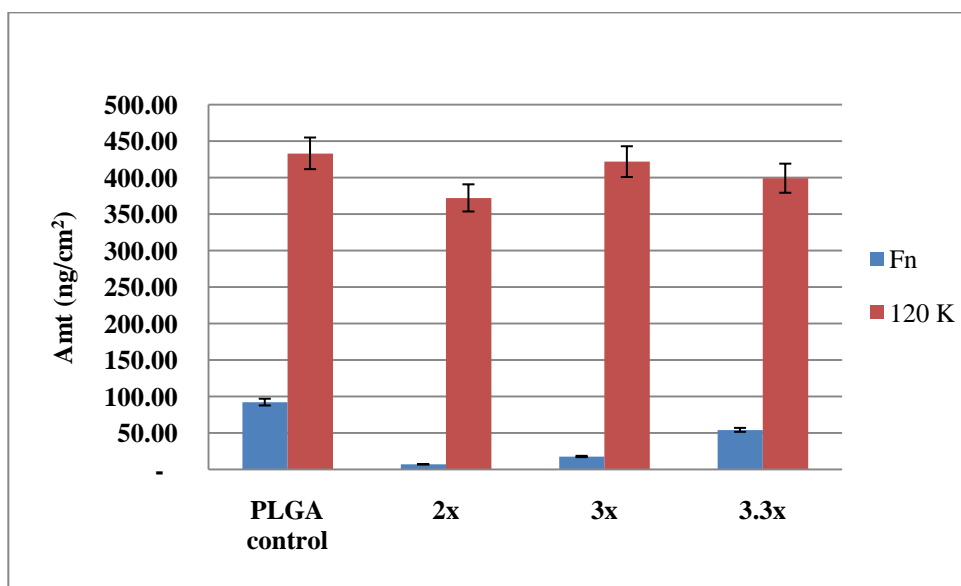


Fig. 6- 15. Fn and Fn 120 kDa Fragment Adsorption on PLGA Surfaces. Fn 120 kDa adsorbed equally on all PLGA surfaces.

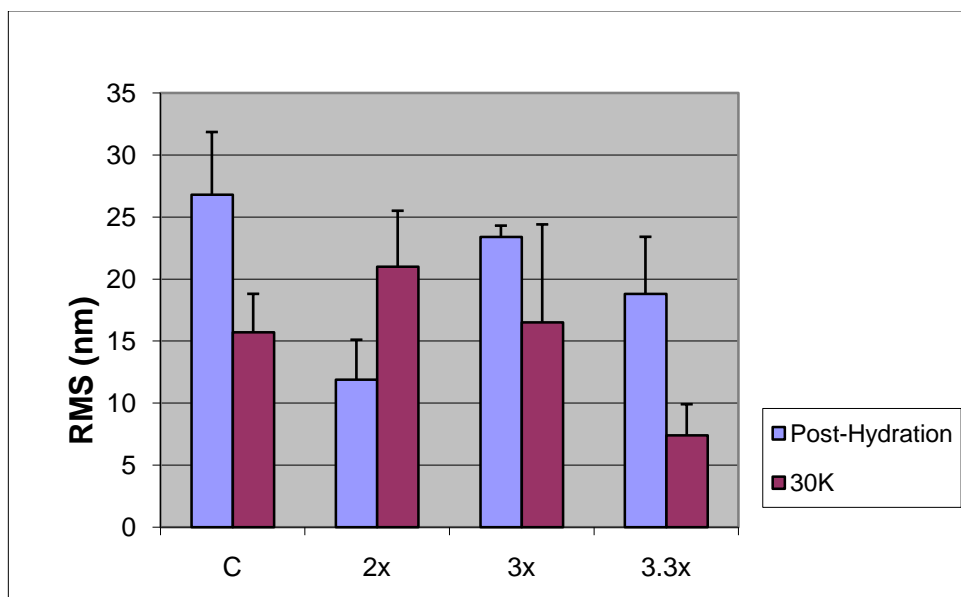


Fig. 6- 16. Roughness of PLGA Films Adsorbed with Fn 30 KDa Fragments.

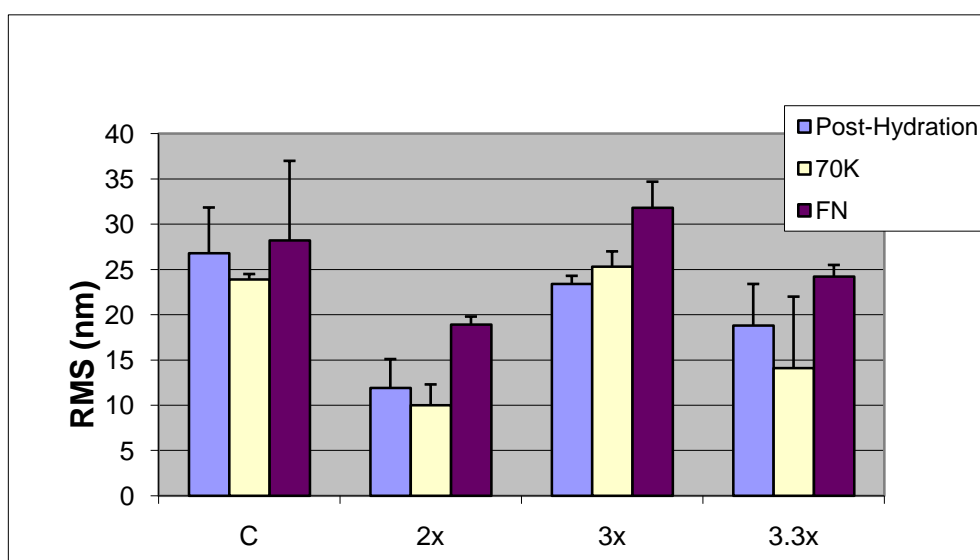


Fig. 6- 17. Roughness of PLGA Films Adsorbed with Fn and Fn 70 KDa Fragments. There doesn't appear to be obvious changes in roughness for all Fn and Fn 70 kDa correlated roughness changes.

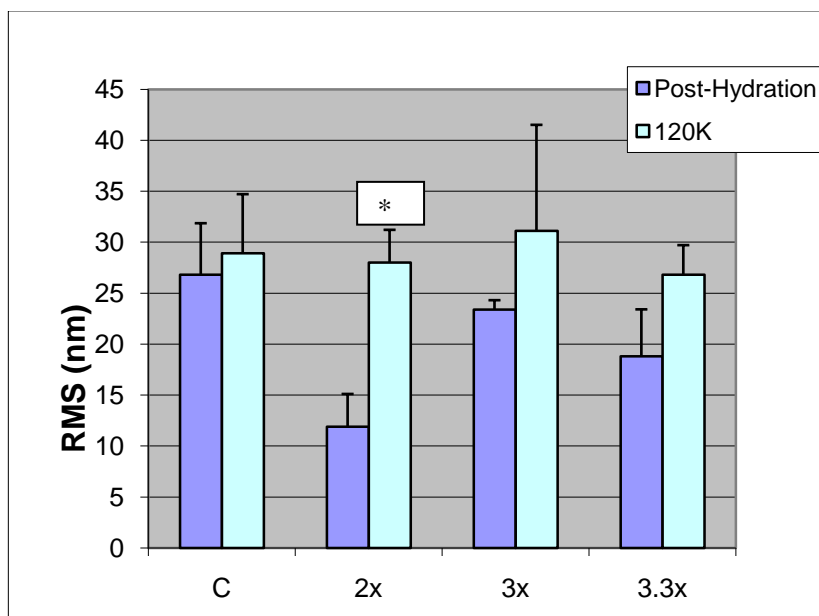


Fig. 6- 18. Roughness of PLGA Films Adsorbed with Fn 120 KDa Fragments. **Roughness increased for 2x stretched PLGA films is significant ($p < 0.05$)**

7 SUMMARY AND CONCLUSIONS

Poly(caprolactone-*co*-glycolide) (PCL-PGA) is a class of biodegradable polymers used for various tissue engineering applications. Previous research suggests that polymer crystallinity impacts biocompatibility. However, there have been no systematic studies to evaluate the role of the crystallinity of PCL-PGA polymers on cellular responses and protein adsorption. This dissertation involves the evaluation of PCL-PGA polymers as substrate materials to study cellular responses and protein adsorption to these surfaces.

Amorphous/flexible PCL-PGA 35:65 was significantly more efficient in supporting the growth of osteoblasts, whereas highly crystalline and rigid PCL and PGA surfaces did not support osteoblast growth. Cellular response studies demonstrated that crystallinity and rigidity played major roles in determining cell responses to PCL-PGA polymers. The chemical composition, morphology, hydrophobicity and surface roughness were similar and held as constant in these studies.

The current results also demonstrated that conformation and hydrophobicity of rhGDF-5 played a major role in determining its adsorption to PCL-PGA surfaces, whereas the physiochemical properties of the materials only played a minor role. The crystallinity of

PCL-PGA surfaces had a slight effect on rhGDF-5 adsorption. Further, the Fn 70 kDa fragment, a hydrophobic heparin and collagen binding motif, strongly impacted the amount of Fn adsorption to PCL-PGA surfaces.

In conclusion, crystallinity of PCL-PGA polymers played a major role in cell responses, and protein conformation/hydrophobicity determined the capacity of adsorption to these polymers.

ABBREVIATIONS

AFM	Atomic Force Microscopy
BCA	Bicinchoninic Acid
CAM	Contact Angle Measurement
DSC	Differential Scanning Calorimetry
ECM	Extra Cellular Matrix
Fibronectin	Fn
G	Gibbs Free Energy
H	Enthalpy
HPLC	High Performance Liquid Chromatography
KDa	Kilo Dalton
PCL	Poly (Caprolactone)
PCL-PGA	Poly (Caprolactone-co-glycolide)
PGA	Poly (Glycolide)
PLGA	Poly (lactide-co-Glycolide)
rhGDF-5	Recombinant Human Growth and Differentiating Factor-5
RMS	Roughness Mean Square
SEM	Scanning Electron Microscopy
XRD	X-Ray Diffraction

8 REFERENCES

1. Engelberg, I. and J. Kohn, *Physico-mechanical properties of degradable polymers used in medical applications: a comparative study*. Biomaterials, 1991. **12**(3): p. 292-304.
2. Agrawal, C.M. and R.B. Ray, *Biodegradable polymeric scaffolds for musculoskeletal tissue engineering*. J Biomed Mater Res, 2001. **55**(2): p. 141-50.
3. Flemming, R.G., et al., *Effects of synthetic micro- and nano-structured surfaces on cell behavior*. Biomaterials, 1999. **20**(6): p. 573-88.
4. Anselme, K., et al., *Effect of grooved titanium substratum on human osteoblastic cell growth*. J Biomed Mater Res, 2002. **60**(4): p. 529-40.
5. Lincks, J., et al., *Response of MG63 osteoblast-like cells to titanium and titanium alloy is dependent on surface roughness and composition*. Biomaterials, 1998. **19**(23): p. 2219-32.
6. Blanco, E.M., M.A. Horton, and P. Mesquida, *Simultaneous investigation of the influence of topography and charge on protein adsorption using artificial nanopatterns*. Langmuir, 2008. **24**(6): p. 2284-7.
7. Fuse, Y., et al., *Cell adhesion and proliferation patterns on mixed self-assembled monolayers carrying various ratios of hydroxyl and methyl groups*. Dent Mater J, 2007. **26**(6): p. 814-9.
8. Kennedy, S.B., et al., *Combinatorial screen of the effect of surface energy on fibronectin-mediated osteoblast adhesion, spreading and proliferation*. Biomaterials, 2006. **27**(20): p. 3817-24.
9. van der Valk, P., et al., *Interaction of fibroblasts and polymer surfaces: relationship between surface free energy and fibroblast spreading*. J Biomed Mater Res, 1983. **17**(5): p. 807-17.
10. van Wachem, P.B., et al., *Interaction of cultured human endothelial cells with polymeric surfaces of different wettabilities*. Biomaterials, 1985. **6**(6): p. 403-8.

11. Harnett, E.M., J. Alderman, and T. Wood, *The surface energy of various biomaterials coated with adhesion molecules used in cell culture*. Colloids Surf B Biointerfaces, 2007. **55**(1): p. 90-7.
12. Cameron, J.B.E., Richard E. Clegg, Ph.D., David I Leavesley, and Mark J Pearcy. , *Mediation of Biomaterial-Cell Interaction by Adsorbed Proteins: A Review*. Tissue Eng., 2005. **11**(2).
13. Ben-Ze'ev, A., S.R. Farmer, and S. Penman, *Protein synthesis requires cell-surface contact while nuclear events respond to cell shape in anchorage-dependent fibroblasts*. Cell, 1980. **21**(2): p. 365-72.
14. Folkman, J. and A. Moscona, *Role of cell shape in growth control*. Nature, 1978. **273**(5661): p. 345-9.
15. Ruoslahti, E. and J.C. Reed, *Anchorage dependence, integrins, and apoptosis*. Cell, 1994. **77**(4): p. 477-8.
16. Singhvi, R., et al., *Engineering cell shape and function*. Science, 1994. **264**(5159): p. 696-8.
17. Takebe, J., et al., *Titanium surface topography alters cell shape and modulates bone morphogenetic protein 2 expression in the J774A.1 macrophage cell line*. J Biomed Mater Res A, 2003. **64**(2): p. 207-16.
18. Howlett, C.R., et al., *Mechanism of initial attachment of cells derived from human bone to commonly used prosthetic materials during cell culture*. Biomaterials, 1994. **15**(3): p. 213-22.
19. Kilpadi, K.L., P.L. Chang, and S.L. Bellis, *Hydroxylapatite binds more serum proteins, purified integrins, and osteoblast precursor cells than titanium or steel*. J Biomed Mater Res, 2001. **57**(2): p. 258-67.
20. Steele, J.G., et al., *Attachment of human bone cells to tissue culture polystyrene and to unmodified polystyrene: the effect of surface chemistry upon initial cell attachment*. J Biomater Sci Polym Ed, 1993. **5**(3): p. 245-57.
21. Schneider, G. and K. Burridge, *Formation of focal adhesions by osteoblasts adhering to different substrata*. Exp Cell Res, 1994. **214**(1): p. 264-9.

22. Steele, J.G., et al., *Polystyrene chemistry affects vitronectin activity: an explanation for cell attachment to tissue culture polystyrene but not to unmodified polystyrene*. J Biomed Mater Res, 1993. **27**(7): p. 927-40.
23. Steele, J.G., et al., *Adsorption of fibronectin and vitronectin onto Primaria and tissue culture polystyrene and relationship to the mechanism of initial attachment of human vein endothelial cells and BHK-21 fibroblasts*. Biomaterials, 1995. **16**(14): p. 1057-67.
24. Lee, Y.J., et al., *MG63 osteoblastic cell adhesion to the hydrophobic surface precoated with recombinant osteopontin fragments*. Biomaterials, 2003. **24**(6): p. 1059-66.
25. Grzesik, W.J. and P.G. Robey, *Bone matrix RGD glycoproteins: immunolocalization and interaction with human primary osteoblastic bone cells in vitro*. J Bone Miner Res, 1994. **9**(4): p. 487-96.
26. Sinha, R.K. and R.S. Tuan, *Regulation of human osteoblast integrin expression by orthopedic implant materials*. Bone, 1996. **18**(5): p. 451-7.
27. Bagambisa, F.B., H.F. Kappert, and W. Schilli, *Cellular and molecular biological events at the implant interface*. J Craniomaxillofac Surg, 1994. **22**(1): p. 12-7.
28. Chou, L., et al., *Substratum surface topography alters cell shape and regulates fibronectin mRNA level, mRNA stability, secretion and assembly in human fibroblasts*. J Cell Sci, 1995. **108** (Pt 4): p. 1563-73.
29. Dalton, B.A., et al., *Role of the heparin binding domain of fibronectin in attachment and spreading of human bone-derived cells*. J Cell Sci, 1995. **108** (Pt 5): p. 2083-92.
30. Martin, J.Y., et al., *Effect of titanium surface roughness on proliferation, differentiation, and protein synthesis of human osteoblast-like cells (MG63)*. J Biomed Mater Res, 1995. **29**(3): p. 389-401.
31. Hormia, M. and M. Kononen, *Immunolocalization of fibronectin and vitronectin receptors in human gingival fibroblasts spreading on titanium surfaces*. J Periodontal Res, 1994. **29**(2): p. 146-52.

32. Singer, II, et al., *Cell surface distribution of fibronectin and vitronectin receptors depends on substrate composition and extracellular matrix accumulation*. J Cell Biol, 1988. **106**(6): p. 2171-82.
33. Saito, T., S.M. Albelda, and C.T. Brighton, *Identification of integrin receptors on cultured human bone cells*. J Orthop Res, 1994. **12**(3): p. 384-94.
34. Aarden, E.M., et al., *Adhesive properties of isolated chick osteocytes in vitro*. Bone, 1996. **18**(4): p. 305-13.
35. Kornu, R., et al., *Osteoblast adhesion to orthopaedic implant alloys: effects of cell adhesion molecules and diamond-like carbon coating*. J Orthop Res, 1996. **14**(6): p. 871-7.
36. Ranucci, C.S. and P.V. Moghe, *Substrate microtopography can enhance cell adhesive and migratory responsiveness to matrix ligand density*. J Biomed Mater Res, 2001. **54**(2): p. 149-61.
37. Leavesley, D.I., et al., *Requirement of the integrin beta 3 subunit for carcinoma cell spreading or migration on vitronectin and fibrinogen*. J Cell Biol, 1992. **117**(5): p. 1101-7.
38. Yang, X., et al., *Induction of human osteoprogenitor chemotaxis, proliferation, differentiation, and bone formation by osteoblast stimulating factor-1/pleiotrophin: osteoconductive biomimetic scaffolds for tissue engineering*. J Bone Miner Res, 2003. **18**(1): p. 47-57.
39. Olbrich, K.C., et al., *Surfaces modified with covalently-immobilized adhesive peptides affect fibroblast population motility*. Biomaterials, 1996. **17**(8): p. 759-64.
40. Dike, L.E., et al., *Geometric control of switching between growth, apoptosis, and differentiation during angiogenesis using micropatterned substrates*. In Vitro Cell Dev Biol Anim, 1999. **35**(8): p. 441-8.
41. Pamula, E., et al., *Cytocompatibility of aliphatic polyesters--in vitro study on fibroblasts and macrophages*. J Biomed Mater Res A, 2008. **87**(2): p. 524-35.
42. Ajami-Henriquez, D., et al., *Evaluation of cell affinity on poly(L-lactide) and poly(epsilon-caprolactone) blends and on PLLA-b-PCL diblock copolymer surfaces*. J Biomed Mater Res A, 2008. **87**(2): p. 405-17.

43. Degirmenbasi, N., et al., *Surface patterning of poly(L-lactide) upon melt processing: in vitro culturing of fibroblasts and osteoblasts on surfaces ranging from highly crystalline with spherulitic protrusions to amorphous with nanoscale indentations*. J Biomed Mater Res A, 2009. **88**(1): p. 94-104.
44. Globus, R.K., et al., *Fibronectin is a survival factor for differentiated osteoblasts*. J Cell Sci, 1998. **111** (Pt 10): p. 1385-93.
45. Stephansson, S.N., B.A. Byers, and A.J. Garcia, *Enhanced expression of the osteoblastic phenotype on substrates that modulate fibronectin conformation and integrin receptor binding*. Biomaterials, 2002. **23**(12): p. 2527-34.
46. Qiu, Q., et al., *Attachment, morphology, and protein expression of rat marrow stromal cells cultured on charged substrate surfaces*. J Biomed Mater Res, 1998. **42**(1): p. 117-27.
47. Linkhart, T.A., S. Mohan, and D.J. Baylink, *Growth factors for bone growth and repair: IGF, TGF beta and BMP*. Bone, 1996. **19**(1 Suppl): p. 1S-12S.
48. Clemmons, D.R. and L.A. Maile, *Minireview: Integral membrane proteins that function coordinately with the insulin-like growth factor I receptor to regulate intracellular signaling*. Endocrinology, 2003. **144**(5): p. 1664-70.
49. Nurcombe, V., et al., *The proliferative and migratory activities of breast cancer cells can be differentially regulated by heparan sulfates*. J Biol Chem, 2000. **275**(39): p. 30009-18.
50. Hlady, V.V. and J. Buijs, *Protein adsorption on solid surfaces*. Curr Opin Biotechnol, 1996. **7**(1): p. 72-7.
51. Tzannis, A.P., et al., *Phase-conjugate resonant holographic interferometry applied to NH concentration measurements in a two-dimensional diffusion flame*. Appl Opt, 1997. **36**(30): p. 7978-83.
52. Lopez-Diez, E.C. and S. Bone, *The interaction of trypsin with trehalose: an investigation of protein preservation mechanisms*. Biochim Biophys Acta, 2004. **1673**(3): p. 139-48.
53. Calonder, C., Y. Tie, and P.R. Van Tassel, *History dependence of protein adsorption kinetics*. Proc Natl Acad Sci U S A, 2001. **98**(19): p. 10664-9.

54. Clarke, M.L. and Z. Chen, *Polymer surface reorientation after protein adsorption*. Langmuir, 2006. **22**(21): p. 8627-30.
55. Giacomelli, C.E., M.G. Bremer, and W. Norde, *ATR-FTIR Study of IgG Adsorbed on Different Silica Surfaces*. J Colloid Interface Sci, 1999. **220**(1): p. 13-23.
56. Giacomelli, C.E. and W. Norde, *The Adsorption-Desorption Cycle. Reversibility of the BSA-Silica System*. J Colloid Interface Sci, 2001. **233**(2): p. 234-240.
57. Long, J.R., et al., *Structure and dynamics of hydrated statherin on hydroxyapatite as determined by solid-state NMR*. Biochemistry, 2001. **40**(51): p. 15451-5.
58. Horbett, T.A. and K.R. Lew, *Residence time effects on monoclonal antibody binding to adsorbed fibrinogen*. J Biomater Sci Polym Ed, 1994. **6**(1): p. 15-33.
59. Mondon, M., S. Berger, and C. Ziegler, *Scanning-force techniques to monitor time-dependent changes in topography and adhesion force of proteins on surfaces*. Anal Bioanal Chem, 2003. **375**(7): p. 849-55.
60. Strathmann, S.C., et al., *Forces between insulin microspheres and polymers surfaces for a dry powder inhaler*. Int J Pharm, 2009. **372**(1-2): p. 147-53.
61. Haggerty, L. and A.M. Lenhoff, *Analysis of ordered arrays of adsorbed lysozyme by scanning tunneling microscopy*. Biophys J, 1993. **64**(3): p. 886-95.
62. Tibbs Jones, T. and E.J. Fernandez, *Alpha-lactalbumin tertiary structure changes on hydrophobic interaction chromatography surfaces*. J Colloid Interface Sci, 2003. **259**(1): p. 27-35.
63. Malmsten, M., *Biopolymer at Interfaces*. 1998, New York: Dekker.
64. Branden, C.T., J., *Introduction to protein structure*. 1991, New York: Garland Publishing;.
65. Williams, T.J., R.P. Schneider, and M.D. Willcox, *The effect of protein-coated contact lenses on the adhesion and viability of gram negative bacteria*. Curr Eye Res, 2003. **27**(4): p. 227-35.
66. Norde, W., *Adsorption of proteins from solution at the solid-liquid interface*. Adv Colloid Interface Sci, 1986. **25**(4): p. 267-340.

67. Baier, R.E. and C.K. Akers, *Blood-surface interactions: recognized factors and unsettled questions*. Trans Am Soc Artif Intern Organs, 1978. **24**: p. 770-3.
68. Cuypers, P.A., W.T. Hermens, and H.C. Hemker, *Ellipsometry as a tool to study protein films at liquid-solid interfaces*. Anal Biochem, 1978. **84**(1): p. 56-67.
69. Hlady, V., J. Buijs, and H.P. Jennissen, *Methods for studying protein adsorption*. Methods Enzymol, 1999. **309**: p. 402-29.
70. Horbett, T.A., ed. *Proteins: Structure, properties, and adsorption to surfaces*. Biomaterials Science, ed. B.D. Ratner, Hoffman, A.S., Schoen, F.J., and Lemons, J. E. 1996, Academic Press: San Diego, CA. 133-141.
71. Lu, W. and T.G. Park, *Protein release from poly(lactic-co-glycolic acid) microspheres: protein stability problems*. PDA J Pharm Sci Technol, 1995. **49**(1): p. 13-9.
72. Tsai, W.B., et al., *The effects of types of degradable polymers on porcine chondrocyte adhesion, proliferation and gene expression*. J Mater Sci Mater Med, 2006. **17**(4): p. 337-43.
73. Calis, S., et al., *Adsorption of salmon calcitonin to PLGA microspheres*. Pharm Res, 1995. **12**(7): p. 1072-6.
74. Cleland, J.L., et al., *Development of poly-(D,L-lactide--coglycolide) microsphere formulations containing recombinant human vascular endothelial growth factor to promote local angiogenesis*. J Control Release, 2001. **72**(1-3): p. 13-24.
75. Kostanski, J.W. and P.P. DeLuca, *A novel in vitro release technique for peptide containing biodegradable microspheres*. AAPS PharmSciTech, 2000. **1**(1): p. E4.
76. Coppi, G., et al., *Protein immobilization in crosslinked alginate microparticles*. J Microencapsul, 2002. **19**(1): p. 37-44.
77. Ghaderi, R. and J. Carlfors, *Biological activity of lysozyme after entrapment in poly(d,l-lactide-co-glycolide)-microspheres*. Pharm Res, 1997. **14**(11): p. 1556-62.
78. van de Weert, M., et al., *The effect of a water/organic solvent interface on the structural stability of lysozyme*. J Control Release, 2000. **68**(3): p. 351-9.

79. Yamaguchi, Y., et al., *Insulin-loaded biodegradable PLGA microcapsules: initial burst release controlled by hydrophilic additives*. J Control Release, 2002. **81**(3): p. 235-49.
80. Cleland, J.L. and A.J. Jones, *Stable formulations of recombinant human growth hormone and interferon-gamma for microencapsulation in biodegradable microspheres*. Pharm Res, 1996. **13**(10): p. 1464-75.
81. Johansen, P., et al., *Improving stability and release kinetics of microencapsulated tetanus toxoid by co-encapsulation of additives*. Pharm Res, 1998. **15**(7): p. 1103-10.
82. Jahng, T.A., et al., *Endoscopic instrumented posterolateral lumbar fusion with Healos and recombinant human growth/differentiation factor-5*. Neurosurgery, 2004. **54**(1): p. 171-80; discussion 180-1.
83. maxwell, J., Theodore Nicholas., *A recombinant bone growth factor and a mineralized collagen matrix (Healos/MP 52) in threaded interbody fusion cages*. Proceedings of the NASS 16th Annual Meeting/The spine Journal, 2002. **2**: p. 35-44.
84. Jennissen, H.P., ed. *Surface and Interracial Aspects of Biomedical Polymers*. ed. J. Andrade. 1985, Plenum: New York.
85. Norde, W. and J. Lyklema, *Why proteins prefer interfaces*. J Biomater Sci Polym Ed, 1991. **2**(3): p. 183-202.
86. Du, C., et al., *Apatite/amelogenin coating on titanium promotes osteogenic gene expression*. J Dent Res, 2005. **84**(11): p. 1070-4.
87. Siebers, M.C., et al., *Integrins as linker proteins between osteoblasts and bone replacing materials. A critical review*. Biomaterials, 2005. **26**(2): p. 137-46.
88. Kieswetter, K., et al., *Surface roughness modulates the local production of growth factors and cytokines by osteoblast-like MG-63 cells*. J Biomed Mater Res, 1996. **32**(1): p. 55-63.
89. Francois, P., et al., *Influence of surface treatments developed for oral implants on the physical and biological properties of titanium. (II) Adsorption isotherms and biological activity of immobilized fibronectin*. Clin Oral Implants Res, 1997. **8**(3): p. 217-25.

90. Deligianni, D.D., et al., *Effect of surface roughness of the titanium alloy Ti-6Al-4V on human bone marrow cell response and on protein adsorption*. Biomaterials, 2001. **22**(11): p. 1241-51.
91. Vroman, L. and A.L. Adams, *Rapid identification of proteins on flat surfaces, using antibody-coated metal oxide suspensions*. J Immunol Methods, 1986. **93**(2): p. 213-6.
92. Vroman, L.A., A.L., Fischer, G.C., Munoz, P.C., and Stanford, M. , *Proteins, plasma and blood in narrow spaces of clot-promoting surfaces*. Biomaterials: Interfacial Phenomena and Applications, ed. S.L. Cooper, and Peppas, N.A. 1982, Washington DC: American Chemical Society.
93. Hanein, D., et al., *Selective interactions of cells with crystal surfaces. Implications for the mechanism of cell adhesion*. J Cell Sci, 1993. **104** (Pt 2): p. 275-88.
94. Brash, J.L., and Horbett, T.A, *Proteins at interfaces: An overview*, in *Proteins at Interfaces II: Fundamentals and Applications*, T.A. Horbett, and Brash, J.L, Editor. 1995, American Chemical Society: Washington DC. p. 1-23.
95. Israelachvili, J. and H. Wennerstrom, *Role of hydration and water structure in biological and colloidal interactions*. Nature, 1996. **379**(6562): p. 219-25.
96. Horbett, T.A., et al., *The kinetics of baboon fibrinogen adsorption to polymers: in vitro and in vivo studies*. J Biomed Mater Res, 1986. **20**(6): p. 739-72.
97. Lee, V.H. and J.R. Robinson, *Topical ocular drug delivery: recent developments and future challenges*. J Ocul Pharmacol, 1986. **2**(1): p. 67-108.
98. Duneas, N., J. Crooks, and U. Ripamonti, *Transforming growth factor-beta 1: induction of bone morphogenetic protein genes expression during endochondral bone formation in the baboon, and synergistic interaction with osteogenic protein-1 (BMP-7)*. Growth Factors, 1998. **15**(4): p. 259-77.
99. Boden, S.D., et al., *Posterolateral lumbar intertransverse process spine arthrodesis with recombinant human bone morphogenetic protein 2/hydroxyapatite-tricalcium phosphate after laminectomy in the nonhuman primate*. Spine (Phila Pa 1976), 1999. **24**(12): p. 1179-85.

100. Ijiri, S., et al., *Ectopic bone induction in porous apatite-wollastonite-containing glass ceramic combined with bone morphogenetic protein*. J Biomed Mater Res, 1997. **35**(4): p. 421-32.
101. Saito, N. and K. Takaoka, *New synthetic biodegradable polymers as BMP carriers for bone tissue engineering*. Biomaterials, 2003. **24**(13): p. 2287-93.
102. Whang, K., et al., *Ectopic bone formation via rhBMP-2 delivery from porous bioabsorbable polymer scaffolds*. J Biomed Mater Res, 1998. **42**(4): p. 491-9.
103. Renier, M.L. and D.H. Kohn, *Development and characterization of a biodegradable polyphosphate*. J Biomed Mater Res, 1997. **34**(1): p. 95-104.
104. Boyne, P.J., et al., *A feasibility study evaluating rhBMP-2/absorbable collagen sponge for maxillary sinus floor augmentation*. Int J Periodontics Restorative Dent, 1997. **17**(1): p. 11-25.
105. Gerhart, T.N., et al., *Healing segmental femoral defects in sheep using recombinant human bone morphogenetic protein*. Clin Orthop Relat Res, 1993(293): p. 317-26.
106. yokota, S., *Processing of the 28th conference on pharmaceutical technology 2003*: p. 69-74.
107. Tabata, Y., et al., *Bone regeneration by basic fibroblast growth factor complexed with biodegradable hydrogels*. Biomaterials, 1998. **19**(7-9): p. 807-15.
108. Stenport, V.F., et al., *Failure to induce supracrestal bone growth between and around partially inserted titanium implants using bone morphogenetic protein (BMP): an experimental study in dogs*. Clin Oral Implants Res, 2003. **14**(2): p. 219-25.
109. Kirkeby, O.J. and A. Ekeland, *No effects of local somatomedin C on bone repair. Continuous infusion in rats*. Acta Orthop Scand, 1992. **63**(4): p. 447-50.
110. Aspenberg, P., T. Albrektsson, and K.G. Thorngren, *Local application of growth-factor IGF-1 to healing bone. Experiments with a titanium chamber in rabbits*. Acta Orthop Scand, 1989. **60**(5): p. 607-10.
111. Luginbuehl, V., et al., *Localized delivery of growth factors for bone repair*. Eur J Pharm Biopharm, 2004. **58**(2): p. 197-208.

112. Buxton, P., et al., *Growth/differentiation factor-5 (GDF-5) and skeletal development*. J Bone Joint Surg Am, 2001. **83-A Suppl 1**(Pt 1): p. S23-30.
113. Dines, J.S., et al., *The effect of growth differentiation factor-5-coated sutures on tendon repair in a rat model*. J Shoulder Elbow Surg, 2007. **16**(5 Suppl): p. S215-21.
114. Wierzbicka-Patynowski, I. and J.E. Schwarzbauer, *The ins and outs of fibronectin matrix assembly*. J Cell Sci, 2003. **116**(Pt 16): p. 3269-76.
115. Pankov, R. and K.M. Yamada, *Fibronectin at a glance*. J Cell Sci, 2002. **115**(Pt 20): p. 3861-3.
116. Daniels, A.U., M.K. Chang, and K.P. Andriano, *Mechanical properties of biodegradable polymers and composites proposed for internal fixation of bone*. J Appl Biomater, 1990. **1**(1): p. 57-78.
117. Anderson, J.M., A. Rodriguez, and D.T. Chang, *Foreign body reaction to biomaterials*. Semin Immunol, 2008. **20**(2): p. 86-100.
118. Yang, X.B., et al., *Human osteoprogenitor growth and differentiation on synthetic biodegradable structures after surface modification*. Bone, 2001. **29**(6): p. 523-31.
119. Harber GM, G.D., *Cell-material interactions: fundamental design issues for tissue engineering and clinical considerations*. . An introduction to biomaterials ed. H.J. Guelcher SA. 2006: CRC Press Taylor & Francis Group.
120. Kalbacova, M., et al., *Nanoscale topography of nanocrystalline diamonds promotes differentiation of osteoblasts*. Acta Biomater, 2009. **5**(8): p. 3076-85.
121. Biggs, D.L., et al., *In vitro and in vivo evaluation of the effects of PLA microparticle crystallinity on cellular response*. J Control Release, 2003. **92**(1-2): p. 147-61.
122. Kawamoto, N., et al., *Blood compatibility of polypropylene surfaces in relation to the crystalline-amorphous microstructure*. J Biomater Sci Polym Ed, 1997. **8**(11): p. 859-77.

123. Park, A. and L.G. Cima, *In vitro cell response to differences in poly-L-lactide crystallinity*. J Biomed Mater Res, 1996. **31**(1): p. 117-30.
124. Wang, S., et al., *The roles of matrix polymer crystallinity and hydroxyapatite nanoparticles in modulating material properties of photo-crosslinked composites and bone marrow stromal cell responses*. Biomaterials, 2009. **30**(20): p. 3359-70.
125. Washburn, N.R., et al., *High-throughput investigation of osteoblast response to polymer crystallinity: influence of nanometer-scale roughness on proliferation*. Biomaterials, 2004. **25**(7-8): p. 1215-24.
126. Winet, H. and J.Y. Bao, *Comparative bone healing near eroding polylactide-polyglycolide implants of differing crystallinity in rabbit tibial bone chambers*. J Biomater Sci Polym Ed, 1997. **8**(7): p. 517-32.
127. Wang, D., et al., *Isolation and characterization of MC3T3-E1 preosteoblast subclones with distinct in vitro and in vivo differentiation/mineralization potential*. J Bone Miner Res, 1999. **14**(6): p. 893-903.
128. Tiaw, K.S., et al., *Processing methods of ultrathin poly(epsilon-caprolactone) films for tissue engineering applications*. Biomacromolecules, 2007. **8**(3): p. 807-16.
129. Cheng, Z. and S.H. Teoh, *Surface modification of ultra thin poly (epsilon-caprolactone) films using acrylic acid and collagen*. Biomaterials, 2004. **25**(11): p. 1991-2001.
130. Rosen, S., ed. *Fundamental Principles of Polymeric Materials, 2nd edition*. ed. S. Rosen, John Wiley & Sons: New York.
131. Jones, D.S., et al., *Poly(epsilon-caprolactone) and poly(epsilon-caprolactone)-polyvinylpyrrolidone-iodine blends as ureteral biomaterials: characterisation of mechanical and surface properties, degradation and resistance to encrustation in vitro*. Biomaterials, 2002. **23**(23): p. 4449-58.
132. Bramfeldt, H. and P. Vermette, *Enhanced smooth muscle cell adhesion and proliferation on protein-modified polycaprolactone-based copolymers*. J Biomed Mater Res A, 2009. **88**(2): p. 520-30.

133. Chung, T.W., et al., *Poly (epsilon-caprolactone) grafted with nano-structured chitosan enhances growth of human dermal fibroblasts*. Artif Organs, 2006. **30**(1): p. 35-41.
134. Ishaug-Riley, S.L., et al., *Human articular chondrocyte adhesion and proliferation on synthetic biodegradable polymer films*. Biomaterials, 1999. **20**(23-24): p. 2245-56.
135. Lee, S.H., et al., *Elastic biodegradable poly(glycolide-co-caprolactone) scaffold for tissue engineering*. J Biomed Mater Res A, 2003. **66**(1): p. 29-37.
136. Otten, J.E., et al., *Bacterial colonization on different suture materials--a potential risk for intraoral dentoalveolar surgery*. J Biomed Mater Res B Appl Biomater, 2005. **74**(1): p. 627-35.
137. Baman, N.K., et al., *Spatial control over cell attachment by partial solvent entrapment of poly lysine in microfluidic channels*. Int J Nanomedicine, 2006. **1**(2): p. 213-7.
138. Clapper, J.D., et al., *Biotinylated biodegradable nanotemplated hydrogel networks for cell interactive applications*. Biomacromolecules, 2008. **9**(4): p. 1188-94.
139. Phillips, J.E., C.A. Gersbach, and A.J. Garcia, *Virus-based gene therapy strategies for bone regeneration*. Biomaterials, 2007. **28**(2): p. 211-29.
140. Ducey, P., T. Schinke, and G. Karsenty, *The osteoblast: a sophisticated fibroblast under central surveillance*. Science, 2000. **289**(5484): p. 1501-4.
141. Rath, B., et al., *Compressive forces induce osteogenic gene expression in calvarial osteoblasts*. J Biomech, 2008. **41**(5): p. 1095-103.
142. Idris, S.B., et al., *Polyester copolymer scaffolds enhance expression of bone markers in osteoblast-like cells*. J Biomed Mater Res A, 2010.
143. Mo, X., H.J. Weber, and S. Ramakrishna, *PCL-PGLA composite tubular scaffold preparation and biocompatibility investigation*. Int J Artif Organs, 2006. **29**(8): p. 790-9.

144. Tang, Z.G., J.T. Callaghan, and J.A. Hunt, *The physical properties and response of osteoblasts to solution cast films of PLGA doped polycaprolactone*. Biomaterials, 2005. **26**(33): p. 6618-24.
145. Muller, A.J., et al., *Self-nucleation and crystallization kinetics of double crystalline poly(p-dioxanone)-b-poly(epsilon-caprolactone) diblock copolymers*. Faraday Discuss, 2005. **128**: p. 231-52; discussion 321-39.
146. Hamley W, C.V., Castillo RV, Muller AJ, *Crystallization in poly(l-lactide)-b-poly(epsilon-caprolactone) double crystalline diblock copolymers: A study using x-ray scattering, differential scanning calorimetry, and polarized optical microscopy*. macromolecules, 2005. **38**: p. 463-472.
147. Pelham, R.J., Jr. and Y. Wang, *Cell locomotion and focal adhesions are regulated by substrate flexibility*. Proc Natl Acad Sci U S A, 1997. **94**(25): p. 13661-5.
148. Tzvetkova-Chevolleau, T., et al., *The motility of normal and cancer cells in response to the combined influence of the substrate rigidity and anisotropic microstructure*. Biomaterials, 2008. **29**(10): p. 1541-51.
149. Gough, J.E., et al., *Craniofacial osteoblast responses to polycaprolactone produced using a novel boron polymerisation technique and potassium fluoride post-treatment*. Biomaterials, 2003. **24**(27): p. 4905-12.
150. Ducy, P., et al., *Osx/Cbfa1: a transcriptional activator of osteoblast differentiation*. Cell, 1997. **89**(5): p. 747-54.
151. Franceschi, R.T., *The developmental control of osteoblast-specific gene expression: role of specific transcription factors and the extracellular matrix environment*. Crit Rev Oral Biol Med, 1999. **10**(1): p. 40-57.
152. Komori, T. and T. Kishimoto, *Cbfa1 in bone development*. Curr Opin Genet Dev, 1998. **8**(4): p. 494-9.
153. Perinpanayagam, H., et al., *Alveolar bone osteoblast differentiation and Runx2/Cbfa1 expression*. Arch Oral Biol, 2006. **51**(5): p. 406-15.
154. Richert, L., et al., *Elasticity of native and cross-linked polyelectrolyte multilayer films*. Biomacromolecules, 2004. **5**(5): p. 1908-16.

155. Mendelsohn, J.D., et al., *Rational design of cytophilic and cytophobic polyelectrolyte multilayer thin films*. Biomacromolecules, 2003. **4**(1): p. 96-106.
156. Schwarzbauer, J.E., *Identification of the fibronectin sequences required for assembly of a fibrillar matrix*. J Cell Biol, 1991. **113**(6): p. 1463-73.
157. Jenner, J.M., et al., *Effect of transforming growth factor-beta and growth differentiation factor-5 on proliferation and matrix production by human bone marrow stromal cells cultured on braided poly lactic-co-glycolic acid scaffolds for ligament tissue engineering*. Tissue Eng, 2007. **13**(7): p. 1573-82.
158. Jennissen, H.P. and G. Botzet, *The binding of phosphorylase kinase to immobilized calmodulin*. J Mol Recognit, 1993. **6**(3): p. 117-30.
159. Tollefen DM, F.J., Majerus PWJ, J. Biol. Chem, 1971. **246**: p. 2646.
160. Garcia, A.J., M.D. Vega, and D. Boettiger, *Modulation of cell proliferation and differentiation through substrate-dependent changes in fibronectin conformation*. Mol Biol Cell, 1999. **10**(3): p. 785-98.
161. Keselowsky, B.G., D.M. Collard, and A.J. Garcia, *Surface chemistry modulates fibronectin conformation and directs integrin binding and specificity to control cell adhesion*. J Biomed Mater Res A, 2003. **66**(2): p. 247-59.
162. McFarlane, A.S., *In Vivo Behavior of I-Fibrinogen*. J Clin Invest, 1963. **42**(3): p. 346-61.
163. Burmeister, J.S., et al., *Effect of fibronectin amount and conformation on the strength of endothelial cell adhesion to HEMA/EMA copolymers*. J Biomed Mater Res, 1996. **30**(1): p. 13-22.
164. Webster, T.J., et al., *Mechanisms of enhanced osteoblast adhesion on nanophase alumina involve vitronectin*. Tissue Eng, 2001. **7**(3): p. 291-301.
165. Agheli, H., et al., *Large area protein nanopatterning for biological applications*. Nano Lett, 2006. **6**(6): p. 1165-71.
166. Meadows, P.Y. and G.C. Walker, *Force microscopy studies of fibronectin adsorption and subsequent cellular adhesion to substrates with well-defined surface chemistries*. Langmuir, 2005. **21**(9): p. 4096-107.

167. Carsons, S., ed. *The structure and function of fibronectin*. Fibronectin in health and disease, ed. C. SE. 1989, CRC press: Boca Raton, FL.
168. Saren, A., et al., *The cellular form of human fibronectin as an adhesion target for the S fimbriae of meningitis-associated Escherichia coli*. Infect Immun, 1999. **67**(5): p. 2671-6.
169. Woodley, D.T., et al., *Specific affinity between fibronectin and the epidermolysis bullosa acquisita antigen*. J Clin Invest, 1987. **79**(6): p. 1826-30.
170. Corbett, S.A. and J.E. Schwarzbauer, *Fibronectin-fibrin cross-linking: a regulator of cell behavior*. Trends Cardiovasc Med, 1998. **8**(8): p. 357-62.
171. Sechler, J.L. and J.E. Schwarzbauer, *Control of cell cycle progression by fibronectin matrix architecture*. J Biol Chem, 1998. **273**(40): p. 25533-6.
172. Chang, I.a.H.J., *Orientation of acid-pretreated antibodies on hydrophobic dichlorodimethylsilane-treated silica surfaces*. Langmuir, 1995. **1995**(11): p. 2083-2089.
173. Kowalczyńska, H.M., et al., *Atomic force microscopy evidence for conformational changes of fibronectin adsorbed on unmodified and sulfonated polystyrene surfaces*. J Biomed Mater Res A, 2009. **91**(4): p. 1239-51.
174. Kowalczyńska, H.M., et al., *Adsorption characteristics of human plasma fibronectin in relationship to cell adhesion*. J Biomed Mater Res, 2002. **61**(2): p. 260-9.
175. Kowalczyńska, H.M., et al., *Fibronectin adsorption and arrangement on copolymer surfaces and their significance in cell adhesion*. J Biomed Mater Res A, 2005. **72**(2): p. 228-36.
176. Kowalczyńska, H.M., et al., *Semiquantitative evaluation of fibronectin adsorption on unmodified and sulfonated polystyrene, as related to cell adhesion*. J Biomed Mater Res A, 2008. **87**(4): p. 944-56.
177. Toworfe, G.K., et al., *Effect of functional end groups of silane self-assembled monolayer surfaces on apatite formation, fibronectin adsorption and osteoblast cell function*. J Tissue Eng Regen Med, 2009. **3**(1): p. 26-36.

178. Toworfe, G.K., et al., *Fibronectin adsorption on surface-activated poly(dimethylsiloxane) and its effect on cellular function*. J Biomed Mater Res A, 2004. **71**(3): p. 449-61.
179. Rouxhet, L., et al., *Adsorption of albumin, collagen, and fibronectin on the surface of poly(hydroxybutyrate-hydroxyvalerate) (PHB/HV) and of poly (epsilon-caprolactone) (PCL) films modified by an alkaline hydrolysis and of poly(ethylene terephthalate) (PET) track-etched membranes*. J Biomater Sci Polym Ed, 1998. **9**(12): p. 1279-304.
180. Sethuraman, A., et al., *Effect of surface wettability on the adhesion of proteins*. Langmuir, 2004. **20**(18): p. 7779-88.
181. Garcia, A.J., P. Ducheyne, and D. Boettiger, *Effect of surface reaction stage on fibronectin-mediated adhesion of osteoblast-like cells to bioactive glass*. J Biomed Mater Res, 1998. **40**(1): p. 48-56.

9 CURRICULUM VITA

Helen Han Cui

July 1994: Bachelor of Science, Beijing Polytechnic University, Beijing, China.

Dec 1998: Master of Science, Bioengineering, The University of Illinois at Chicago, Chicago, IL.

May 2010: Ph.D., Pharmaceutical Science, Rutgers University, New Brunswick, NJ.

Publications

Research articles

- **Cui, H, Sinko PJ.** The Role of Crystallinity on Differential Attachment and Proliferation of Osteoblasts and Fibroblasts on Poly(caprolactone-*co*-glycolide) Polymeric Surfaces. To be submitted to J. of Biomed. Mater: Mater in Tissue E. and Reg. Med.
- **Helen Cui**, Jeffrey Geesin and Patrick Sinko. Fn Adsorbed to Poly(caprolactone-*co*-glycolide) Surfaces via Its Heparin/Collagen Binding Motif Module under influence of varied crystallinity of the matrix. To be submitted to Biomat.
- Nathan A, Rosenblatt J, **Cui H** and Borgia M. Sustained delivery of Risperidone using polyester materials. Proceedings in the Con. Rel Society Annual Mtg, 2003, Glasgow, Scotland.

- **Cui H** and Messersmith PB. A controlled release formulation using thermal gelation. Chapter 13, Biopolymers, Marcel dekker, New York, 1998.

▪

Patent application

- Rosenblatt J, Cui H, Wu CB and Kataria R. "Compositions for parenteral administration and sustained-release of therapeutic agents", A61K000916.
- Rosenblatt J, Cui H, Wu CB and Kataria R. "Polymer coated microparticles for sustained release", A61F001300
- Brown L, Cui H and Wu D. " METHOD OF TREATMENT FOR OSTEOARTHRITIS BY LOCAL INTRA-ARTICULAR INJECTION OF MICROPARTICLES", A61K0031726
- Wadsworth S, Rosenblatt J, Cui H and Do H. " Hollow Foam Beads for Treatment of Glioblastoma", A61K000914
- Cooper K, Wadsworth S, Rosenblatt J, Cui H. " DRUG-ENHANCED ADHESION PREVENTION", A61K0031519
- Cooper K, Wadsworth S, Rosenblatt J, Cui H. " DRUG-ENHANCED ADHESION PREVENTION", A61K000916
- Cooper K, Wadsworth S, Rosenblatt J, Cui H. " DRUG-ENHANCED ADHESION PREVENTION", A61K0009127
- Agenter D, Brown L, Cui H and Geesin J. " Pharmaceutical composition and method for treating a joint-capsule arthropathy", A61K0031726
- Nathan A, Cui H, Li Z. " PUNCTAL PLUGS FOR THE DELIVERY OF ACTIVE AGENTS", A61F000214
- Nathan A, Cui H, Li Z. " PUNCTAL PLUGS FOR THE DELIVERY OF ACTIVE AGENTS", A61F000900
- Nathan A, Cui H, Li Z. " PUNCTAL PLUGS FOR THE DELIVERY OF ACTIVE AGENTS", A61F000200
- Schachter D, Cui H and Zhang J. "Sustained release formulation for HIV agents".